

MECHANISTIC STUDIES OF BETA PROTEIN AMYLOID FORMATION IN ALZHEIMER'S DISEASE: IDENTIFICATION AND CHARACTERIZATION OF PROTOFIBRIL INTERMEDIATES

by

James D. Harper

B.S. Chemistry, Furman University (1993)

Submitted to the Department of Chemistry in Partial Fulfillment of the Requirements for the Degree of

DOCTOR OF PHILOSOPHY

at the

Massachusetts Institute of Technology

June 1998

© 1998 Massachusetts Institute of Technology All rights reserved

Signature of Author [Signature] Department of Chemistry April 28, 1998

Certified by [Signature] Peter T. Lansbury, Jr. Associate Professor of Chemistry Thesis Supervisor

Accepted by [Signature] Dietmar Seyferth Chairman, Departmental Committee on Graduate Students

MASSACHUSETTS INSTITUTE OF TECHNOLOGY


JUN 15 1998

Science

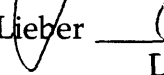
LIBRARIES

This doctoral thesis has been examined by a Committee of the Department of Chemistry as follows:

Professor Joanne Stubbe  \_\_\_\_\_  
Chairperson

Professor Peter T. Lansbury, Jr.  \_\_\_\_\_  
Thesis Supervisor

Professor Jonathan King  \_\_\_\_\_  
Department of Biology

Professor Charles M. Lieber  \_\_\_\_\_  
Department of Chemistry & Chemical Biology  
Harvard University

# MECHANISTIC STUDIES OF BETA PROTEIN AMYLOID FORMATION IN ALZHEIMER'S DISEASE: IDENTIFICATION AND CHARACTERIZATION OF PROTOFIBRIL INTERMEDIATES

by

James D. Harper

Submitted to the Department of Chemistry  
on April 28, 1998 in Partial Fulfillment of the  
Requirements for the Degree of Doctor of Philosophy

## ABSTRACT

Ordered protein aggregation in the brain is a hallmark of Alzheimer's disease (AD). The disease-specific amyloid fibrils which form the core of neuritic plaques are formed by the 4-kilodalton  $\beta$  amyloid protein ( $A\beta$ ). This protein can be induced to form aggregates *in vitro* which are indistinguishable from brain-derived fibrils. Consequently, a large amount of effort has been invested in the development of *in vitro* model systems to study the details of the aggregation process and the effects of endogenous molecules which have been implicated in disease. A simple mechanistic model has emerged for  $A\beta$  amyloid formation which involves a nucleation-dependent polymerization process. To test the basic features of the model, a series of experiments have been performed using atomic force microscopy (AFM) to follow the progress of  $A\beta$  fibril formation *in vitro*. These studies have detected a heterogeneous group of oligomeric  $A\beta$  species which are transiently populated before the onset of fibril formation. Among these species is an elongated flexible species with a diameter of approximately 4 nm that we have termed  $A\beta$  amyloid protofibrils. Protofibrils elongate slowly with time under a variety of *in vitro* conditions with a rate that is sensitive to changes in  $A\beta$  concentration, incubation temperature, and ionic strength, and ultimately disappear as amyloid fibrils of at least two types are formed. An expanded model of  $A\beta$  fibril formation is presented, based on these and other observations, in which  $A\beta$  amyloid fibrils are formed by lateral association and winding of protofibrils and stabilized by a conformational change. The presence of protofibrils during the initial stages of fibril formation *in vitro* suggests that protofibrils may also form early in AD. If these transient intermediates are found in the brain, they would provide attractive targets for AD therapeutics aimed at inhibiting amyloid formation and AD diagnostics aimed at detecting presymptomatic disease.

Thesis Supervisor: Peter T. Lansbury, Jr.  
Title: Associate Professor of Chemistry

## **Table of Contents**

List of Illustrations.....	8
Acknowledgments.....	11
List of Abbreviations.....	13

### **Chapter 1**

#### **A $\beta$ Amyloid Fibril Formation: A Nucleation Dependent Process.**

Introduction.....	14
Nucleation-Dependent A $\beta$ Amyloid Formation.....	17
Critical Concentration.....	18
A $\beta$ 1-40 Has a Slightly Higher Critical Concentration than A $\beta$ 1-42.....	20
Suggestions of an Intermediate in A $\beta$ Fibril Formation.....	21
How is the A $\beta$ Critical Concentration Exceeded in the AD Brain?.....	22
Proteins and Other Molecules May Raise the A $\beta$ Critical Concentration.....	23
Lag Time .....	24
A $\beta$ 1-40 is Significantly More Kinetically Soluble than A $\beta$ 1-42....	25
ApoE Inhibits Amyloid Nucleation .....	26
Seeding.....	27
Amyloid Formation by A $\beta$ 1-40 is Seeded by A $\beta$ 1-40 Fibrils,28 A $\beta$ 1-42 Fibrils, and NAC Fibrils.....	28
Measuring Amyloid Formation is Difficult.....	29
Existing Methods Have Complementary Strengths and Weaknesses.....	30
Electron Microscopy .....	30
Turbidity .....	31
Sedimentation.....	31
Birefringent Congo Red Binding.....	32
Thioflavine T-Induced Fluorescence .....	32
Quasi-Elastic Light Scattering.....	33
Atomic Force Microscopy.....	33
The Purity and Aggregation State of Synthetic A $\beta$ Substrates Influences the Kinetics of Amyloid Formation.....	34
Stochastic Variability of Kinetic Experiments is Unavoidable .....	34
Physiological Consequences of the Seeded Polymerization Mechanism.....	35
References for Chapter 1.....	39



## **Chapter 2**

### **Observation and Characterization of Transiently Populated Oligomeric**

#### **Intermediates in A $\beta$ Fibril Formation**

Introduction.....	46
Atomic Force Microscopy.....	48
AFM is a Physical Imaging Technique.....	48
Interpretation of Lateral Dimensions.....	49
Interpretation of Height Measurements.....	50
Specimen Preparation.....	51
Evolution of Aggregated Species Observed by AFM.....	52
A $\beta$ 1-40 Rapidly Formed Discrete Protofibrils.....	52
A $\beta$ 1-40 Protofibrils Disappeared, Concurrent With the Appearance of Fibrils.....	54
Rapid Assembly of A $\beta$ 1-42.....	54
Description of Aggregate Morphologies.....	56
Globular Particles.....	56
Protofibrils.....	60
Type 1 Fibrils.....	63
Type 2 Fibrils.....	65
Other Fibril Morphologies are Observed.....	67
Morphologies On a Different Substrate Are Similar.....	68
A $\beta$ 1-42 and A $\beta$ 1-40 Aggregate Morphologies Have Similar Dimensions.....	69
Physical Separation of Aggregate Morphologies.....	69
Filtration.....	69
Sedimentation.....	70
Time Course for the Formation of Protein Secondary Structure.....	74
A Potential Role for the Protofibril as a Fibril Assembly Intermediate.....	76
Experimental.....	80
Materials.....	80
In Vitro Fibril Formation.....	80
AFM Experiments.....	80
CD/AFM Time Course Experiments.....	80
Atomic Force Microscopy.....	81
Specimen Preparation.....	81
AFM Operation.....	81
Measurements.....	81
Separation Studies.....	82
Filtration.....	82
Low Speed Sedimentation.....	82
High Speed Sedimentation.....	82
Equilibrium Density Ultracentrifugation.....	82
Circular Dichroism.....	83
References for Chapter 2.....	85

### **Chapter 3**

#### **AFM Measurements of A $\beta$ 1-40 Protofibril Growth**

Introduction.....	89
AFM-Based Methods for Monitoring Protofibril Growth.....	90
Measuring Average Protofibril Length.....	90
Measuring the Length of the Longest Protofibril Observed.....	91
Effects of Specimen Preparation Conditions on Measurements.....	92
Controlling for the Effect of Brief Dilution.....	93
The Effect of Extended Dilution.....	95
Controlling for the Effect of Incubation Time on the Mica Substrate.....	97
Measurements of Protofibril Growth.....	98
Time-Dependent Elongation of Protofibrils.....	98
Concentration-Dependent Elongation of Protofibrils.....	100
Temperature-Dependent Elongation of Protofibrils.....	105
Ionic Strength-Dependent Protofibril Growth.....	109
Protofibril Growth at Acidic pH.....	112
Summary.....	114
Experimental.....	116
Protein Substrate.....	116
Preparation of Seed-Free A $\beta$ 1-40 Stock Solutions.....	116
In Vitro Aggregation of A $\beta$ 1-40.....	116
General Methods for AFM Analysis.....	117
Specimen Preparation.....	117
Optimization of Protofibril Adsorption Density.....	117
Atomic Force Microscopy.....	118
Protofibril Length Measurements.....	119
Average Protofibril Length.....	119
Length of Longest Protofibril.....	120
References for Chapter 3.....	121

### **Chapter 4**

#### **Seeding Behavior and Morphological Clues Lead to an Expanded Model for the A $\beta$ Fibril Assembly Process**

Introduction.....	123
Protofibril Elongation and Fibril Elongation May be Distinct Processes.....	124
Evidence From Seeding Behavior.....	125
Evidence From Growth Rate Estimates.....	130
Evidence That Fibrils Grow By Incorporation of Protofibrils.....	132
Evidence From the Effects of Pre-Incubation on Seeding Efficiency.....	132
Morphological Observations Are Also Consistent With Fibril Growth by Protofibril Incorporation.....	136

Fibrils have an Inherent Helical Twist.....	136
Observation of Staggered Filaments at Type 1 Fibril Ends.....	138
Imperfections In Type 1 Fibrils.....	139
Observations of Partially Wound Type 1 Fibrils and Isolated Filaments.....	141
Branched Type 1 Fibrils Were Observed.....	143
A Conformational Change May Occur During Fibril Formation.....	145
Indications From Denaturation Studies.....	145
Indications From Differences Between Protofibrils and Filaments.....	149
A Model For A $\beta$ Fibril Formation.....	150
Experimental Section.....	155
Protein Substrate.....	155
Preparation of Seed-Free A $\beta$ 1-40 Stock Solutions.....	155
In Vitro Aggregation of A $\beta$ 1-40.....	155
Seeding Experiments.....	155
GuHCl Denaturation Experiments.....	156
Atomic Force Microscopy.....	156
References for Chapter 4.....	158

## List of Illustrations

<b>Figure</b>		<b>Page</b>
1.1	Sequences of the two major AD amyloid fibril proteins, A $\beta$ 1-40 and A $\beta$ 1-42	15
1.2	A schematic depicting the simplest nucleation-dependent mechanism	17
1.3	Fibril formation is concentration-dependent	19
1.4	An idealized kinetic curve for amyloid formation	25
1.5	Amyloid formation can be seeded	28
1.6	Amyloid formation in vivo must involve a local concentration step	36
1.7	Seeded polymerization of A $\beta$ must occur in a locally concentrated environment	37
2.1	Schematic diagram of an atomic force microscope	49
2.2	AFM tip shape influences lateral dimensions	50
2.3	Representative AFM images of the time course of fibril formation	53
2.4	Representative image and sections of A $\beta$ 1-40 globular particles	57
2.5	Distribution of globular aggregate diameters	59
2.6	Representative image and sections of A $\beta$ 1-40 protofibrils	61
2.7	Representative image and sections of A $\beta$ 1-40 type 1 fibrils	64
2.8	Representative image and sections of A $\beta$ 1-40 type 2 fibrils	66
2.9	A $\beta$ 1-40 Aggregate morphologies on HOPG	68
2.10	Filtration and low speed sedimentation of an A $\beta$ 1-40 solution containing protofibrils and fibrils	70

2.11	Sedimentation of protofibrils at 100,000 x g for 1 hour	71
2.12	Equilibrium density ultracentrifugation of A $\beta$ 1-40 aggregates	73
2.13	Parallel observations of aggregate morphologies and secondary structure formation during A $\beta$ 1-40 fibril formation	76
2.14	Possible A $\beta$ fibril assembly pathways	78
3.1	Typical protofibril distributions used for measuring protofibril lengths	94
3.2	Images of protofibrils following dilution	95
3.3	Images and histograms of protofibril growth	99
3.4	Time course of measured protofibril dimensions	100
3.5	Time course of protofibril growth at different A $\beta$ 1-40 concentrations	102
3.6	Concentration dependence of protofibril growth	104
3.7	AFM images of A $\beta$ 1-40 protofibrils grown at different temperatures	106
3.8	Temperature dependence of protofibril average length	107
3.9	Temperature dependence of protofibril growth based on longest protofibril method	108
3.10	Images of protofibrils grown at different [NaCl]	109
3.11	[NaCl] dependence of average protofibril length	110
3.12	A $\beta$ 1-40 aggregates differ with changing pH	113
4.1	Images of unseeded samples and samples seeded with preformed fibrils	127
4.2	The effect of adding preformed protofibrils or fibrils to freshly diluted A $\beta$ solutions	128
4.3	Seeding behavior with enantiomeric A $\beta$ fibrils	129

4.4	Images used for estimating protofibril and fibril elongation rates	131
4.5	Two possible roles for the protofibril in fibril formation	134
4.6	The effect of pre-incubation time on seeding efficiency	135
4.7	Helicity of A $\beta$ 1-40 type 1 fibrils	137
4.8	Images of staggered filaments at the end of type 1 fibrils	139
4.9	Imperfect winding in type 1 fibrils	140
4.10	Rigid filaments are seen both in isolation and as part of partially wound A $\beta$ 1-40 type 1 fibrils	142
4.11	Images of branched type 1 fibrils	144
4.12	Comparison of the resistance of protofibrils and filaments & fibrils to denaturation by GuHCl	146
4.13	GuHCl does not decrease adsorption of protofibrils to mica at short incubation times	147
4.14	Temporal evolution of A $\beta$ 1-40-derived species	151
4.15	A working hypothesis to explain seeded amyloid fibril growth	152
<b>Table</b>		<b>Page</b>
3.1	Protofibril lengths measured with and without dilution	94
3.2	Effect of extended dilution on protofibril lengths	96
3.3	The effect of NaCl concentration on protofibril adsorption	112

## Acknowledgments

My earliest memories of my interest in science trace back to seemingly endless hours spent in front of public television watching programs like Nova and The Undersea World of Jacques Cousteau. This general curiosity and interest continues through to this day with the help of people who took the time to encourage me and nurture my natural curiosity and creativity. Thanks to Mr. Don Hawk at Parkview High School, I developed a particular fondness for chemistry that initiated the series of events that have ultimately led to the completion of my graduate studies and this thesis. I could not have made it without the support and encouragement of many people over the last five years.

Peter Lansbury has been the best advisor and boss a graduate student could hope for. His relatively "hands-off" approach forced me to struggle with my own ideas for first couple of years and helped me to learn how to think and work independently as a scientist. As my project took shape and began to produce results, Peter helped me learn to focus on understanding the key aspects of the results and to avoid getting sidetracked by my tendency to pay too much attention to less significant details. I am also grateful to Peter for providing a supportive and flexible environment which allowed me to make it through graduate school without ever feeling forced to choose between being a good graduate student and being a good husband and father.

Professor Charles Lieber and his graduate student Stan Wong introduced me to atomic force microscopy and helped me get started on the work that ultimately turned into my thesis project and provided valuable expertise and feedback along the way.

My labmates have helped make my time here a memorable and enjoyable experience. Paul Weinreb and Krista Evans taught me how to aggregate A $\beta$  and make turbidity measurements with the Ted2000 in my early days and helped form the core of the Lansbury group poker night crowd. Raul Zambrano and Anna Poon joined the lab with me and their bay was always a frequent stop on my pacing tours when I was trying to decide what to do next. Ted Ashburn gave me a new appreciation for the pros (and cons) of the "sledgehammer" approach to science. As Lansbury group postdocs and good friends, Santosh Nandan, Cheon-Gyu Cho, Weiguo Zhen, and Tomas Ding each took turns providing the voice of reason and experience that I often needed to stay on track inside and outside the lab. Kelly Conway and Magdalena Anguiano will be the last Lansbury Lab MIT graduates and have been great companions in the lab. Matt Goldberg and Seung-Jae Lee are bravely pioneering molecular biology projects in the chemistry oriented Lansbury lab and have contributed to the broadening of my scientific experience. Lara Fallon and Jongmin Kang have recently resurrected the

Ted2000 and started to make turbidity measurements again ensuring that the agonizing legacy of amyloid aggregation irreproducibility will not end with my departure.

One of the last things that Dr. Larry Trzupek told me as I left Furman University to start my graduate studies at MIT turned out to be one of the most valuable pieces of advice I have received. He warned me that there would be times when I would question my motivation for being in graduate school and want to leave, but that if I would just stick it out through the first couple of years that things would get better. When things got tough, the memory of this conversation and the support of my friends and family (who always had more confidence in my ability to finish than I did) helped me persevere.

My parents have never wavered in their unconditional support of me, no matter what I was doing. Their confidence in my abilities and willingness to do whatever they could to ease my burden has helped me make it this far. Thanks Mom and Dad.

Most importantly, I want to thank my wife, Michelle, for being my partner in everything. Your help and encouragement have kept me going when I couldn't have made it on my own. We came to Cambridge to get this degree together and will be leaving with something much more lasting and rewarding--a family.



## List of Abbreviations

A $\beta$	$\beta$ amyloid protein
AChE	protein acetylcholinesterase
AD	Alzheimer's disease
AFM	atomic force microscopy
ApoE	apolipoprotein E
APP	$\beta$ amyloid precursor protein
CD	circular dichroism
CMC	critical micelle concentration
CR	Congo red
CSF	Cerebrospinal fluid
DMSO	dimethyl sulfoxide
EM	electron microscopy
FAD	familial Alzheimer's disease
FTIR	Fourier-transform infrared spectroscopy
HOPG	highly ordered pyrolytic graphite
NAC	non-A $\beta$ component of AD amyloid
QLS	quasielastic light scattering
RMS	root mean square
SAP	serum amyloid P component
SDS-PAGE	sodium dodecyl sulfate polyacrylamide gel electrophoresis
thioT	thioflavine T

## Chapter 1

### A $\beta$ Amyloid Fibril Formation: A Nucleation Dependent Process

Alzheimer's disease (AD) is a late-onset, progressive neurodegenerative disease which is characterized by ordered protein aggregation in the brain.<sup>1-5</sup> The highly insoluble AD-specific aggregates, known as amyloid fibrils, comprise primarily variants of the A $\beta$  protein (Figure 1.1).<sup>3</sup> Circumstantial evidence suggests that the A $\beta$  amyloid fibril may initiate neurodegeneration *in vivo*.<sup>1,3,6-8</sup> Hence, the inhibition of A $\beta$  aggregation may represent a feasible therapeutic strategy against AD.<sup>9-12</sup> It is, therefore, critical to understand the detailed molecular mechanism of A $\beta$  amyloid formation and to elucidate the role of endogenous factors which appear to inhibit amyloidogenesis in the normal brain and/or promote it in the AD brain.

The family of A $\beta$  variants are derived from the amyloid precursor protein (APP), a widely-expressed *ca.* 700-amino acid cell-surface protein of unknown function.<sup>1,3</sup> All forms of early-onset AD affect the expression and/or processing of APP.<sup>8</sup> Trisomy of the APP-bearing chromosome (chromosome 21) is characteristic of Down syndrome; these individuals invariably develop the neuropathological features of AD in their forties.<sup>13</sup> Mutations in the APP gene cause early-onset familial AD (FAD) and affect the production of A $\beta$  variants from APP in culture by transfected mammalian cell lines.<sup>3,8</sup> Two variants, A $\beta$ 1-40 and A $\beta$ 1-42, which differ by truncation at the carboxyl terminus (Figure 1.1), are the predominant plaque proteins.<sup>8</sup> Both are found in the blood and cerebrospinal fluid (CSF) at nanomolar levels.<sup>14</sup> The combined concentration of the A $\beta$  variants in plasma and CSF does not vary significantly in most AD patients.<sup>14,15</sup> However, the plasma concentration of the minor plasma protein

A $\beta$ 1-42 increases in FAD patients bearing an APP mutation, and also, strikingly, in FAD patients bearing mutations on chromosomes 1 (presenilin 2) or 14 (presenilin 1).<sup>16</sup> In addition, A $\beta$ 1-42 constitutes a larger portion of total A $\beta$  in amyloid plaques from FAD patients as compared to those from late-onset AD patients.<sup>17,18</sup> These findings suggest a possible role for A $\beta$ 1-42 in AD pathogenesis, a possibility discussed below.

<b>A<math>\beta</math>1-40</b>	<b>DAEFRHDSGYEVHHQKLVFFAEDVGSNKGAIIGLMVGGVV</b>
<b>A<math>\beta</math>1-42</b>	<b>DAEFRHDSGYEVHHQKLVFFAEDVGSNKGAIIGLMVGGVVIA</b>

**Figure 1.1 Sequences of the two major AD amyloid fibril proteins, A $\beta$ 1-40 and A $\beta$ 1-42.**

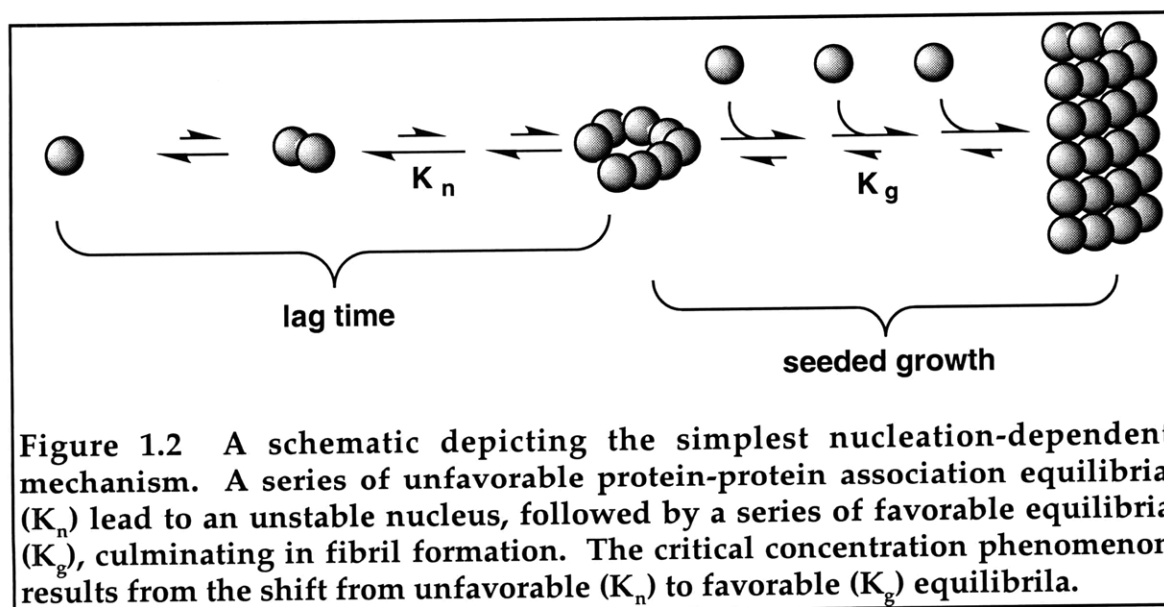
Native-like A $\beta$  amyloid fibrils have been produced from synthetic A $\beta$  variants (see below).<sup>19,20</sup> It is therefore possible to devise simple *in vitro* models of the complex *in vivo* aggregation process. Such models have been used to screen compound libraries for inhibitors of aggregation which may have therapeutic efficacy against AD.<sup>11</sup> In addition, *in vitro* models will be useful for elucidating the molecular details of the aggregation processes, for facilitating the understanding of known genetic risk factors for AD, and, possibly, for discovering novel potential protein risk factors, which could then be investigated by targeted genetic screening.<sup>5</sup> A prerequisite to elucidation of the pathway is the understanding of the structural aspects of the aggregation process; the conformational properties of the starting A $\beta$  protein and the structure of the product A $\beta$  amyloid fibril.<sup>5,21,22</sup>

Once a simple *in vitro* model for amyloidogenesis has been developed and shown to recapitulate what is known about the *in vivo* process, it can be used to evaluate the effects of disease-associated biochemical changes characteristic of AD (increases in A $\beta$  concentration, Apolipoprotein E (apoE) genotype, etc.--see below) on the aggregation process. In doing so, it is critical to distinguish between effects on the structure, solubility, or stability of aggregates and effects on the rate of aggregate formation. Perturbations of the structural properties of a protein in its soluble or fibrillar state can be measured (SSNMR, FTIR, CD, gel filtration, SDS-PAGE, electron microscopy, etc.) but do not necessarily correlate to effects on the aggregation rate. Conversely, perturbations of the rate of amyloid formation are not necessarily linked to structural effects. For example, ApoE3 decreases the rate of A $\beta$ 1-40 amyloid formation *in vitro* but does not seem to affect the structure or solubility of the product amyloid fibril<sup>23,24</sup> (this interpretation has been disputed by other laboratories,<sup>25,26</sup> see below).

The key to understanding the rate of amyloid formation involves the identification of its slowest, or rate-determining, step in the overall process. This is the step which may be responsible for protecting normal individuals from amyloid formation. The disease may result from acceleration of this step and, therefore, the overall process; perturbation of other steps may have no effect. For instance, since most protein conformational changes are much faster than amyloid formation, perturbations of the monomer conformational dynamics are unlikely to affect the overall rate. The slow step in amyloid formation seems to be the formation of an ordered oligomeric nucleus (Figure 1.2).<sup>27</sup>

## NUCLEATION-DEPENDENT A $\beta$ AMYLOID FORMATION

Protein crystallization is a highly ordered process which occurs *via* a nucleation-dependent pathway.<sup>28</sup> Physiological ordered protein aggregation processes as diverse as viral coat assembly,<sup>29</sup> microtubule formation,<sup>30</sup> flagellum formation,<sup>31</sup> and sickle-cell hemoglobin fibril formation<sup>32</sup> also occur by a nucleation-dependent polymerization pathway. These processes are characterized by (a) a slow nucleation phase, in which the protein undergoes a series of unfavorable association steps to form an ordered oligomeric nucleus, (b) a growth phase in which the nucleus rapidly grows to form larger polymers, and (c) a steady state phase, in which the ordered aggregate and the monomer appear to be at equilibrium.<sup>33,34</sup>



The characteristic features of a typical nucleation-dependent polymerization are as follows: (a) No aggregation occurs at a protein concentration below the **critical concentration**, (b) At protein concentrations which exceed the critical concentration by a small amount, there is a **lag time** before polymerization occurs, and (c) During the lag time, addition of a **seed**

results in immediate polymerization.<sup>31-34</sup> Each of these characteristics will be considered in turn, citing specific experiments involving in vitro A $\beta$  amyloid formation.

### **Critical Concentration**

In a typical nucleation-dependent polymerization, polymer is not observed at equilibrium until the monomer concentration exceeds a certain level, known as the critical concentration (Figure 1.3). Below the critical concentration, the monomer is the predominant species. As the protein concentration is increased beyond the critical concentration, the polymer concentration continues to rise, but the monomer concentration remains the same (Figure 1.3). The critical concentration phenomenon reflects the cooperativity of nucleus formation; formation of the nucleus involves a series of unfavorable equilibria (the rate of these association steps could be fast or slow, both scenarios are precedented), while the equilibrium constant which characterizes the growth phase is very favorable ( $K_g \gg K_n$ , Figure 1.2).<sup>33,34</sup> The critical concentration is equivalent to the growth equilibrium constant ( $K_g$ ) and describes the solubility of the protein under steady-state conditions.<sup>33,34</sup>

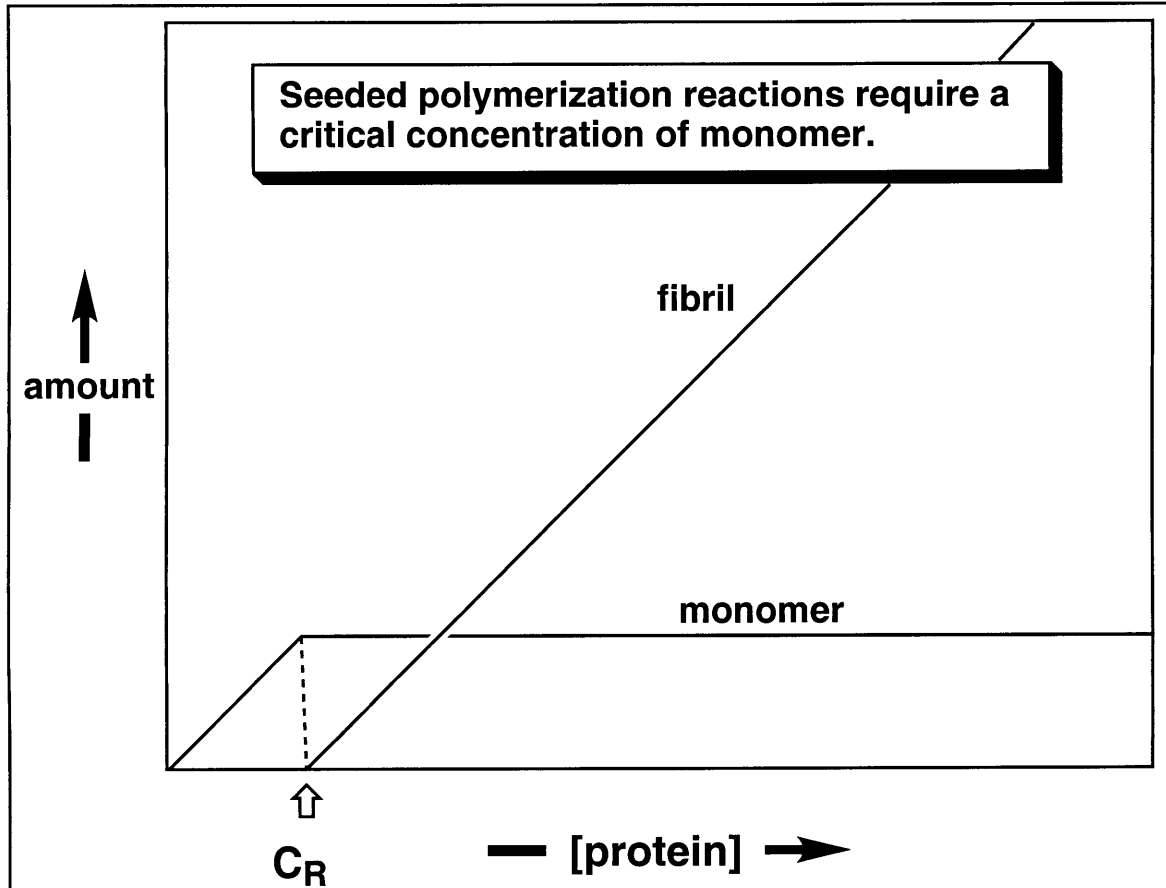


**Figure 1.3: Fibril formation is concentration-dependent. Below the critical concentration ( $C_R$ ), no fibril formation will occur. Above that concentration, all added protein will be incorporated into the fibrils such that the monomer concentration never exceeds  $C_R$ . This behavior is seen at equilibrium.**

Micelle formation also requires a critical concentration, referred to as the critical micelle concentration (CMC). Amyloid fibril nucleation is much slower than micelle formation, possibly due to the greater entropic barrier involved in organizing a fibril.<sup>22</sup> As a consequence, supersaturated protein solutions are metastable, or kinetically soluble (see discussion of lag time below). By definition, the kinetic solubility of an amyloid protein is time-dependent; at infinite time, the kinetic solubility and the critical concentration are equivalent. The kinetic solubility of amyloid proteins may play an important role in the in

vivo process leading to disease; this will be discussed in detail at the end of this chapter.

*Aβ1-40 has a slightly higher critical concentration than Aβ1-42.* The critical concentration is typically measured by determining the concentration at which fibril formation and fibril dissolution are equal.<sup>33,35</sup> The concentration of Aβ remaining in solution after amyloid fibril formation should also equal the critical concentration, provided that equilibrium<sup>33</sup> has been reached. That concentration should also be equal to the concentration of soluble material reached by dissolving fibrillar Aβ. Two Aβ model peptides (Aβ26-40, Aβ26-43) have been analyzed in this way,<sup>36</sup> but the full-length Aβ variants have not.

Comparing literature reports of Aβ critical concentration determinations is difficult, since buffer compositions and methods for measuring monomeric Aβ and fibrillar Aβ vary. However, there is a qualitative consensus among experiments performed under "physiological" conditions (pH 7-8, 5-100 mM salt, 25-37°C): (1) Aβ1-40 rapidly forms amyloid fibrils at concentrations over 100 μM,<sup>19,37</sup> (2) At Aβ1-40 concentrations between 20 μM and 80 μM, a period of kinetic solubility precedes fibril formation.<sup>9,11,23,38-40</sup> Some researchers have observed instantaneous aggregation in the latter concentration range, possibly due to the presence of a small amount of undissolved seed fibril in the protein stock solution (vide infra). Using complementary methods, the operational solubility of Aβ1-40 has been measured to be *ca.* 35 μM,<sup>23,41</sup> 6-9 μM,<sup>27</sup> and 10 μM (in 1M urea).<sup>35</sup> Thus the critical concentration of Aβ1-40 at neutral pH is *ca.* 10-40 μM, and significant kinetic solubility will be observed at concentrations less than 100μM.

The Aβ variant Aβ1-42 has not been studied in as much detail as Aβ1-40 due to its limited availability<sup>42</sup> and its greater insolubility.<sup>19,27,43</sup> The difference



in critical concentration is demonstrated by the fact that the supernatant after A $\beta$ 1-42 fibril formation contained four- to fivefold less soluble monomer (interpreted as dimer in reference based on calibration of size exclusion elution profile calibrated with globular proteins, a 4 kDa A $\beta$  monomer would likely migrate with an apparent molecular weight of 8-9 kDa due to its nonglobular structure--extended random coil proteins typically behave in this manner<sup>44</sup>) than did the supernatant after A $\beta$ 1-40 fibril formation.<sup>45</sup> At A $\beta$ 1-42 concentrations as low as 20-25  $\mu$ M (37, 41), aggregation has been observed within the few minutes required to make the initial measurement. This may be due to the difficulties with the complete solubilization of the commercial material, (vide infra) leaving seed fibrils in the stock solution. At 8  $\mu$ M A $\beta$ 1-42, significant aggregation has been observed within 12 hours, but, since earlier time points were not measured, the existence of a significant lag time cannot be ruled out.<sup>46</sup> The post-aggregation solubility of A $\beta$ 1-42 is difficult to accurately measure; reported values between 2 and 15  $\mu$ M,<sup>27,46</sup> reflect the intrinsic critical concentration of A $\beta$ 1-42. Thus the critical concentration of A $\beta$ 1-42 appears to be in the low micromolar range, *ca.* 5-fold lower than the critical concentration of A $\beta$ 1-40.<sup>45</sup> A $\beta$ 1-42 has shown little or no evidence of kinetic solubility.

*Suggestions of an intermediate in A $\beta$  fibril formation.* Analytical ultracentrifugation has shown that A $\beta$ 1-40, below its critical concentration (25  $\mu$ M), exists predominantly as a monomer.<sup>47</sup> The same method indicated that, well above its critical concentration (*ca.* 450  $\mu$ M), monomeric A $\beta$ 1-40 coexists with with insoluble fibrillar high molecular weight oligomers.<sup>37</sup> In addition, slow-sedimenting (operationally soluble) A $\beta$ 1-40 oligomers were detected. Based on sedimentation properties, the molecular weight of the putative intermediate has been proposed to be *ca.* 4,000 kD (an A $\beta$  1000 mer?).<sup>37</sup> An A $\beta$ -apoE complex of

comparable size has been purified by gel filtration (see below).<sup>48</sup> These findings suggest that the actual mechanism for A $\beta$  amyloid formation may be more complex than the simple model presented in Figure 1.2. Other A $\beta$  aggregates have been detected under different conditions. The surfactant properties of A $\beta$  have been documented: both A $\beta$ 1-40 and A $\beta$ 1-42 show surface activity at the air-water interface, probably due to monolayer formation (critical concentration = 25  $\mu$ M). A form of A $\beta$ 1-40 with behavior resembling that of a micelle (diameter based on a spherical model = 14 nm) was detected by quasielastic light scattering (QLS) studies of A $\beta$ 1-40 in 0.1 N aqueous HCl (CMC = 100  $\mu$ M, critical conc. for fibril growth under these conditions < 25  $\mu$ M).<sup>49</sup> It was proposed that these species slowly convert into fibril nuclei.<sup>49</sup>

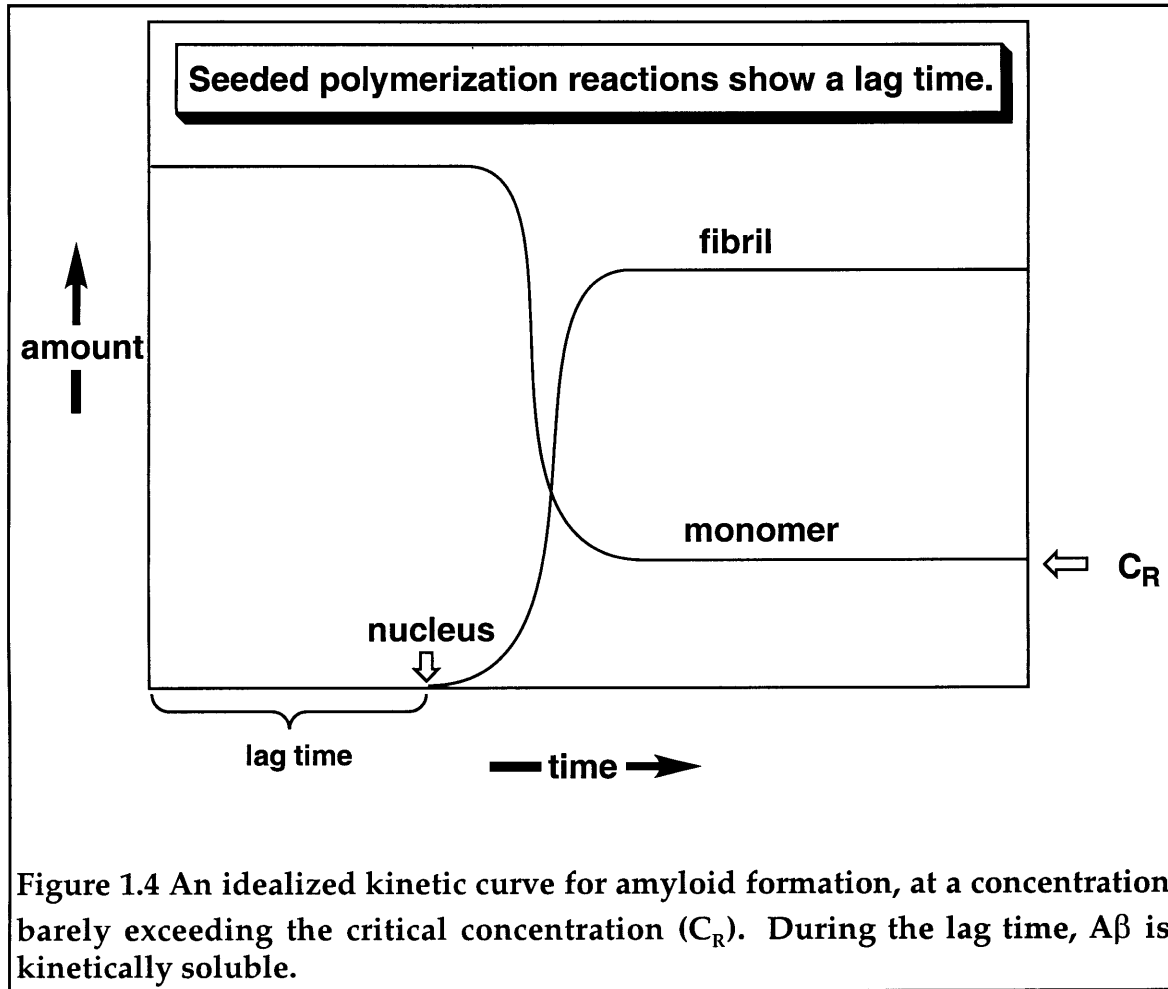
*How is the A $\beta$  critical concentration exceeded in the AD brain?* The concentration of A $\beta$  in cerebrospinal fluid is in the low nanomolar range.<sup>15,50</sup> However, *in vitro* amyloid fibril growth in single component A $\beta$  1-40 or A $\beta$ 1-42 solutions has not been detected at submicromolar A $\beta$  concentrations. In order for A $\beta$  amyloid formation to occur in the brain, there must either exist a process whereby a local A $\beta$  concentration in the  $\mu$ M range is created, or the *in vivo* critical concentration must be lowered by an endogenous substance. We will consider these possibilities in turn. Two general mechanisms for local A $\beta$  concentration can be proposed based on *in vitro* studies; (1) concentrate A $\beta$  in a cellular compartment, (2) create a high effective concentration, for example, by A $\beta$  binding to proteoglycan<sup>51</sup> or directly to the membrane surface.<sup>47</sup> Mechanism (1) is consistent with cell-culture studies of A $\beta$  production from APP which demonstrate the proteolysis may occur in a cellular compartment.<sup>1</sup> Lysosomal pH clearly induces rapid A $\beta$  aggregation,<sup>37,38,43,52</sup> but the low pH precipitate is not fibrillar.<sup>38</sup> Mechanism (2) is supported by the observation that phospholipid

vesicles lower the A $\beta$ 1-40 concentration required to observe a random coil-to- $\beta$ -sheet transition indicative of amyloid formation.<sup>47</sup> In addition to mechanisms that create a high local concentration of A $\beta$  *in vivo*, endogenous proteins or other factors could lower the critical concentration of A $\beta$ . The amyloid-associated protein acetylcholinesterase (AChE), at a 1% relative concentration (2.4  $\mu$ M AChE vs. 240  $\mu$ M A $\beta$ 1-40), decreased the critical concentration of A $\beta$ 1-40 approximately 3-fold (at pH 5).<sup>53</sup> The effect of AChE on the *rate* of amyloid formation was not determined. In addition, endogenous metals may also lower the A $\beta$  critical concentration. Zinc is capable of inducing precipitation of A $\beta$  at subnanomolar A $\beta$  concentration,<sup>54,55</sup> although it has not been demonstrated that the Zn-induced A $\beta$  aggregates are ordered amyloid fibrils.

*Proteins and other molecules may raise the A $\beta$  critical concentration.* This effect, which could be important *in vivo*, could be achieved by destabilizing the amyloid fibril or by stabilizing the A $\beta$  monomer. The amyloid-associated protein serum amyloid P component (SAP, 2% by moles) was shown to increase the *in vitro* critical concentration of A $\beta$ 1-42 by approximately three-fold (see discussion of sedimentation assay below). SAP also inhibited A $\beta$ 1-42 amyloid formation.<sup>46</sup> However, it is not necessarily the case that molecules which raise the critical concentration would decrease the rate of amyloid formation (or vice versa, see discussion of apoE below). Monoclonal antibodies raised against peptides based on the A $\beta$  sequence increase the A $\beta$ 1-40 critical concentration (at equimolar concentration vs. A $\beta$ 1-40), possibly by binding A $\beta$  monomer.<sup>56</sup> Analogs of the antibiotic rifampicin (5% by moles)<sup>9</sup> and a long-chain alkyl piperidinium salt (*ca.* 10% by moles)<sup>11</sup> have similar effects. The detailed kinetic behavior of A $\beta$  in the presence of these compounds has not been reported.

## Lag Time

The length of time during which a supersaturated solution remains kinetically soluble before amyloid formation commences is called the lag time (Figure 1.4). During the lag time, small, but not necessarily detectable, amounts of prenucleus oligomers sequentially build up according to the simplified mechanistic scheme presented in Figure 2. The rate of nucleus formation is slow, due primarily to the unfavorability of the preceding association equilibria, rather than to the intrinsically slow association rates.<sup>34</sup> The length of the lag time can be extremely sensitive to protein concentration, depending on the oligomer size of the nucleus and other details of mechanism which are unclear in the case of A $\beta$ . Extremely large concentration-dependences of the lag time for sickle-cell fibril formation (*ca.* 25 - 50-fold) have been measured.<sup>57</sup> The magnitude of the concentration-dependence may be due to the coexistence of a secondary nucleation pathway, which involves nucleus formation at the fibril surface.<sup>58</sup> A similar phenomenon could exist in A $\beta$  amyloid fibril formation. The concentration-dependences of the A $\beta$ 1-40 and A $\beta$ 1-42 lag times have not been measured, due, in part, to experimental inconsistencies which are unavoidable at the low concentrations of A $\beta$  required to observe a significant lag time (see below). However, a large concentration-dependence may not be seen if the observed lag time for A $\beta$  fibril formation arises from the slow conversion of a relatively rapidly formed oligomeric intermediate form of A $\beta$  to an ordered nucleus.



*A $\beta$ 1-40 is significantly more kinetically soluble than A $\beta$ 1-42.* The critical concentration of  $A\beta$ 1-42 is only four- to five-fold greater than  $A\beta$ 1-40 (see above). However, the kinetic solubility of  $A\beta$ 1-40 has been demonstrated to be significantly greater than that of  $A\beta$ 1-42.<sup>27</sup> For example, a supersaturated solution of  $A\beta$ 1-40 (20  $\mu$ M) is kinetically soluble for days (lag time = 96 h), whereas kinetic solubility has not been demonstrated for  $A\beta$ 1-42 at the identical concentration (lag time  $\ll$  1h).<sup>27</sup> The difference in lag times could arise from a stabilizing effect of the C-terminus on each step preceding nucleus formation. However, this possibility should not be overemphasized, since  $A\beta$ 1-42 amyloidogenesis may follow a pathway that is mechanistically distinct from the

A $\beta$ 1-40 pathway. Resolution of this issue will require the direct comparison of the A $\beta$ 1-40 and A $\beta$ 1-42 mechanisms, using multiple techniques.

*ApoE inhibits amyloid nucleation.* ApoE2 and other endogenous proteins which inhibit amyloid formation may protect against AD. There are three isoforms of human apolipoprotein E, apoE2, apoE3, and apoE4. ApoE2 and apoE4 differ from apoE3 at a single residue (out of 299). The E3 allele is the most widespread, followed by E4 and E2. ApoE4 homozygotes have a significantly increased risk of contracting AD, at an earlier age, than do apoE3 homozygotes.<sup>59</sup> ApoE2 homozygotes, though very rare, seem to be protected against AD.<sup>59</sup> The apoE2 allele is underrepresented (and the apoE4 allele is overrepresented) in the AD population, implicating ApoE2 as a protective factor against AD.<sup>59</sup> ApoE4-bearing AD patients have a high amyloid burden at the time of death as compared to the average AD patient.<sup>60</sup> Thus, apoE4 may promote amyloid formation relative to apoE3. This phenotype could result either from apoE4 being a better amyloid promoter than apoE3,<sup>25,26</sup> or from apoE4 being a less efficient amyloid inhibitor than apoE3.<sup>23,24,61,62</sup> Experimental support for both of these scenarios has been presented. The inhibitory scenario is supported by the fact that apoE3, at molar ratio of 0.1% to 1% as compared to A $\beta$ 1-40, significantly increases the observed lag time.<sup>23,61,62</sup> The apoE3 dimer is a much more potent inhibitor than monomeric apoE3 or monomeric apoE4 (apoE4 cannot dimerize).<sup>23</sup> Based on these results, a mechanistic model, in which apoE binds to a prenucleus A $\beta$  oligomer, was proposed.<sup>23</sup> Recently other laboratories have confirmed the inhibitory activity of apoE3<sup>24,61,62</sup> and isolated an apoE-A $\beta$  oligomer.<sup>61</sup> This complex was not an effective seed of A $\beta$  polymerization, rather, it was an inhibitor of A $\beta$  seeding.<sup>61</sup> ApoE3 inhibits amyloid formation when

coexpressed in doubly transfected cell cultures, and attenuates A $\beta$  fibril-induced neurotoxicity.<sup>63,64</sup> Finally, the observation that plaques in apoE4-bearing individuals were more numerous, yet no larger than plaques in apoE3 homozygotes, suggests that the inhibitory effect is focused on the initiation of plaque formation.<sup>65</sup> Earlier studies, which led to the proposal that apoE4 promoted amyloid formation, were based on single time point measurements of amyloid using a method not suited for the quantitation of amyloid (see below).<sup>25,26</sup>

### **Seeding**

At concentrations above the critical concentration, the slow nucleation step can be bypassed by the introduction of exogenous nucleus or seed.<sup>34</sup> As a consequence of seeding, the A $\beta$ 1-40 lag time is eliminated and a first-order growth process occurs (Figure 1.5).<sup>35,49,66,67</sup> Seeding of amyloid formation, like seeding of a crystallization, is extremely discriminating, since it relies on a complementarity between the growth face of the seed fibril and the substrate.<sup>68</sup> However, as is the case in the growth of inorganic crystals, a seed of a different constitution can function as a heterogeneous seed, provided that its growth face is complementary to the native substrate. Both homogeneous and heterogeneous seeding may be important in accelerating amyloid formation in AD.

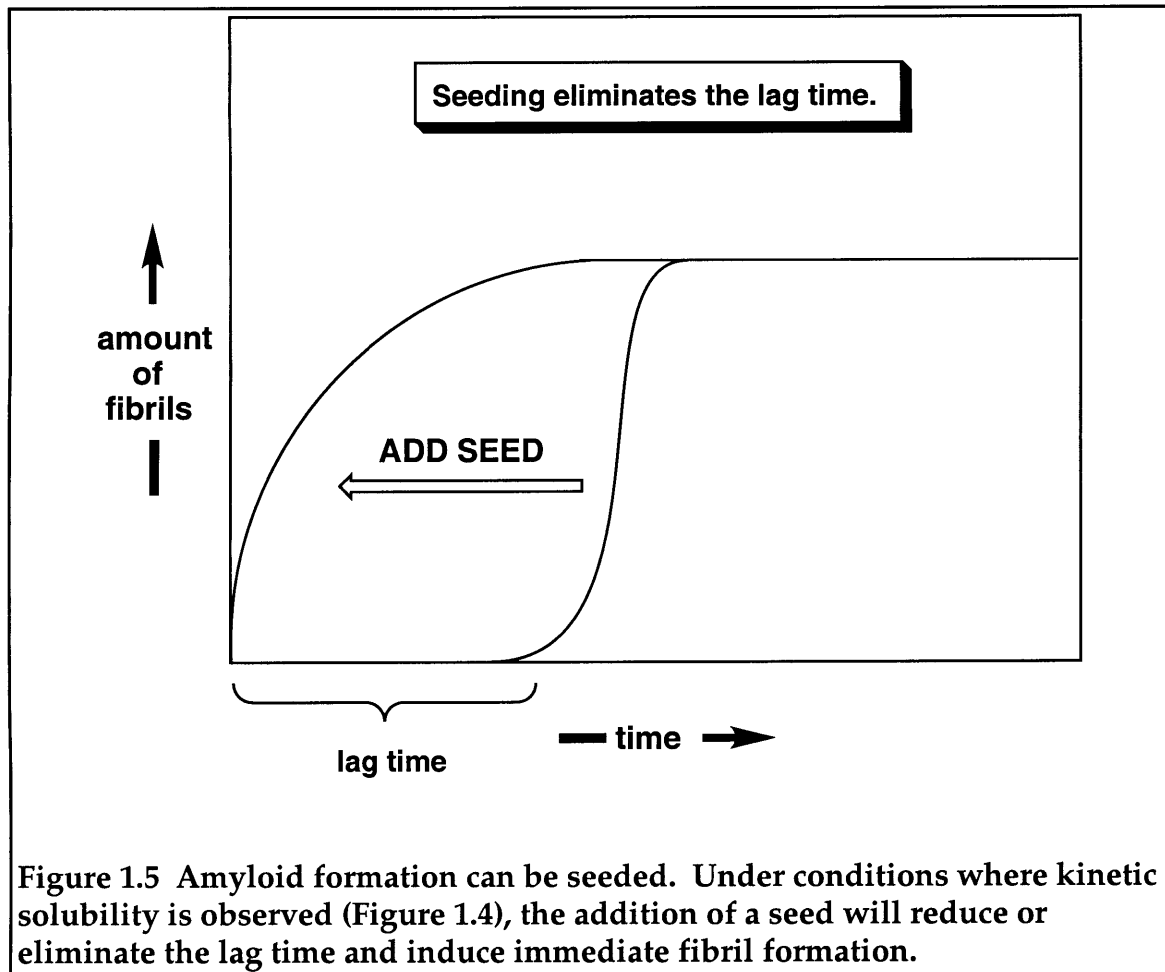


**Figure 1.5 Amyloid formation can be seeded. Under conditions where kinetic solubility is observed (Figure 1.4), the addition of a seed will reduce or eliminate the lag time and induce immediate fibril formation.**

*Amyloid formation by A $\beta$ 1-40 is seeded by A $\beta$ 1-40 fibrils, A $\beta$ 1-42 fibrils, and NAC fibrils. Addition of preformed fibrillar A $\beta$ 1-40 to unseeded solutions of A $\beta$ 1-40 at concentrations barely exceeding its critical concentration can reduce<sup>61,62</sup> (addition of *ca.* 0.02% by weight) or eliminate<sup>27,61,62</sup> (addition of *ca.* 5-10% by weight) the observance of a lag time. A $\beta$ 1-42 fibrils are also efficient heterogeneous seeds for A $\beta$  polymerization.<sup>27,37,38</sup> The initial observation of this effect led to the proposal that seeding of amyloid formation by A $\beta$ 1-42 may be a mechanism of familial early-onset AD (FAD).<sup>27</sup> Subsequent information from neuropathological studies supports the feasibility of this proposed mechanism to*



explain several forms of FAD (involving mutations on chromosomes 1, 21, and 14).<sup>8,17,18</sup>

The 35-amino acid peptide NAC (Non A $\beta$  component of AD amyloid) is an intrinsic component of the insoluble fibrillar core of AD amyloid.<sup>69</sup> This peptide contains an eight amino-acid sequence which is very similar to the critical C-terminus of the A $\beta$ 1-42 and a sequence in the prion protein, a brain amyloid protein implicated in scrapie.<sup>70</sup> NAC amyloid fibrils are efficient seeds for amyloid formation by A $\beta$ 1-40.<sup>70</sup> Conversely, A $\beta$ 1-40 fibrils efficiently seed amyloid formation by NAC.<sup>70</sup> This *in vitro* activity suggests that NAC may trigger A $\beta$  aggregation *in vivo* or, alternatively, may be a target of an A $\beta$  oligomeric seed.<sup>70</sup>

## **MEASURING AMYLOID FORMATION IS DIFFICULT**

The studies of A $\beta$  aggregation discussed above all suffer from a major experimental problem, that is, the lack of a single accurate method to quantitate amyloid fibrils and, especially, to compare fibrils formed under different conditions. Amyloid is not well understood at the structural or morphological level;<sup>21,22</sup> in fact, the existence of more than one type of amyloid fibril suggests that there may be more than one conformational state or packing arrangement for A $\beta$  in amyloid.<sup>71,72</sup> Amyloid has, therefore, been defined operationally as an insoluble fibrous protein aggregate with affinity for Congo red (CR) and thioflavine T (thioT).<sup>21</sup> None of these individual properties is unique to amyloid. Therefore, no single property should be the basis for a quantitative assay. Instead, a combination of methods must be used to increase the specificity of the measurement. The value of this approach is clearly demonstrated in a study of the pH-dependence of A $\beta$  amyloid formation.<sup>38</sup> It has been widely

reported that the pH maximum for A $\beta$  aggregation is in the 5-6 range,<sup>19,37,43,52</sup> suggesting that in vivo amyloid formation may take place in the lysosome. Sedimentable A $\beta$ 1-40 aggregates grown under unstirred conditions at pH 5.8 and at pH 7.4 bind to CR and thioT but are clearly different.<sup>38</sup> First, the aggregates formed at pH 5.8 bind more CR on a molar basis than do A $\beta$ 1-40 aggregates formed at pH 7.4.<sup>38</sup> Second, the pH 7.4 A $\beta$ 1-40 aggregates are fibrillar (as shown by EM) but do not exhibit turbidity at 405 nm, while the turbid aggregates formed at pH 5.8 do not appear to be fibrillar by EM (although they induce a significant enhancement in the thioT fluorescence emission spectrum).<sup>38</sup> Third, the aggregates grown at pH 5.8 are unable to seed polymerization of A $\beta$ 1-40 at pH 7.4.<sup>38</sup> The two aggregate morphologies do not interconvert when incubated under the conditions used to grow the alternate morphology.<sup>38</sup> The existence of distinct A $\beta$  amyloid morphologies could add considerable complexity to the idealized mechanism depicted in Figure 1.2.

### **Existing Methods Have Complementary Strengths and Weaknesses**

The commonly used methods for identifying and quantitating amyloid will be briefly discussed below.

*Electron microscopy.* EM is useful for identifying amyloid fibrils and describing, at low resolution, their morphology. However, it is not possible to quantitate the amount of amyloid protein in fibrillar form by this method. Attempts have been made to utilize the number of fibril crossovers per field to quantitate total amyloid,<sup>26</sup> however, in our experience, it is difficult to select a “typical” field for fibril counting due to clumping of the fibrils. Fibril-fibril associations could alter the amount of crossovers in selected regions (as compared to an ideal homogeneous distribution of straight fibrils) without affecting the total amount

of fibrillar protein. Finally, it is impractical to follow a kinetic run by EM, since sample preparation (fixing, staining, etc.) is time-consuming and may affect fibril morphology.

*Turbidity.* Turbidity detects all particles with a hydrodynamic radius greater than the wavelength of the incident light (e.g., 400 nm).<sup>73</sup> For a homogenous population of fibrils, turbidity correlates with oligomer size.<sup>73</sup> The following findings suggest that turbidity alone is not sufficient to quantify the total amount of fibrillar protein: (a) Turbidity is not specific to amyloid fibrils.<sup>38</sup> (b) The total turbidity will depend on the aggregate morphology (in a nonobvious way).<sup>38</sup> (c) Early intermediates in the fibrillization process may be too small to be detected.<sup>73</sup> For example, the fact that AChE increases the final turbidity of A $\beta$ 1-40 by three-fold could be explained in at least two ways: either AChE decreases the A $\beta$ 1-40 critical concentration or it induces a morphological shift to a fibril type which produces more turbidity.<sup>53</sup> An independent measurement of the amount of A $\beta$ 1-40 remaining in solution after sedimentation of fibrils supports the former scenario.<sup>46,53</sup> Any study using turbidity as a quantitative measure of amyloid should confirm the legitimacy of the method using an independent method to assure that a morphological shift has not occurred.<sup>38,40</sup>

*Sedimentation.* Separation of the soluble monomeric protein from the insoluble amyloid by centrifugation and/or by filtration has been attempted. However, sedimentation does not distinguish ordered amyloid (the morphology of interest) from insoluble amorphous aggregates. For example, 100 mM Zn induces precipitation (measured by sedimentation) of A $\beta$ 1-40 at *subnanomolar* concentrations; a decrease in the solubility of A $\beta$ 1-40 by 10<sup>6</sup>-fold.<sup>55,74</sup> This work does not differentiate between zinc-induced amorphous aggregation and zinc-

induced amyloid formation. Finally, sedimentation may not be able to separate ordered oligomers with low molecular weights (compared to fibrils) from A $\beta$  monomer. Soluble A $\beta$  oligomers, which may be important intermediates in amyloid fibril formation, have been observed in two studies.<sup>37,45</sup>

*Birefringent Congo red binding.* Birefringent CR binding, a defining property of amyloid fibrils, requires that the binding sites be ordered with respect to one another, as may be the case along the surface of an ordered aggregate.<sup>21</sup> Bound CR can be quantitated because there is a spectral shift on binding.<sup>38,75</sup> Unfortunately, CR birefringence cannot be quantified in the same way as CR binding can, so it is not possible to determine what portion of the CR-protein complex is fibrillar. Thus the conclusion, based on CR birefringence, that 25  $\mu$ M A1-40 forms amyloid, as opposed to amorphous aggregate, in the presence of equimolar zinc<sup>54</sup> requires confirmation by another method.

*Thioflavine T-induced fluorescence.* The induced fluorescence of thioT has been widely applied to study amyloid formation, because of its sensitivity and practicality.<sup>24,35,76,77</sup> Fluorescence enhancement is assumed to be common to amyloid fibrils, but this generality has not been demonstrated, and magnitude of this effect has been shown to vary as a function of A $\beta$ 1-40 aggregate morphology.<sup>38</sup> Furthermore, there is also evidence that thioT binds to soluble oligomers of A $\beta$ .<sup>78</sup> In addition, the magnitude of the induced fluorescence emission depends on the morphology of the aggregate.<sup>38</sup> Consequently, the thioT fluorescence assay should not be used to compare fibril growth under conditions that vary slightly, unless it is shown independently that these changes do not result in a morphological change in the aggregate.

*Quasi-elastic light scattering.* QLS directly measures the diffusion coefficient of a species in solution.<sup>49,79-82</sup> The diffusion coefficient is related to hydrodynamic radius and, depending on the shape of the species, to molecular weight. Thus if complementary information about aggregate morphology is available from EM or atomic force microscopy (AFM), the kinetics of amyloidogenesis can be measured.<sup>49</sup> Also, since multiple species can sometimes be simultaneously detected and distinguished (depending on their relative size), some low molecular weight species may be identified and quantified with this method.<sup>49</sup>

*Atomic Force Microscopy.* AFM is a method of imaging material on surfaces with a resolution currently comparable to electron microscopy.<sup>71,72</sup> Recent technological advances may provide a significant increase in AFM resolution of biological features.<sup>83</sup> However, unlike EM, AFM requires little or no sample preparation and can, in some cases, be used to image species in buffer in a continuous mode, which is ideal for kinetic studies. This method has demonstrated a morphological heterogeneity of A $\beta$  amyloid fibrils which is not readily apparent from negative stain EM analysis (often because of the variability of the staining procedure).<sup>71,72</sup> AFM offers the potential to simultaneously study the morphology and assembly kinetics of a single fibril provided that suitable binding to substrate can be achieved. Since AFM imaging ordinarily requires non-specific adsorption of species to an atomically smooth surface (e.g., mica), studies using AFM must control for the effect of the adsorption process on aggregate morphology and/or assembly.

## **The Purity and Aggregation State of Synthetic A $\beta$ Substrates Influences the Kinetics of Amyloid Formation**

The synthesis of insoluble proteins, such as the A $\beta$  variants, is extremely difficult. A typical solid-phase synthesis will average *ca.* 99.5% yield per coupling. However, at the completion of a 39-step process, the crude product will contain a significant amount of 39-mers, each missing a single amino acid.<sup>42</sup> These deletion impurities can be extremely difficult to separate from the desired product and, to make matters worse, can be extremely difficult to detect, since each single deletion impurity constitutes less than 1% of the crude mixture. However, these impurities could have a significant effect on the aggregation kinetics, possibly acting as crystal poisons.<sup>34</sup> For example, the inhibitory effect of A $\beta$ 1-40 on A $\beta$ 1-42 aggregation has been reported.<sup>37</sup> In addition to chemical impurities, it is important to eliminate "structural impurities" from the A $\beta$  substrate. A very small amount of preexisting ordered aggregate in a stock solution may be capable of seeding polymerization of the A $\beta$  protein.<sup>27,61,62,68</sup> Extensive precautions should be followed to remove any aggregated A $\beta$  from commercial lots before kinetic experiments are attempted.<sup>23,81</sup>

## **Stochastic Variability of Kinetic Experiments is Unavoidable**

The timing of an improbable event like homogeneous nucleation is difficult to predict and measure reproducibly. This experimental limitation has been encountered in studies of sickle-cell hemoglobin polymerization.<sup>58,84-86</sup> Finally, there are many variables (e.g., tube surfaces, stirring rate) which are known to influence nucleation and growth but are extremely difficult to control.

## PHYSIOLOGICAL CONSEQUENCES OF THE SEEDED POLYMERIZATION MECHANISM

The ordered aggregation of A $\beta$  follows a nucleation-dependent pathway, which means that both protein concentration and time are important in predicting their aggregation state. Since the "intrinsic" critical concentration of A $\beta$ , measured *in vitro*, is *ca.* three to four orders of magnitude greater than the average brain concentration, a local supersaturation mechanism must exist in order for the A $\beta$  nucleus to form and grow. The factor responsible for the local supersaturation event may be unique to AD (e.g. overexpression of an abnormal proteoglycan).<sup>51</sup> However, the prevalence of sporadic AD which has no relationship to known genetic abnormalities suggests that concentration can also be the result of a process to which the protein is normally exposed. It is possible that A $\beta$  is normally exposed, for times too short to allow nucleation, to a local concentration exceeding its critical concentration. A slight increase in the local concentration of A $\beta$  during that time could result in immediate intracellular aggregation. This scenario may explain the early age of AD onset in Down syndrome patients who overproduce A $\beta$ . At least two other variables that are unique characteristics of the nucleation-dependent mechanism may play a role *in vivo*. First, since kinetic solubility is, by definition, metastable, the *time* during which the protein is locally concentrated is critical (Figure 1.6). Dilution of protein before nucleus formation ( $t < \text{lag time}$ , Figure 1.6, arrow A) may reflect the normal course of events. However, dilution of A $\beta$  after nucleation ( $t > \text{lag time}$ , Figure 1.6, arrow B) will result in the release of fibrillar material. Although fibrillar A $\beta$  will be far below its critical concentration, the slowness of disaggregation may allow the fibril to be irreversibly trapped, or "fixed", leading to its deposition in amyloid plaque.

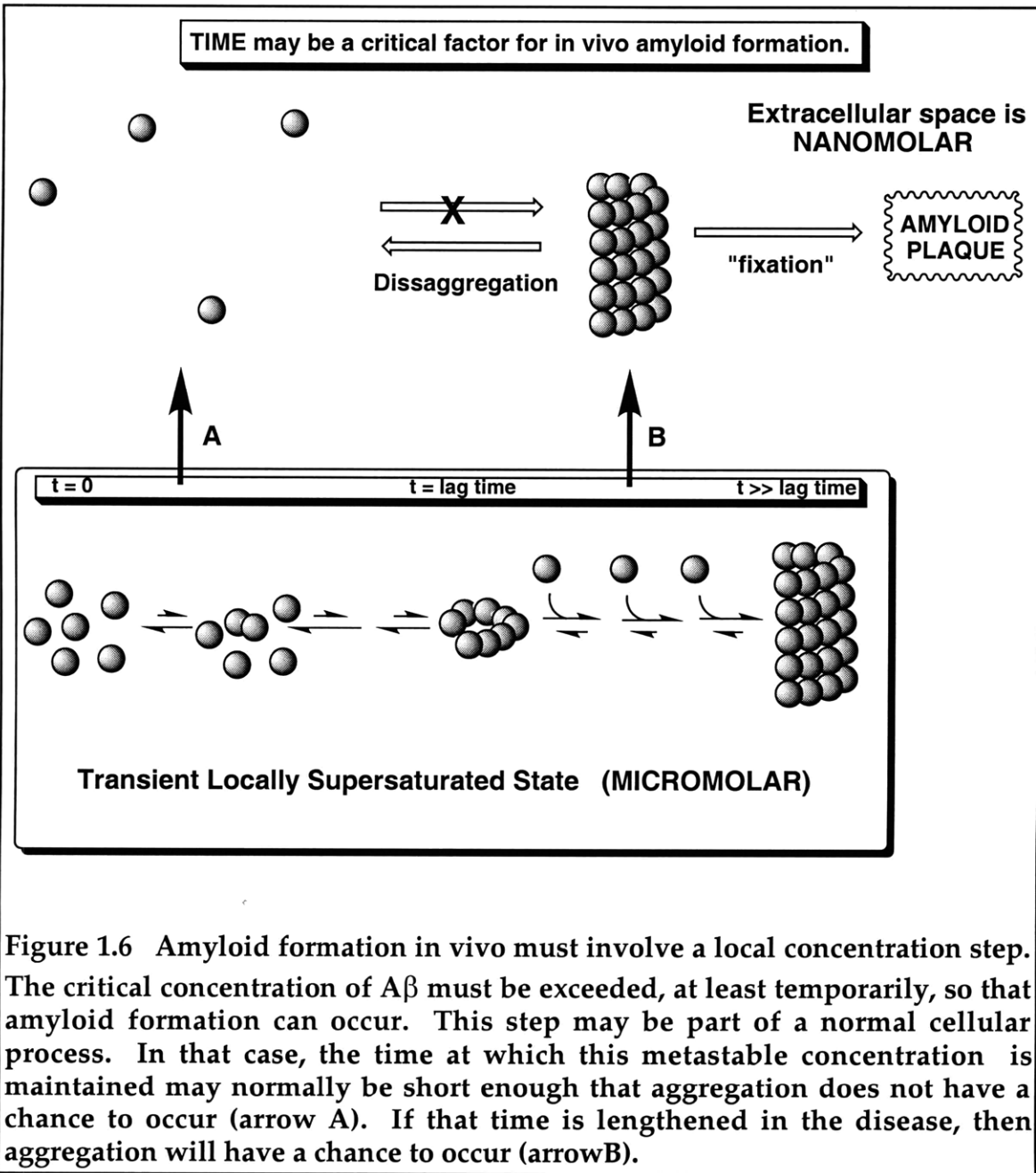
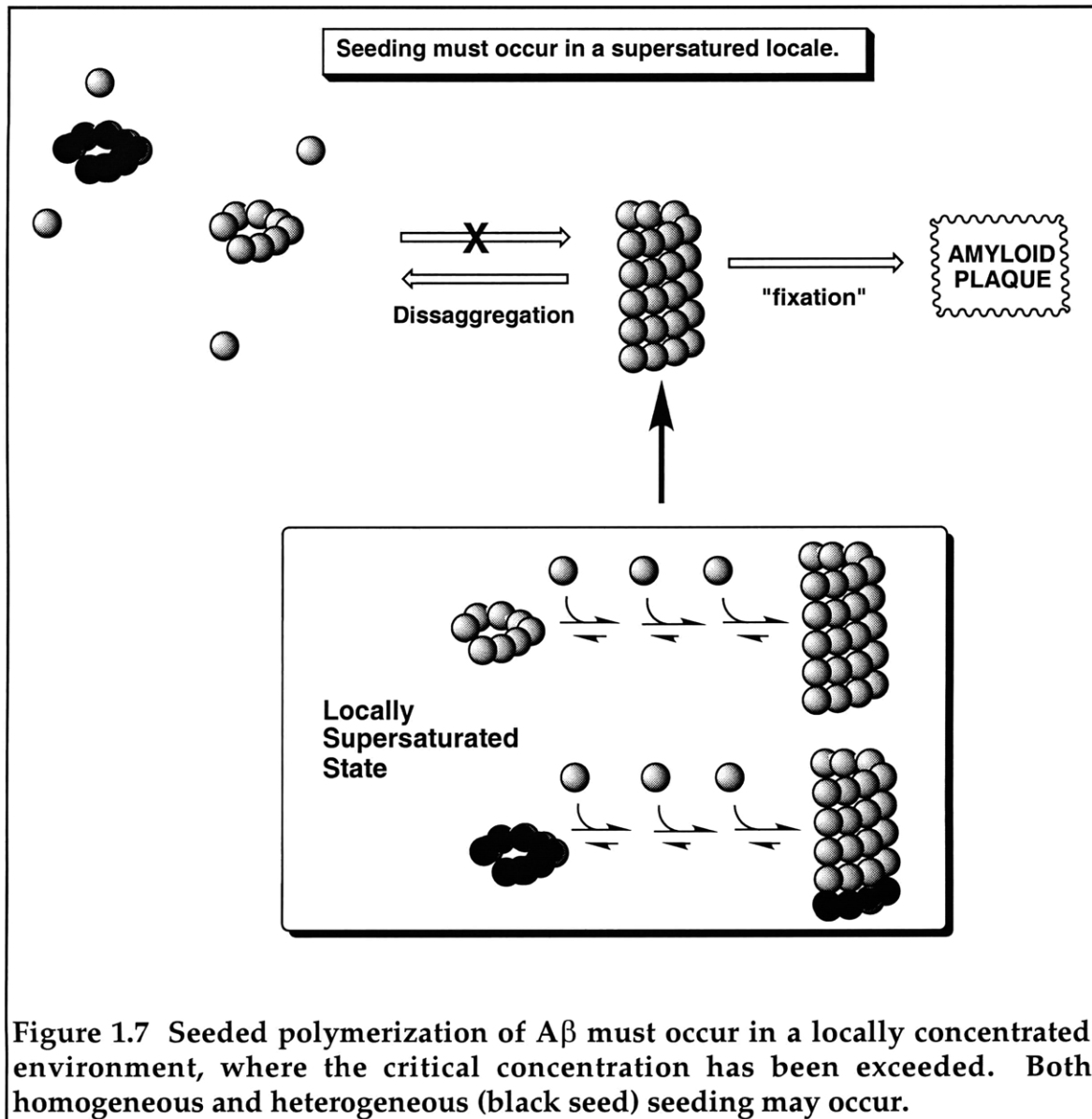


Figure 1.6 Amyloid formation in vivo must involve a local concentration step. The critical concentration of  $A\beta$  must be exceeded, at least temporarily, so that amyloid formation can occur. This step may be part of a normal cellular process. In that case, the time at which this metastable concentration is maintained may normally be short enough that aggregation does not have a chance to occur (arrow A). If that time is lengthened in the disease, then aggregation will have a chance to occur (arrow B).

Clearly, endogenous molecules could be very important in slowing disaggregation, accelerating fixation, or both. It is also critical to identify the mechanism of local supersaturation (compartmentalization, surface-binding, etc) that allows nucleation to occur. Once this mechanism has been identified, it will be critical to study the factors which control the duration of local



supersaturation. It is not difficult to imagine that some of these factors (e.g. protein trafficking time) may be sensitive to age, the strongest risk factor for AD.



**Figure 1.7 Seeded polymerization of A $\beta$  must occur in a locally concentrated environment, where the critical concentration has been exceeded. Both homogeneous and heterogeneous (black seed) seeding may occur.**

Another feature of the nucleation-dependent mechanistic model which may have physiological consequences, is the seeding of a locally supersaturated solution to induce immediate aggregation (Figure 1.7). Seeded growth can only occur in the locally concentrated state. In the case of A $\beta$  aggregation in AD,

NAC fibrils could also induce polymerization of A $\beta$ 1-40 by heterogeneous seeding.<sup>70</sup>

Despite our relative ignorance, the general features of the nucleation dependent mechanism offer insights into the *in vivo* amyloid formation process. However, much work remains to be done in order to completely characterize the molecular mechanism of ordered A $\beta$  aggregation *in vitro*. The structural and morphological features of the aggregates are only beginning to be probed in detail.<sup>21,38,71</sup> In addition, the operationally soluble oligomeric species have been detected using analytical ultracentrifugation<sup>37</sup> and QLS.<sup>49</sup> The simplest form of the nucleation dependent model does not predict the presence of significant amounts of oligomeric A $\beta$  preceding fibril formation, and so the detection of these species suggests that the actual pathway to fibril formation may be considerably more complex. Furthermore, most of the methods that have previously been used to follow the kinetics of amyloid formation are not capable of adequately addressing the potential role that these species may play as intermediates in amyloid fibril formation. The work that will be described in the remainder of this thesis has been inspired by these indications of additional complexity and has focussed on developing and applying new AFM methodologies to test and refine the nucleation dependent model for amyloid formation reviewed in this chapter.

## References for Chapter 1

1. Selkoe, D. The Molecular Pathology of Alzheimer's Disease. *Neuron* **1991**, 6, 487-498.
2. Kosik, K.S. The Alzheimer's Disease Sphinx: A Riddle with Plaques and Tangles. *J. Cell. Biol.* **1994**, 127, 1501-1504.
3. Selkoe, D. Deciphering Alzheimer's Disease: Molecular Genetics and Cell Biology Yield Major Clues. *J. NIH. Research.* **1995**, 7, 57-64.
4. Schellenberg, G.D. Genetic Dissection of Alzheimer Disease, a Heterogeneous Disorder. *Proc. Nat. Acad. Sci. USA* **1995**, 92, 8552-8559.
5. Lansbury, P.T., Jr. A Reductionist view of alzheimer's disease. *Acc. Chem. Res.* **1996**, 29, 317-321.
6. Yankner, B.A. Mechanisms of neuronal degeneration in Alzheimer's disease. *Neuron* **1996**, 16, 921-32.
7. El Khoury, J., Hickman, S.E., Thomas, C.A., Cao, L., Silverstein, S.C., and Lokie, J.D. Scavenger receptor-mediated adhesion of microglia to  $\beta$ -amyloid fibrils. *Nature* **1996**, 382, 716-719.
8. Selkoe, D.J. Alzheimer's disease: genotypes, phenotypes, and treatments. *Science* **1997**, 275, 630-631.
9. Tomiyama, T., Asano, S., Suwa, Y., Morita, T., Kataoka, K., Mori, H., and Endo, N. Rifampicin prevents the aggregation and neurotoxicity of amyloid beta protein in vitro. *Biochem. Biophys. Res. Commun.* **1994**, 204, 76-83.
10. Tjernberg, L.O., Naslund, J., Lindqvist, F., Johansson, J., Karlstrom, A.R., Thyberg, J., Terenius, L., and Nordstedt, C. Arrest of beta-amyloid fibril formation by a pentapeptide ligand. *J. Biol. Chem.* **1996**, 271, 8545-8548.
11. Wood, S.J., MacKenzie, L., Maleeff, B., Hurle, M.R., and Wetzel, R. Selective inhibition of A-beta fibril formation. *J. Biol. Chem.* **1996**, 271, 4086-4092.
12. Lansbury, P.T. Jr. Inhibition of amyloid formation: a strategy to delay the onset of Alzheimer's disease. *Curr. Opin. Chem. Biol.* **1997**, 1, 260-267.
13. Selkoe, D.J. Amyloid beta-protein and the genetics of Alzheimer's disease. *J. Biol. Chem.* **1996**, 271, 18295-18298.
14. Seubert, P., Vigo-Pelfrey, C., Esch, F., Lee, M., Dovey, H., Davis, D., Sinha, S., Schlossmacher, M., Whaley, J., Swindlehurst, C., McCormack, R., Wolfert, R., Selkoe, D., Lieberburg, I., and Schenk, D. Isolation and quantification of soluble Alzheimer's  $\beta$ -peptide from biological fluids. *Nature* **1992**, 359, 325-327.
15. van Gool, W.A., Kuiper, M.A., Walstra, G.J.M., and Bolhuis, P.A. Concentrations of Amyloid  $\beta$  Protein in Cerebrospinal Fluid of Patients with Alzheimer's Disease. *Ann. Neurol.* **1995**, 37, 277-279.
16. Schneener, D., Eckman, C., Jensen, M., Song, X., Citron, M., Suzuki, N., Bird, T.D., Hardy, J., and Hutton, M. Secreted amyloid  $\beta$ -protein similar to that in the senile plaques of Alzheimer's disease is increased in vivo by the

- presenilin 1 and 2 and APP mutations linked to familial Alzheimer's disease. *Nat. Med.* **1996**, *2*, 864- 870.
17. Lemere, C.A., Lopera, F., Kosik, K.S., Lendon, C.L., Ossa, J., Saido, T.C., Yamaguchi, H., Ruiz, A., Martinez, A., Madrigal, L., Hincapie, L., Arango, J.C., Anthony, D.C., Koo, E.H., Goate, A.M., Selkoe, D.J., and Arango, J.C. The E280A presenilin 1 Alzheimer mutation produces increased A beta 42 deposition and severe cerebellar pathology. *Nat. Med.* **1996**, *2*, 1146-50.
  18. Iwatsubo, T., Odaka, A., Suzuki, N., Mizusawa, H., Nukina, N., and Ihara, Y. Visualization of A $\beta$ 42(43) and A $\beta$ 40 in senile plaques with end-specific A $\beta$  monoclonals: evidence that an initially deposited species is A $\beta$ 42(43). *Neuron* **1994**, *13*, 45-53.
  19. Burdick, D., Soreghan, B., Kwon, M., Kosmoski, J., Knauer, M., Henschen, A., Yates, J., Cotman, C., and Glabe, C. Assembly and Aggregation Properties of Synthetic Alzheimer's A4/ $\beta$  Amyloid Peptide Analogs. *J. Biol. Chem.* **1992**, *267*, 546-554.
  20. Hilbich, C., Kisters-Woike, B., Reed, J., Masters, C.L., and Beyreuther, K. Aggregation and Secondary Structure of Synthetic Amyloid  $\beta$ A4 Peptides of Alzheimer's Disease. *J. Mol. Biol.* **1991**, *218*, 149-163.
  21. Lansbury, P.T., Jr. In Pursuit of the Molecular Structure of Amyloid Plaque: New Technology Provides Unexpected and Critical Information. *Biochemistry* **1992**, *31*, 6865-6870.
  22. Lansbury, P.T., Jr., Costa, P.R., Griffiths, J.M., Simon, E.J., Auger, M., Halverson, K.J., Kocisko, D.A., Hendsch, Z.S., Ashburn, T.T., Spencer, R.G., and et al. Structural model for the beta-amyloid fibril based on interstrand alignment of an antiparallel-sheet comprising a C-terminal peptide. *Nat. Struct. Biol.* **1995**, *2*, 990-998.
  23. Evans, K.C., Berger, E.P., Cho, C.-G., Weisgraber, K.H., and Lansbury, P.T., Jr. Apolipoprotein E is a kinetic, but not a thermodynamic inhibitor of amyloid formation: Implications for the pathogenesis and treatment of Alzheimer's disease. *Proc. Natl. Acad. Sci. USA* **1995**, *92*, 763-767.
  24. Naiki, H., Gejyo, F., and Nakakuki, K. Concentration-dependent inhibitory effects of apolipoprotein E on Alzheimer's beta-amyloid fibril formation in vitro. *Biochemistry* **1997**, *36*, 6243-50.
  25. Sanan, D.A., Weisgraber, K.H., Russell, S.J., Mahley, R.W., Huang, D., Saunders, A., Schmechel, D., Wisniewski, T., Frangione, B., Roses, A.D., and Strittmatter, W.J. Apolipoprotein E associates with amyloid b peptide of Alzheimer's disease to form novel monofibrils. *J. Clin. Invest.* **1994**, *94*, 860-869.
  26. Ma, J., Yee, A., Brewer, H.B., Das, S., and Potter, H. Amyloid-associated proteins a antichymotrypsin and apolipoprotein E promote assembly of Alzheimer b protein into filaments. *Nature* **1994**, *372*, 92-94.
  27. Jarrett, J.T., Berger, E.P., and Lansbury, P.T., Jr. The Carboxy Terminus of  $\beta$  Amyloid Protein is Critical for the Seeding of Amyloid Formation: Implications for the Pathogenesis of Alzheimer's Disease. *Biochemistry* **1993**, *32*, 4693-4697.

28. Blow, D.M., Chayen, N.E., Lloyd, L.F., and Saridakis, E. Control of Nucleation of Protein Crystals. *Prot. Sci.* **1994**, 3, 1638-1643.
29. Prevelige, P.E., Jr., Thomas, D., and King, J. Scaffolding protein regulates the polymerization of P22 coat subunits into icosahedral shells in vitro. *J. Mol. Biol.* **1988**, 202, 743-757.
30. Mitchison, T. and Kirschner, M. Microtubule assembly is nucleated by isolated centrosomes. *Nature* **1984**, 312, 232-236.
31. Asakura, L. Polymerization of flagellin and polymorphism of flagella. *Adv. Biophys.* **1970**, 1, 99-155.
32. Eaton, W.A. and Hofrichter, J. The biophysics of sickle cell hydroxyurea therapy. *Science* **1995**, 268, 1142-1143.
33. Andreu, J.M. and Timasheff, S.N. The measurement of cooperative protein self-assembly by turbidity and other techniques. *Meth. Enzymol.* **1986**, 130, 47-59.
34. Jarrett, J.T. and Lansbury, P.T., Jr. Seeding the "One-Dimensional Crystallization" of Amyloid: a Pathogenic Mechanism in Alzheimer's Disease and Scrapie? *Cell* **1993**, 73, 1055-1058.
35. Naiki, H. and Nakakuki, K. First-order kinetic model of Alzheimer's  $\beta$ -amyloid fibril extension *in vitro*. *Lab. Invest.* **1996**, 74, 374-383.
36. Jarrett, J.T., Costa, P.R., Griffin, R.G., and Lansbury, P.T., Jr. Models of the  $\beta$  protein C-terminus: Differences in amyloid structure may lead to segregation of "long" and "short" fibrils. *J. Am. Chem. Soc.* **1994**, 116, 9741-9742.
37. Snyder, S.W., Lardor, U.S., S., W.W., Wang, G.T., Barrett, L.W., Matayoshi, E.D., Huffaker, H.J., Krafft, G.A., and Holzman, T.F. Amyloid- $\beta$  aggregation: selective inhibition of aggregation in mixtures of amyloid with different chain lengths. *Biophys. J.* **1994**, 67, 1216-1228.
38. Wood, S.J., Maleeff, B., Hart, T., and Wetzel, R. Physical, morphological and functional differences between pH 5.8 and 7.4 aggregates of the Alzheimer's amyloid peptide A-beta. *J. Mol. Biol.* **1996**, 256, 870-877.
39. Pike, C.J., Overman, M.J., and Cotman, C.W. Amino-terminal deletions enhance aggregation of beta-amyloid peptides in vitro. *J. Biol. Chem.* **1995**, 270, 23895-23898.
40. Jarrett, J.T., Berger, E.P., and Lansbury, P.T., Jr. The C-terminus of the beta protein is critical in amyloidogenesis. *Ann. NY. Acad. Sci.* **1993**, 695, 144-148.
41. Seelig, J., Lehrmann, R., and Terzi, E. Domain formation induced by lipid-ion and lipid-peptide interactions. *Mol. Membr. Biol.* **1995**, 12, 51-57.
42. Hendrix, J.C., Halverson, K.J., and Lansbury, P.T., Jr. A Convergent Synthesis of the Amyloid Protein of Alzheimer's Disease. *J. Am. Chem. Soc.* **1992**, 114, 7930-7931.
43. Barrow, C.J., Yasuda, A., Kenny, P.T.M., and Zagorski, M.G. Solution Conformations and Aggregational Properties of Synthetic Amyloid  $\beta$ -peptides of Alzheimer's Disease. Analysis of Circular Dichroism Spectra. *J. Mol. Biol.* **1992**, 225, 1075-1093.

44. Weinreb, P.H., Zhen, W., Poon, A.W., Conway, K.A., and Lansbury, P.T., Jr. NACP, a protein implicated in Alzheimer's disease and learning, is natively unfolded. *Biochemistry* **1996**, 35, 13709-13715.
45. Soreghan, B., Kosmoski, J., and Glabe, C. Surfactant Properties of Alzheimer's A $\beta$  Peptides and the Mechanism of Amyloid Aggregation. *J. Biol. Chem.* **1994**, 269, 28551-28554.
46. Janciauskiene, S., Garcia de Frutos, P., Carlemalm, E., Dahlback, B., and Eriksson, S. Inhibition of Alzheimer beta-peptide fibril formation by serum amyloid P component. *J. Biol. Chem.* **1995**, 270, 26041-26044.
47. Terzi, E., Holzemann, G., and Seelig, J. Self-association of beta-amyloid peptide (1-40) in solution and binding to lipid membranes. *J. Mol. Biol.* **1995**, 252, 633-642.
48. Chan, W., Fornwald, J., Brawner, M., and Wetzel, R. Native complex formation between apolipoprotein E isoforms and the Alzheimer's Disease Peptide A $\beta$ . *Biochemistry* **1996**, 35, 7123-7130.
49. Lomakin, A., Chung, D.S., Benedek, G.B., Kirschner, D.A., and Teplow, D.B. On the nucleation and growth of amyloid beta-protein fibrils: detection of nuclei and quantitation of rate constants. *Proc. Natl. Acad. Sci. USA* **1996**, 93, 1125-1129.
50. Nitsch, R.M., Rebeck, G.W., Deng, M., Richardson, I., Tennis, M., Schenk, D.B., Vigo-Pelfrey, C., Lieberberg, I., Wurtman, R.J., Hyman, B.T., and Growdon, J.H. Cerebrospinal fluid levels of amyloid beta-protein in alzheimer's disease: Inverse correlation with weverity of dementia and effect of apolipoprotein E genotype. *Ann. Neurol.* **1995**, 37, 512-518.
51. Snow, A.D. and Wight, T.N. Proteoglycans in the pathogenesis of Alzheimer's disease and other amyloidoses. *Neurobiology of Aging* **1989**, 10, 481-497.
52. Barrow, C.J. and Zagorski, M.G. Solution Structures of  $\beta$ -Peptide and Its Constituent Fragments: Relation to Amyloid Deposition. *Science* **1991**, 253, 179-182.
53. Inestrosa, N.C., Alvarez, A., Perez, C.A., Moreno, R.D., Vicente, M., Linker, C., Casanueva, O.I., Soto, C., and Garrido, J. Acetylcholinesterase accelerates assembly of amyloid-beta-peptides into Alzheimer's fibrils: Possible role of the peripheral site of the enzyme. *Neuron* **1996**, 16, 881-891.
54. Bush, A.I., Pettingell, W.H., Multhap, G., Paradis, M.D., Vonsattel, J.-P., Gusella, J.F., Betreuther, K., Masters, C.L., and Tanzi, R.E. Rapid induction of Alzheimer A $\beta$  amyloid formation by zinc. *Science* **1994**, 265, 1464-1467.
55. Mantyh, P.W., Ghilardi, J.R., Rogers, S., DeMaster, E., Allen, C.J., Stimson, E.R., and Maggio, J.E. Aluminum, Iron and Zinc Ions Promote Aggregation of Physiological Concentrations of  $\beta$ -Amyloid Peptide. *J. Neurochem.* **1993**, 61, 1171-1174.
56. Solomon, B., Koppel, R., Hanan, E., and Katzav, T. Monoclonal antibodies inhibit *in vitro* fibrillar aggregation of the Alzheimer  $\beta$ -amyloid peptide. *Proc. Natl. Acad. Sci. USA* **1996**, 93, 452-455.

57. Cao, Z. and Ferrone, F.A. A 50th order reaction predicted and observed for sickle hemoglobin nucleation. *J. Mol. Biol.* **1996**, 256, 219-222.
58. Ferrone, F.A., Hofrichter, J., and Eaton, W.A. Kinetics of sickle Hemoglobin polymerization. II. A double nucleation mechanism. *J. Mol. Biol.* **1985**, 183, 611-631.
59. Corder, E.H., Saunders, A.M., Strittmatter, W.J., Schmechel, D.E., Gaskell, P.C., Small, G.W., Roses, A.D., Haines, J.L., and Pericak-Vance, M.A. Gene Dose of Apolipoprotein E Type 4 Allele and the Risk of Alzheimer's Disease in Late Onset Families. *Science* **1993**, 261, 921-923.
60. Schmechel, D.E., Saunders, A.M., Strittmatter, W.J., Crain, B.J., Hulette, C.M., Joo, S.H., Pericak-Vance, M.A., Goldgaber, D., and Roses, A.D. Increased amyloid  $\beta$ -peptide deposition in cerebral cortex as a consequence of apolipoprotein E genotype in late-onset Alzheimer disease. *Proc. Natl. Acad. Sci. USA* **1993**, 90, 9649-9653.
61. Wood, S.J., Chan, W., and Wetzel, R. An ApoE-A $\beta$  inhibition complex in A $\beta$  fibril extension. *Chem. Biol.* **1996**, 3, 949-56.
62. Wood, S.J., Chan, W., and Wetzel, R. Seeding of A $\beta$  fibril formation is inhibited by all three isotypes of apolipoprotein E. *Biochemistry* **1996**, 35, 12623-12628.
63. Whitson, J.S., Mims, M.P., Strittmatter, W.J., Yamaki, T., Morrisett, J.D., and Appel, S.H. Attenuation of the neurotoxic effect of A $\beta$  amyloid peptide by apolipoprotein E. *Biochem. Biophys. Res. Commun.* **1994**, 199, 163-170.
64. Ohman, T., Dang, N., LeBoeuf, R.C., Furlong, C.E., and Fukuchi, K. Expression of apolipoprotein E inhibits aggregation of the C-terminal fragments of beta-amyloid precursor protein. *Neurosci. Lett.* **1996**, 210, 65-68.
65. Hyman, B.T., West, H.L., Rebeck, G.W., Buldyrev, S.V., Mantegna, R.N., Ukleja, M., Havlin, S., and Stanley, H.E. Quantitative analysis of senile plaques in Alzheimer's disease: Observation of log-normal distribution and molecular epidemiology of differences associated with apolipoprotein E genotype and trisomy 21 (Down syndrome). *Proc. Nat. Acad. Sci. USA* **1995**, 92, 3586-3590.
66. Esler, W.P., Stimson, E.R., Ghilardi, J.R., Vinters, H.V., Lee, J.P., Mantyh, P.W., and Maggio, J.E. In vitro growth of Alzheimer's disease beta-amyloid plaques displays first-order kinetics. *Biochemistry* **1996**, 35, .
67. Esler, W.P., Stimson, E.R., Ghilardi, J.R., Felix, A.M., Lu, Y.A., Vinters, H.V., Mantyh, P.W., and Maggio, J.E. A  $\beta$  deposition inhibitor screen using synthetic amyloid. *Nat. Biotechnol.* **1997**, 15, 258-63.
68. Jarrett, J.T. and Lansbury, P.T., Jr. Amyloid Fibril Formation Requires a Chemically Discriminating Nucleation Event: Studies of an Amyloidogenic Sequence from the Bacterial Protein OsmB. *Biochemistry* **1992**, 31, 12345-12352.
69. Ueda, K., Fukushima, H., Masliah, E., Xia, Y., Iwai, A., Yoshimoto, M., Otero, D.A.C., Kondo, J., Ihara, Y., and Saitoh, T. Molecular cloning of

- cDNA encoding an unrecognized component of amyloid in Alzheimer disease. *Proc. Natl. Acad. Sci. USA* **1993**, 90, 11282-11286.
70. Han, H., Weinreb, P.H., and Lansbury, P.T. The core Alzheimer's peptide NAC forms amyloid fibrils which seed and are seeded by  $\beta$ -amyloid: is NAC a common trigger or target in neurodegenerative disease? *Chem. Biol.* **1995**, 2, 163-169.
  71. Stine, W.B., Jr., Snyder, S.W., Lador, U.S., Wade, W.S., Miller, M.F., Perun, T.J., Holzman, T.F., and Krafft, G.A. The nanometer-scale structure of amyloid-beta visualized by atomic force microscopy. *J. Prot. Chem.* **1996**, 15, 193-203.
  72. Roher, A.E., Chaney, M.O., Kuo, Y.-M., Webster, S.D., Stine, W.B., Haverkamp, L.J., Woods, A.S., Cotter, R.J., Tuohy, J.M., Krafft, G.A., Bonnell, B.S., and Emmerling, M.R. Morphology and toxicity of A $\beta$ -(1-42) dimer derived from neuritic and vascular amyloid deposits of Alzheimer's disease. *J. Biol. Chem.* **1996**, 271, 20631-20635.
  73. Berne, B.J. Interpretation of the light scattering from long rods. *J. Mol. Biol.* **1974**, 89, 755-758.
  74. Esler, W.P., Stimson, E.R., Jennings, J.M., Ghilardi, J.R., Mantyh, P.W., and Maggio, J.E. Zinc-induced aggregation of human and rat beta-amyloid peptides in vitro. *J. Neurochem.* **1996**, 66, 723-732.
  75. Klunk, W.E., Pettegrew, J.W., and Abraham, D.J. Two simple methods for quantifying low-affinity dye-substrate binding. *J. Histochem. Cytochem.* **1989**, 37, 1293-1297.
  76. Naiki, H., Higuchi, K., Hosokawa, M., and Takeda, T. Fluorometric determination of amyloid fibrils in vitro using the fluorescent dye, thioflavin T1. *Anal. Biochem.* **1989**, 177, 244-249.
  77. LeVine, H.I. Thioflavine T interaction with synthetic Alzheimer's disease  $\beta$ -amyloid peptides: detection of amyloid aggregation in solution. *Prot. Sci.* **1993**, 2, 404-410.
  78. Levine, H.r. Soluble multimeric Alzheimer beta(1-40) pre-amyloid complexes in dilute solution. *Neurobiol. Aging* **1995**, 16, 755-64.
  79. Shen, C.L., Scott, G.L., F., M., and Murphy, R.M. Light scattering analysis of fibril growth from the amino-terminal fragment beta(1-28) of beta amyloid peptide. *Biophys. J.* **1993**, 65, 2383-2395.
  80. Shen, C.L., Fitzgerald, M.C., and Murphy, R.M. Effect of acid predissolution on fibril size and flexibility of synthetic beta-amyloid peptide. *Biophys. J.* **1994**, 67, 1238-1246.
  81. Shen, C.L. and Murphy, R.M. Solvent effects on self-assembly of beta-amyloid peptide. *Biophys. J.* **1995**, 69, 640-651.
  82. Tomski, S.J. and Murphy, R.M. Kinetics of Aggregation of Synthetic  $\beta$ -Amyloid Peptide. *Arch. Biochem. Biophys.* **1992**, 294, 630-638.
  83. Wong, S.S., Harper, J.D., Lansbury, P.T.J., and Lieber, C.M. Carbon nanotubes tips: High resolution probes for imaging biological systems. *J. Am. Chem. Soc.* **1998**, 120, 603-604.



84. Ferrone, F.A., Hofrichter, J., and Eaton, W.A. Kinetics of sickle hemoglobin polymerization. I. Studies using temperature-jump and laser photolysis techniques. *J. Mol. Biol.* **1985**, 183, 591-610.
85. Ferrone, F.A., Hofrichter, J., and Eaton, W.A. Kinetics of sickle hemoglobin polymerization. III. Nucleation rates determined from stochastic fluctuations in polymerization progress curves. *J. Mol. Biol.* **1986**, 189, 553-571.
86. Ferrone, F.A. Kinetic models and the pathophysiology of sickle cell disease. *Ann. NY. Acad. Sci.* **1989**, 565, 63-74.

## Chapter 2

### **Observation and Characterization of Transiently Populated Oligomeric Intermediates in A $\beta$ Fibril Formation**

The presence of amyloid fibrils, ordered protein aggregates comprising A $\beta$  protein variants, in the brain is a defining feature of AD. Because it is very difficult to reconstruct the *in vivo* pathway based on neuropathological data, our lab studies the *in vitro* mechanism of A $\beta$  amyloid formation on the assumption that it may be analogous to the situation in AD. These initial *in vitro* studies led to a mechanistic model of amyloid formation as a nucleation-dependent polymerization that offers a plausible explanation for FAD.<sup>1-3</sup> However, details of the early steps in the *in vitro* mechanism have proved elusive because the methods most commonly used to measure the time course of amyloid formation (turbidometry, sedimentation, CR binding and thioT fluorescence) share two significant limitations. First, these methods do not distinguish between or detect all aggregate morphologies, so a single product morphology has been tacitly assumed. Second, these methods are unable to detect small A $\beta$  oligomers, so the early steps of the assembly process have not been elucidated.

We sought a method which would allow us to observe and characterize any small A $\beta$  species that might be present during the early stages of aggregation prior to fibril formation. AFM appeared to have the potential to provide this information since it is capable of directly detecting *and* measuring with nanometer scale resolution the dimensions of small proteinaceous species that are adsorbed from aqueous media.<sup>4,5</sup> Previous studies have demonstrated the ability of AFM to distinguish multiple A $\beta$  fibril morphologies and suggest that fibril formation follows a more complex pathway than previously thought.<sup>6-9</sup> By using less destructive AFM imaging modes<sup>4</sup> and carefully examining the time

course for the formation of these morphologies, we believed that it would be possible to improve the morphological characterization of these species and establish their temporal relationship. This additional information is necessary to begin to elucidate the molecular events that occur during A $\beta$  fibril formation.

In the experiments described in this chapter we used AFM to follow the aggregation of the two predominant A $\beta$  variants at concentrations slightly in excess of the critical concentration for amyloid formation (we used [A $\beta$ 1-40] = 45-50  $\mu$ M, compared to reported critical concentrations (solubilities) of A $\beta$ 1-40 of ca. 10-40  $\mu$ M (35  $\mu$ M,<sup>10,11</sup> 6-9  $\mu$ M,<sup>1</sup> and 10  $\mu$ M (in 1 M urea)<sup>12</sup>; and we used [A $\beta$ 1-42] = 20  $\mu$ M, compared to reported critical concentrations of A $\beta$ 1-42 of ca 2-15  $\mu$ M<sup>1,13</sup>. These concentrations were selected on the grounds that these conditions should approximate as closely as possible the *in vivo* amyloid formation in most types of AD and should result in the slowest time courses for *in vitro* fibril formation. Maximizing the time prior to the nucleation should also maximize the opportunity to observe potential pre-nucleation intermediate species.

For both A $\beta$ 1-40 and A $\beta$ 1-42, the first-formed species were not the amyloid fibrils. Instead, much smaller oligomeric species were observed, including an elongated, apparently structured, morphology with constant diameter. These elongated features gradually increased in length with time (rarely exceeding 200 nm in length), then they rapidly disappeared in favor of typical amyloid fibrils (usually > 1  $\mu$ M in length). We refer to this transiently observed species as the A $\beta$  amyloid protofibril, to indicate the possibility that it represents a fibril assembly intermediate. The overall process was much more rapid in the case of the 42 amino-acid variant A $\beta$ 1-42 when compared with the truncated variant A $\beta$ 1-40 consistent with the fact that increased expression of the former variant is associated with early-onset AD.

## **Atomic force microscopy**

*AFM is a physical imaging technique.*

Atomic force microscopy (AFM) creates images of surfaces by measuring the position of a sensitive cantilever with a silicon probe tip as a sample is moved underneath (Figure 2.1). The AFM can be operated in several modes, with the most common modes being the contact mode and the tapping mode. In the contact mode (the first AFM imaging mode developed), the tip remains in constant contact with the surface during a scan. This works very well for hard surfaces, which resist compression and damage due to lateral shear forces generated by the sweeping motion of the tip. However, biomolecules adsorbed to substrates for imaging do not always withstand these forces well and can be deformed or swept off the surface in this mode of operation. In the tapping mode, the cantilever is oscillated at its resonant frequency (60-400 kHz depending on the cantilever) and positioned above the sample so that it contacts the surface briefly at the bottom of its swing. The time the tip contacts the surface is very short when compared to the time required to trace across the surface. As a result, shear forces are almost completely eliminated making this mode of imaging better suited for imaging biomolecules.

In all imaging modes, the position of the sample under the tip is precisely controlled by a piezoelectric ceramic-based scanner which can reposition the sample under the tip in three dimensions in angstrom scale increments. Keeping track of the movements required to raster the sample underneath the tip while maintaining a constant deflection (contact mode) or oscillation amplitude (tapping mode) at each position in the region results in an digitized topograph of the surface. Visual representations of this data can then be generated by assigning each point in the area a color or brightness based on its relative height.

For images in this thesis, the smooth surface of the mica substrate will appear dark gray with the brightness of the adsorbed features increasing as a function of their height.

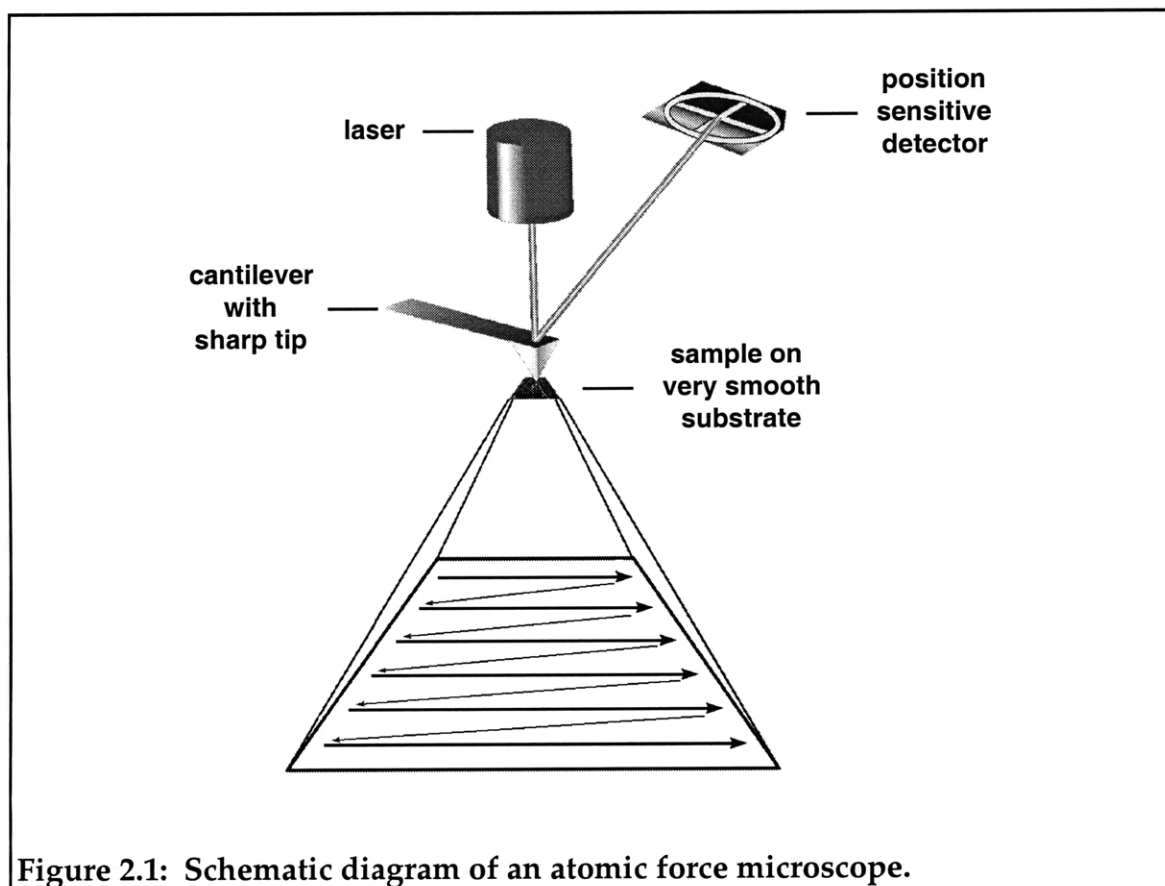


**Figure 2.1: Schematic diagram of an atomic force microscope.**

*Interpretation of lateral dimensions.*

The resulting topographical data for the area can also be used to obtain 3 dimensional measurements of adsorbed features with a high degree of precision, but it is important to consider several limitations which arise as a result of the physical nature of the technique when discussing dimensions measured by AFM. In general, the height of an object above the surface can be determined, but the lateral dimension in the plane of the image (the width) is difficult to measure accurately, due to the shape and the finite size of the tip(Figure 2.2). The

overestimation of width is related to the height and true width of the feature and the shape of the 5 - 10 nm diameter silicon tip, which is difficult to accurately determine.<sup>4</sup> Consequently, we use measurements of the height rather than the width as estimates of the diameters of A $\beta$  aggregate species, although the cross-section may not be circular or square (see discussion of morphologies below).

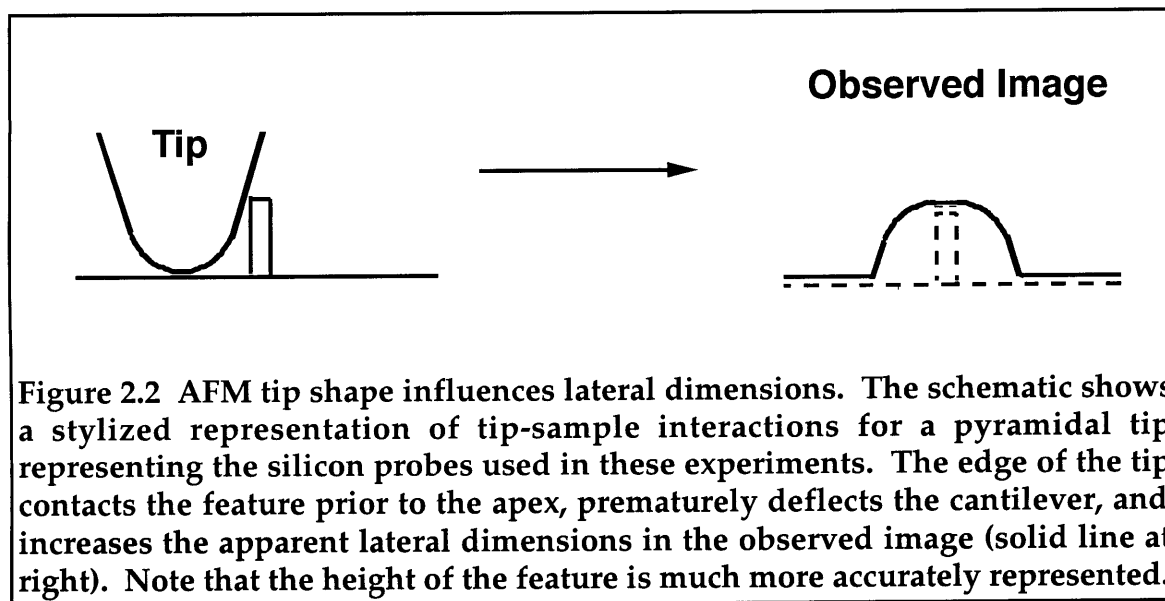


**Figure 2.2 AFM tip shape influences lateral dimensions. The schematic shows a stylized representation of tip-sample interactions for a pyramidal tip representing the silicon probes used in these experiments. The edge of the tip contacts the feature prior to the apex, prematurely deflects the cantilever, and increases the apparent lateral dimensions in the observed image (solid line at right). Note that the height of the feature is much more accurately represented.**

#### *Interpretation of height measurements.*

There are a number of reasons why the height of features measured by AFM in air may underestimate the actual diameters of features as they exist in solution:<sup>5</sup> 1) The force applied by the cantilever may compress soft biological features. 2) Dehydration of the protein following the removal of buffer prior to imaging could reduce measured dimensions. 3) Height measurements may be reduced if features deform during the adsorption process to maximize the surface area of contact to the substrate (similar to the deformation that results when a spherical water droplet adheres to a surface). Differences in cantilevers, tips, instrument parameters, and/or sample preparation conditions can result in variability in the measured dimensions of the same species in different scans.

Therefore, comparisons of height between morphologies are made, when possible, from single images clearly resolving both species. This is done to ensure that variability in measurements among scans does not cause the relative dimensions of morphologies to be misrepresented. When this is not possible the diameter of a distinct morphology present with each species is used as a reference to allow comparisons of their relative heights to be made with more confidence (for example, protofibrils are generally not observed in the same specimen with type 2 fibrils, but standardization of their diameters relative to type 1 fibrils commonly present alongside each species can be used to compare their heights).

#### *Specimen preparation.*

To prepare specimens for imaging, aliquots of protein solutions/suspensions are applied to the atomically smooth surface of freshly cleaved mica and allowed to incubate (typically for 30 seconds to several minutes). Following incubation, excess protein and buffer salts are rinsed away with water and the material that remains bound to the mica surface is analyzed by AFM. Because all aggregate species may not be equally well adsorbed, it is not possible to quantitate the relative amounts of species present in solution based on their abundance on the mica substrate, nor is it possible to rule out the existence of additional species that might be very poorly adsorbed. There is little reason to suspect, however, that the ability of a species to adsorb will change with time. Therefore, the relative amounts of a species observed (using the same specimen preparation) at each time point during an experiment should provide reliable qualitative information about the changes in abundance of a particular morphology during the course of aggregation.

## Evolution of aggregated species observed by AFM

*A $\beta$ 1-40 rapidly formed discrete protofibrils.*

We prepared A $\beta$ 1-40 solutions for analysis by AFM using essentially identical conditions to those used previously in this lab for turbidity based investigations of amyloid formation.<sup>11,14</sup> Briefly, concentrated stock solutions of the peptide (in this case A $\beta$ 1-40) were made in DMSO, and aliquots of the stock solution were added to buffer (10 mM Phosphate, 100 mM NaCl, pH 7.4) to achieve the desired final peptide concentration. Solutions were incubated without agitation at room temperature. At the indicated times, each of these A $\beta$ 1-40 solutions were briefly vortexed to evenly suspend any aggregates which may have precipitated before aliquots were removed and placed on a freshly cleaved mica surface. After brief (0.5-2 min.) incubation on the mica surface under ambient conditions, filtered ultrapure water was used to gently rinse away excess protein and buffer salts, and the structural properties of the species adsorbed onto mica were analyzed immediately by AFM.

The top panel of Figure 2.3 shows a representative time course for the aggregation of A $\beta$ 1-40 (45  $\mu$ M). In each image, the mica surface appears dark gray, and the brightness of the features increases as a function of their height. After four days, the adsorbed material consisted mostly of small species with uniform diameters of about 4 nm (the measured heights of features will be referred to as diameters herein, although the cross-section may not be circular or square). There were also a few larger globular features with diameters ranging widely between 13 - 23 nm (larger bright white spots in image). Some of the ~4 nm diameter features at 4 days appeared to be roughly spherical while many others were clearly elongated with lengths between 40-60 nm being the most common. We will refer to these ~ 4 nm diameter species as A $\beta$  amyloid protofibrils (to reflect their early appearance before the observation of



prototypical A $\beta$  amyloid fibrils and the possibility that they represent a fibril assembly intermediate, see below). The protofibrils elongated over three weeks while retaining a constant diameter, commonly reaching lengths of 100 - 200 nm. A parallel incubation with a much higher A $\beta$ 1-40 concentration (200  $\mu$ M) developed protofibrils of comparable length in two days (data not shown, the concentration dependence of protofibril formation will be discussed in more detail in chapter 3). The small size of these protofibrils precludes their observation by turbidity measurements at 400 nm (unless they become associated in large aggregates).

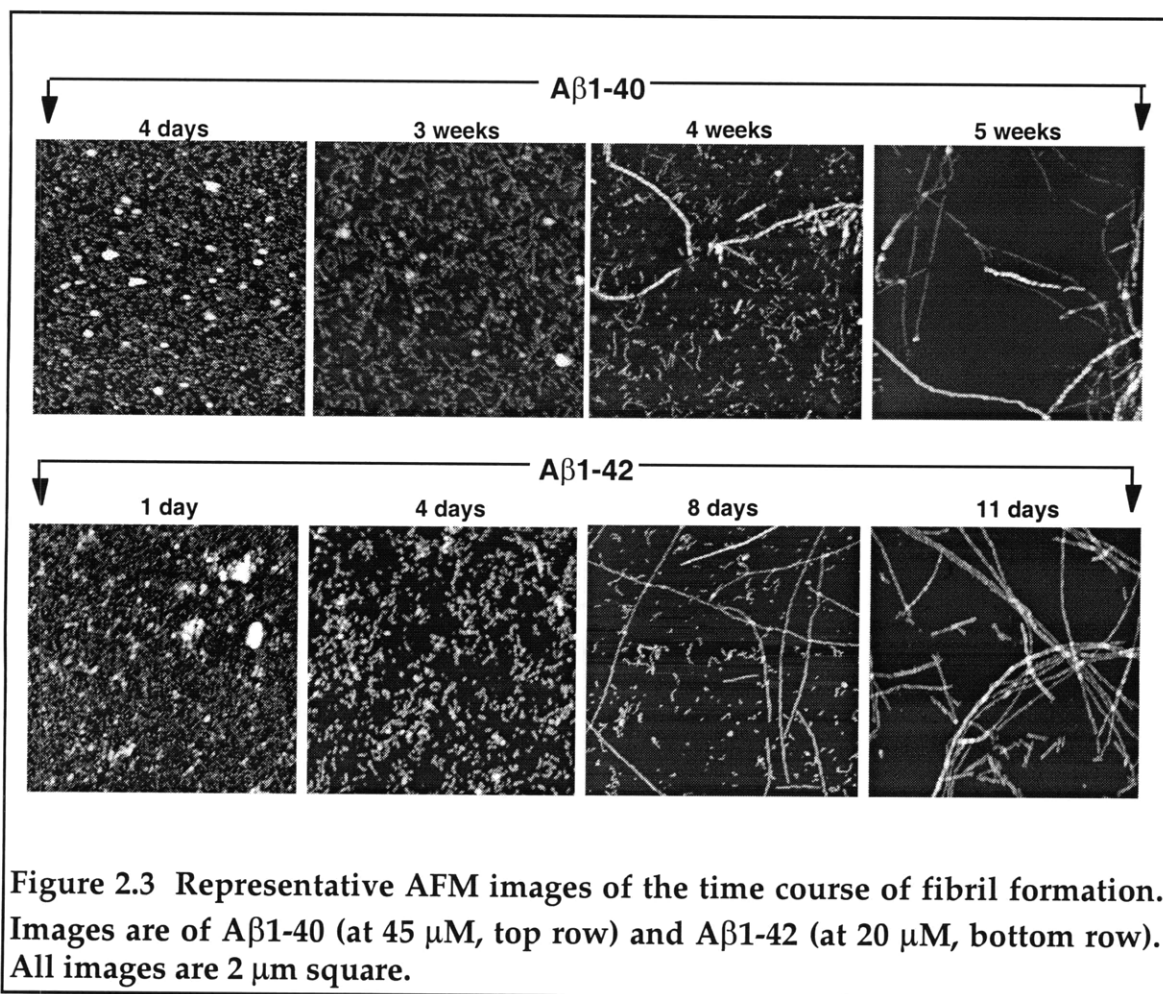


**Figure 2.3** Representative AFM images of the time course of fibril formation. Images are of A $\beta$ 1-40 (at 45  $\mu$ M, top row) and A $\beta$ 1-42 (at 20  $\mu$ M, bottom row). All images are 2  $\mu$ m square.

*Aβ1-40 protofibrils disappeared, concurrent with the appearance of fibrils.*

After four weeks of incubation, the first long (typically > 1 μm) Aβ1-40 species resembling prototypical amyloid fibrils appeared (designated type 1 fibrils since they were the earliest type of fibrils to be observed). Type 1 fibrils had a beaded appearance indicating periodic modulations in height which reached maximum diameters of approximately twice the diameter of the protofibril (detailed measurements below). Strikingly, short (< 500 nm) type 1 fibrils were rarely seen. After five weeks, the protofibrils had disappeared completely and a second fibril type (type 2 fibril) appeared which had a smaller diameter than the type 1 fibril and was characterized by a segmented rather than a beaded appearance.

*Rapid assembly of Aβ1-42.*

Amyloid fibril formation by Aβ1-42 followed a similar, but accelerated, time course (Figure 2.3 bottom) compared to Aβ1-40 producing analogous intermediate species and fibril morphologies. The accelerated time course was observed despite the fact that the Aβ1-42 concentration in these experiments was, as it is *in vivo*,<sup>15</sup> significantly lower (20 μM) than the Aβ1-40 concentration (45 μM). Protofibrils formed within the first day of incubation and elongated over the next eight days. Long (almost always > 1 μm, usually > 5 μm) Aβ1-42 type 1 and type 2 fibrils were detected after 8 days of incubation and all protofibrils had disappeared by 11 days. The observed kinetic differences between Aβ1-42 and Aβ1-40, which are consistent with previous turbidometric studies in this lab,<sup>1</sup> support the proposal that elevated levels of Aβ1-42 lead to more rapid amyloid formation in early-onset familial AD (FAD).<sup>1,16</sup> This scenario has been supported by numerous studies of the levels of Aβ1-42 and Aβ1-40 in the

plasma<sup>15</sup> and brain tissue<sup>17,18</sup> of FAD patients and in the culture media of cells stably transfected with FAD mutant gene products.<sup>19-22</sup>

For both A $\beta$ 1-40 and A $\beta$ 1-42, the transient population of small oligomeric intermediates prior to the appearance of fibrils is clear. Small oligomeric A $\beta$  species have also been separated and/or detected by other methods. Analysis by analytical ultracentrifugation of A $\beta$ 1-40 (450  $\mu$ M) detected a slowly sedimenting species (proposed to contain ~1000 A $\beta$ 1-40 molecules), which was observed in addition to the rapidly sedimenting, probably fibrillar material.<sup>23</sup> Dynamic light scattering of A $\beta$ 1-40 aggregation under acidic conditions detected the rapid formation of an oligomeric A $\beta$ 1-40 species (diameter based on a spherical model = 14 nm), proposed to be a micelle (critical concentration in 0.1N HCl = 100  $\mu$ M).<sup>24</sup> Small globular and elongated species have also been observed previously by AFM, but rather harsh modifications were required to achieve stable contact mode imaging of these features (imaging under isopropanol<sup>6-8</sup> or coating with platinum carbon<sup>9</sup>). The absence of a kinetic component to these AFM experiments left the relevance of these species to fibril formation in aqueous conditions unresolved.

Of particular relevance is the analysis of the initial stages of fibril formation using gel filtration chromatography. Walsh et al. showed that both A $\beta$ 1-40 and A $\beta$ 1-42 (at 220  $\mu$ M) produce slowly sedimenting species that eluted from a size exclusion column with an estimated MW > 100 kDa.<sup>25</sup> Negative stain EM analysis of these high molecular weight fractions revealed curved fibrils 6-8 nm in diameter and < 200 nm in length which they also call protofibrils.<sup>25</sup> The results of Walsh et al. also show that there is a time dependent increase in the amount of material that correlates with the increase in protofibril length with time that we have observed by AFM.<sup>25</sup> Furthermore, the kinetics of protofibril formation and disappearance (observed by the time dependent increase and then

decrease in the magnitude of the protofibril containing peak) also confirm that this species is only transiently populated during fibril formation.<sup>25</sup>

### **Description of aggregate morphologies.**

Images produced during numerous experiments were screened to find well resolved images clearly displaying the morphologies observed during the aggregation of A $\beta$ 1-40. Although aggregation conditions (including time, [A $\beta$ 1-40], temperature) were not always identical for each image chosen, these alterations have not been observed to affect the measured dimensions for A $\beta$ 1-40 aggregate morphologies.

#### *Globular particles*

Well resolved images of A $\beta$ 1-40 samples obtained at early time points regularly show numerous globular features with diameters ranging from ~1 nm to 20 nm or more. These features are more commonly observed at lower concentrations of A $\beta$ 1-40 ( $\leq 50 \mu\text{M}$ ) and become less common as fibril formation proceeds. Figure 2.4 shows a representative image and cross sections of these globular species from a 16  $\mu\text{M}$  solution of A $\beta$ 1-40 2 days after dilution and incubation at RT and from a 45  $\mu\text{M}$  solution 4 days after dilution.

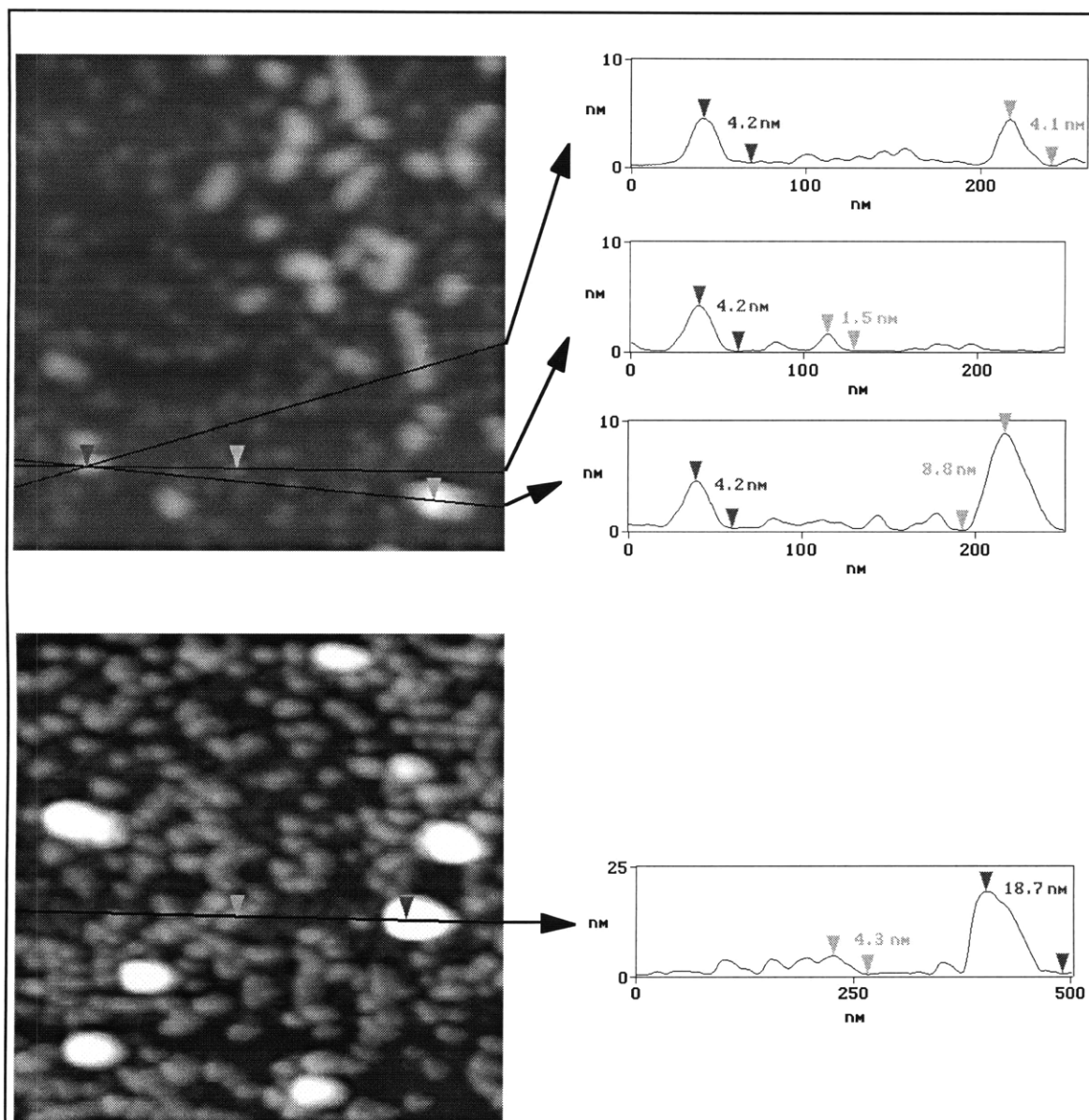
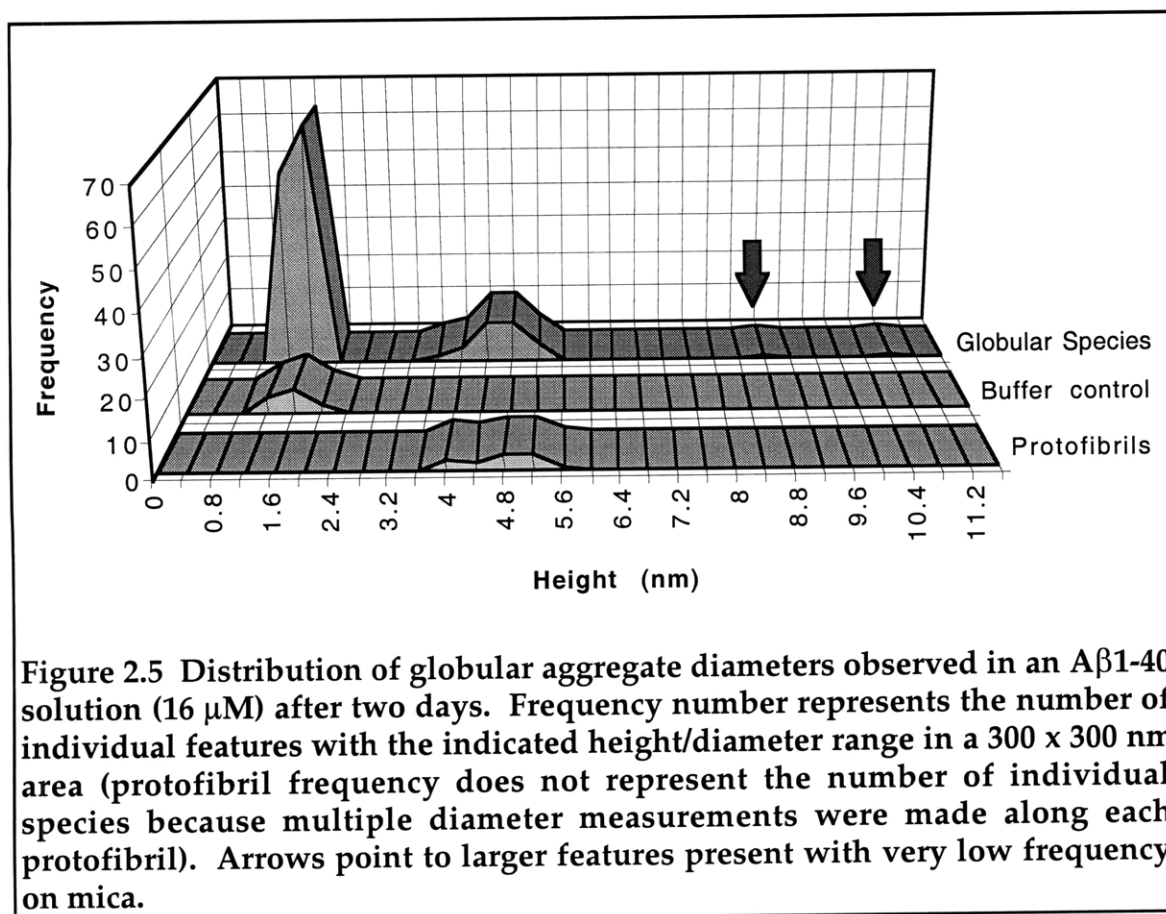


Figure 2.4 Representative image and sections of A $\beta$ 1-40 globular particles. TOP: A 250 nm image of A $\beta$ 1-40 (16  $\mu$ M) after 2 days of incubation at room temperature (left) with sections along the indicated lines (right). BOTTOM: A 500 nm image of A $\beta$ 1-40 (45  $\mu$ M) after 4 days of incubation at room temperature (left) with a section along the indicated line (right) showing an example of a large globular aggregate. Red and green arrowheads in the image correspond to the similarly marked features in the sections shown at right where the heights are indicated.

A representative region ( $300 \times 300 \text{ nm}^2$ ) was selected from the image of the  $16 \mu\text{M}$   $\text{A}\beta_{1-40}$  solution and the diameter of each globular feature present in that region was measured (for the more numerous  $\sim 1 \text{ nm}$  features, a  $150 \times 150 \text{ nm}$  region was analyzed and the frequency of heights was scaled appropriately to represent the larger region). The frequency distribution of the diameters was examined and is shown in Figure 2.5. Clear maxima are observed at  $\sim 1.5 \text{ nm}$  and  $\sim 4.5 \text{ nm}$  and a much less populated peak between  $7\text{-}11 \text{ nm}$ . Only two features in the  $8\text{-}10 \text{ nm}$  diameter range were in the counted area--there were 8 features between  $7$  and  $11 \text{ nm}$  in a  $1 \mu\text{m}$  square region on the same specimen. At higher concentrations and incubation times (for example,  $\text{A}\beta_{1-40}$  at  $45 \mu\text{M}$  after 4 days--Figure 2.4, bottom) even larger globular features with diameters of  $15\text{-}20 \text{ nm}$  are sometimes observed. The coincident distribution of diameters measured for protofibrils present in the same region with the distribution of the  $\sim 4.5 \text{ nm}$  globular species suggests that these features may be related (ie. the  $4.5 \text{ nm}$  particles may be short protofibrils, or protofibril assembly subunits). Comparison to globular particle sizes observed on a different specimen prepared with buffer alone (at same concentration present in  $\text{A}\beta$  solutions) indicates that the  $1.5 \text{ nm}$  particles can be observed with significant frequency without  $\text{A}\beta_{1-40}$ . The presence of the  $\sim 1.5 \text{ nm}$  species in buffer makes it uncertain whether the  $1.5 \text{ nm}$  species is related to  $\text{A}\beta$ , but the significant increase in frequency when  $\text{A}\beta_{1-40}$  is present suggests that some of these particles may be  $\text{A}\beta$ -derived.

The presence of multiple maxima in the distribution suggests that there are multiple distinct globular features with quantized sizes. The decreasing frequency of each consecutive peak of increasing diameter is what one would expect to observe if these species represented oligomers formed by sequential addition of a precursor species of discrete size (the aforementioned problems

associated with adsorption density comparisons could also explain this observation).



**Figure 2.5** Distribution of globular aggregate diameters observed in an A $\beta$ 1-40 solution (16  $\mu$ M) after two days. Frequency number represents the number of individual features with the indicated height/diameter range in a 300 x 300 nm area (protofibril frequency does not represent the number of individual species because multiple diameter measurements were made along each protofibril). Arrows point to larger features present with very low frequency on mica.

Similar indications for multiple small distinct A $\beta$  assemblies have been reported using and AFM<sup>6,7,9</sup> and quasi-elastic light-scattering.<sup>24,25</sup> The smallest A $\beta$ 1-40 particle directly detected by light scattering at pH 1.0 had a hydrodynamic radius of 7 nm.<sup>24</sup> Extrapolation of the linear phase for fibril growth back to  $t = 0$  in the same pH 1.0 experiments predicts the presence of a smaller particle with a hydrodynamic radius of 4 nm.<sup>24</sup> When Walsh et al. examine the included peak from their size exclusion separation of A $\beta$ 1-40 aggregates under conditions more closely resembling our own (at pH 7.4), they are able to detect particles with an even smaller hydrodynamic radius =  $1.8 \pm 0.2$

nm (interpreted to be consistent with monomeric or dimeric A $\beta$ 1-40).<sup>25</sup> Although these independent indications of multiple globular species were obtained under very different conditions, our results are also consistent with the presence of several very small forms of A $\beta$  during (and possibly preceding) the formation of protofibrils. The use of recently developed nanotube AFM probes should significantly improve resolution of these features.<sup>26</sup>

### *Protofibrils*

Protofibrils are also present at very early time points but appear to be more ordered assemblies of A $\beta$  than globular species because their growth occurs essentially in one dimension instead of three. Instead of expanding equally in all directions to form larger spheres they incorporate peptide selectively into one or both ends (of an imaginary cylinder) so that the length of the protofibril increases while it maintains a roughly constant diameter. Figure 2.6 shows a representative image and cross sections of protofibrils from a previously undisturbed (no prior sampling & therefore no prior tapping to suspend aggregates) solution of A $\beta$ 1-40 (45  $\mu$ M) 8 weeks after dilution and incubation at RT. This sample was identical in A $\beta$ 1-40 concentration and peptide stock source yet contained only protofibrils. The only apparent difference between these samples was the lack of agitation. The slower progression toward fibrils observed for this sample (and numerous others) is consistent with previous observations using turbidity<sup>11,27</sup> and congo red binding<sup>28</sup> to follow A $\beta$  aggregation which showed that agitation significantly increased aggregation kinetics in A $\beta$ 1-40 solutions.



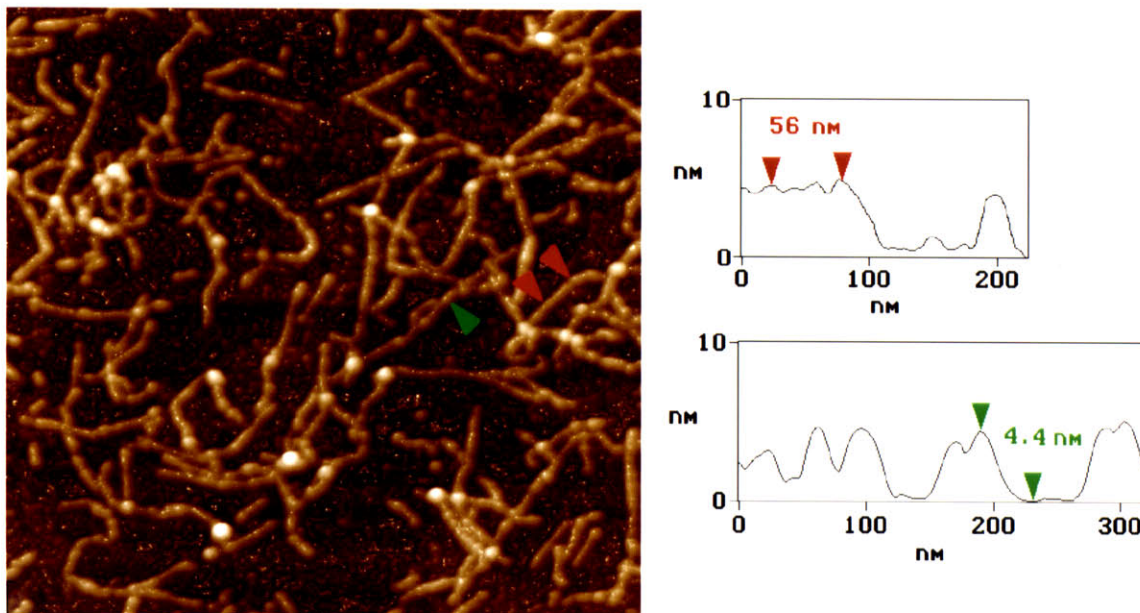


**Figure 2.6** Representative image and sections of A $\beta$ 1-40 protofibrils. Red and green arrowheads in the 1  $\mu$ m square image correspond to the similarly marked features in the sections shown at right. **TOP RIGHT:** An axial section of a protofibril showing 56 nm total distance between arrowheads indicating three periods in the axial substructure of the protofibril. **BOTTOM RIGHT:** A cross section of protofibril indicating the 4.4 nm measured diameter of this representative feature.

In general protofibrils appear to be flexible species as evidenced by the random curvatures they exhibit following adsorption to the mica surface. The average diameter of protofibrils measured from the same image used for analysis of the globular species is  $4.4 \pm 0.4$  nm (based on 15 height measurements). This value is typical of those obtained by similar analyses (based on  $\geq 50$  individual measurements each) of protofibrils grown under a variety of conditions which range from  $3.1 \pm 0.2$  nm to  $4.4 \pm 0.6$  nm (see for example Chapter 3, Figure 3.4). This  $\sim 30\%$  variability in average height measurements from different images is typical even when the same type of probe and similar setpoints are used for imaging (which should result in similar tapping forces) and illustrates the

importance of comparing morphologies from within a single scan whenever possible to ensure the greatest accuracy. Based on the similarity in reported diameter, the 2-3 nm fibrillar species reported by Stine et al. in A $\beta$ 1-40 (250  $\mu$ M) samples after weeks or months in the presence of larger fibrils<sup>8</sup> may be the same species we describe as protofibrils.

In well resolved scans, some protofibrils show small increases in diameter at intervals along their axis. Analyzing longitudinal sections (along the fibril axis) of protofibrils from a typical scan shows that these peaks have an average spacing of  $20 \pm 4.7$  nm. Due to the nonlinear nature of the protofibril, axial sections showing more than three repeats are difficult to obtain so averages included measurements from multiple protofibrils. Individual values for peak to peak distances show considerable variation with values observed ranging from 13 - 31 nm among protofibrils in a single scan, but values obtained on the same protofibril are typically more consistent.

The number of A $\beta$  molecules required to form a protofibril is uncertain from AFM analysis. Slowly sedimenting “soluble aggregates” (which may represent A $\beta$  in protofibrillar form) of A $\beta$ 1-40 and A $\beta$ 1-42 have estimated masses of  $\sim 1,000$  kDa (from analytical ultracentrifugation),<sup>23</sup> and protofibrils elute in the void volume of columns with exclusion limits (for dextrans) of  $\sim 100$  kDa.<sup>25</sup> Rough estimation for the number of A $\beta$ 's ( $\sim 4$  kDa each) in protofibrils based on these observations would suggest that there may be between 25 and 250 molecules of A $\beta$  in protofibrils of varying sizes. Mass-per-length analysis performed using scanning transmission EM for amylin fibrils may also provide a useful comparison.<sup>29</sup> Amylin (also  $\sim 4$  kDa) fibrils and A $\beta$  fibrils appear to share common secondary structures<sup>29,30</sup> and multiple filament wound morphologies (Goldsbury et al.<sup>29</sup> and below). Goldsbury et al. found that 2-5 filaments (referred to as protofibrils) were wound in a left handed helical sense to form

typical amylin fibrils.<sup>29</sup> Each filament had an apparent mass-per-unit length of ~10 kDa/nm (between 2-3 amylin molecules/nm).<sup>29</sup> If the mass-per-length for A $\beta$  protofibrils is similar, then there would be 200-300 A $\beta$ 's in a 100 nm protofibril.

### *Type 1 fibrils*

Type 1 fibrils are generally the earliest fibril type to appear during A $\beta$  fibril formation. A well resolved image of type 1 fibrils (seeded A $\beta$ 1-40 sample at 37°C, t = 1 day--for a complete discussion of seeding behavior see Chapter 4) is shown in Figure 2.7 along with axial and cross sections showing the very regular periodicity of the diameter increases and a representative diameter measurement at one of the peaks. The modulation in diameter has an average period of  $43 \pm 5.0$  nm (range = 35.4-51.5 nm) that appears to be the result of a left handed helical twist of two or more filament subunits. Apparent helicity could arise due to tip induced artifacts, but results presented in Chapter 4 rule out this possibility. The winding of two or more protofibril filament subunits to form these fibrils is also suggested by the diameter of the type 1 fibril ( $7.8 \pm 0.45$  nm, range = range 6.4-9.5 nm) measured at the peaks of the periods. This is roughly twice the diameter of protofibrils (measured from a separate scan). To confirm this relationship of the relative height for protofibrils and type 1 fibrils, the average heights were determined for both morphologies from a well resolved scan where they appeared side by side (not shown). Peak diameters for type 1 fibrils in the scan were  $8.5 \pm 0.9$  nm (range = 6.8-10.0 nm) compared to an average protofibril diameter of  $4.1 \pm 0.6$  nm (range = 3.4-5.1 nm). Therefore, the average diameter of protofibrils appears to be about 48% of the average type 1 fibril diameter.

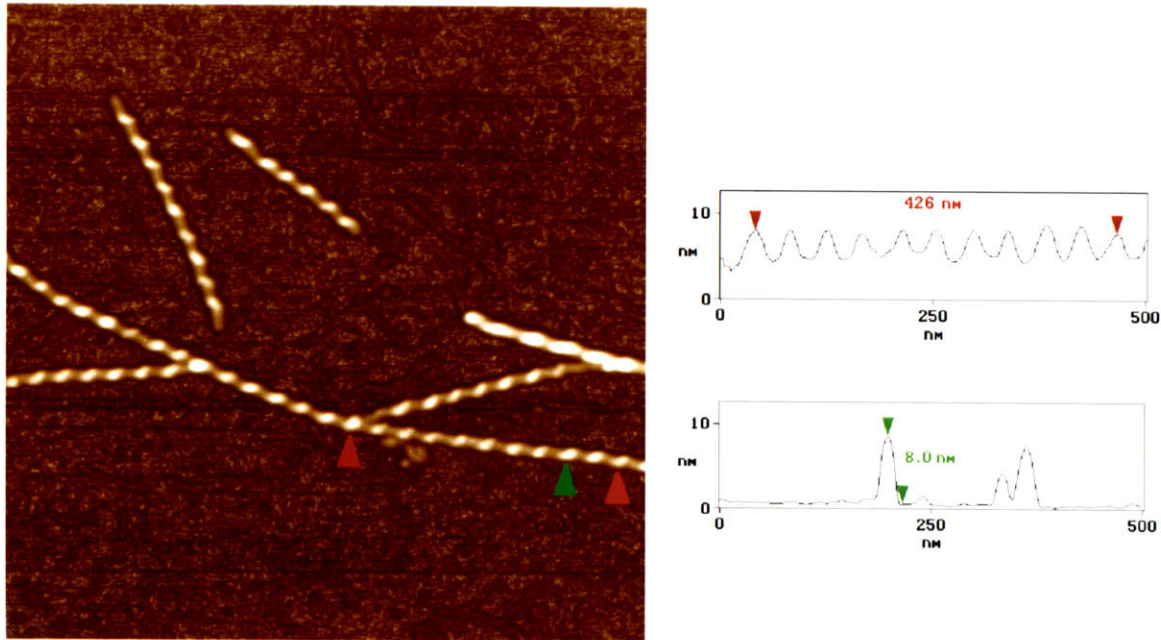


**Figure 2.7** Representative image and sections of A $\beta$ 1-40 type 1 fibrils. Red and green arrowheads in the 1  $\mu$ m square image correspond to the similarly marked features in the sections shown at right. **TOP RIGHT:** An axial section of a type 1 fibril showing 426 nm total distance between arrowheads indicating ten periods in the axial substructure. **BOTTOM RIGHT:** A cross section of type 1 fibril indicating the 8.0 nm measured diameter of this representative feature.

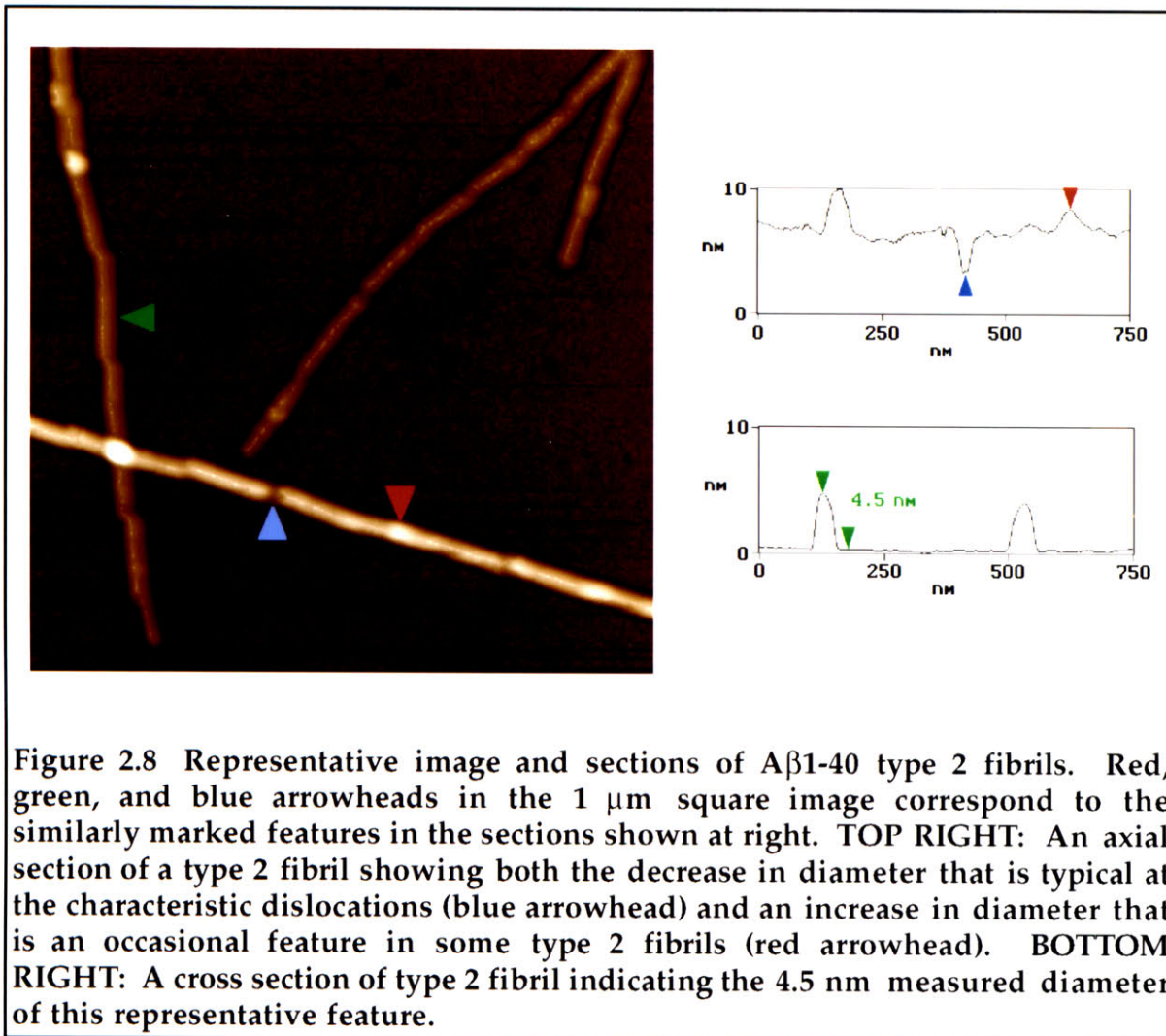
Alzheimer's disease senile plaque amyloid fibrils (presumably A $\beta$  fibrils) with 8-10 nm diameter, and two filament wound morphology (30-50 nm periodicity) have been observed in previous EM studies of tissue sections<sup>31</sup> and purified plaque material.<sup>32,33</sup> This fibril morphology has also been reported previously for A $\beta$ 1-40 fibrils formed from synthetic peptide *in vitro*.<sup>34-36</sup> These reports support the hypothesis that the type-1 fibril morphology is an important product of A $\beta$  fibril formation *in vivo* and that *in vitro* systems which produce this morphology are likely to be useful models for the AD pathogenic process. Furthermore, amyloid fibrils formed by other proteins including transthyretin,<sup>37-</sup>

<sup>39</sup> calcitonin,<sup>40</sup> and amylin,<sup>29</sup> each have been reported to form fibrils containing two or more helically wound filaments suggesting that our observations may also have implications for the general mechanism of amyloid formation (model discussed below).

### *Type 2 fibrils*

Another fibril morphology, the type 2 fibril, commonly appears along with type 1 fibrils at time points following the disappearance of protofibrils. Although they lack the regular height increases which characterize both protofibrils and type 1 fibrils, they do show less regular discontinuities along their axis (Figure 2.8, blue arrow). The interval between these dislocations commonly measured between 100-200 nm, with the intervals along a single fibril typically varying over a smaller range ( $\pm \sim 20\text{nm}$ ). The average diameter of type two fibrils is  $4.5 \pm 0.4$  nm and appears to be very similar to the diameter of protofibrils. For a better comparison, the average diameter of type 1 and type 2 fibrils was measured from another scan where they appeared together on the same specimen (not shown). The average diameters were  $9.0 \pm 0.3$  nm for type 1 fibrils (based on 15 measurements, range = 8.3-9.4 nm) and  $4.4 \pm 0.2$  nm for type 2 fibrils (range 3.9-4.8 nm). Thus, the diameter of type 2 fibrils is roughly 49% of the type 1 fibril diameter. The protofibril has a very similar relative diameter (48%) compared to type 1 fibrils, suggesting that type 2 fibrils may be formed by simple end to end ligation of protofibrils. However several observations indicate that this is probably not the case.





The protofibril has a very similar relative diameter (48%) compared to type 1 fibrils, and so formation of type 2 fibrils by simple end-to-end annealing of protofibrils cannot be ruled out.<sup>25</sup> However, this mechanism seems unlikely since achieving the proper orientation and proximity necessary for a productive collision should be a very rare event. Furthermore, the occasional observance of a height increase rather than a dislocation at an expected interval (red arrow, Figure 2.8) suggests that this species may also be a multi-filament species but with a larger winding pitch than the type 1 fibril. The dislocations observed may

represent breaks or tears in a ribbon-like structure caused by the adsorption process. Therefore the measured height of this feature of type 2 fibrils may underrepresent their maximal diameter which may lie in the plane of the substrate. However, we have not observed grooves along the axis or reproducible differences in width that could confirm the multi-filament nature of the type 2 fibril. This may be due to significant variability in resolving power and apparent widths that result from normal variability of tip radius (5-10 nm or more) for the silicon probes used for these studies. The use of carbon nanotube probes (which significantly improve resolution) should allow us to determine whether these features are truly multi-filament species.<sup>26</sup> Narrow ribbon-like fibrils with a periodicity of ~150 nm clearly made from multiple filaments have been described as products of A $\beta$ 1-42 aggregation *in vitro*.<sup>41</sup> Interestingly, these fibrils were termed 'mature fibrils' to indicate their prevalence after long aggregation times.<sup>41</sup> Other species were also described at earlier aggregation times including globular structures and more granular 'immature fibrils' which disappeared with time in favor of the mature fibrils.<sup>41</sup> These results are qualitatively very similar to our own.

*Other fibril morphologies are observed.*

Although type 1 and type 2 fibrils are the predominant fibril morphologies, fibrillar species which do not fit into these categories are also observed in some specimens(not shown). Generally, the diameters of these fibrils are similar to or slightly larger (diameter ~10-12 nm) than the two fibril types described above. These may represent fibrils formed from different numbers of filaments (as suggested by previous observations of multiple higher order assemblies of filaments in calcitonin<sup>40</sup> and amylin filaments<sup>29</sup>) or alternate lateral association modes of similar numbers of filaments (similar to the

polymorphism of flagella which has also been proposed to be the result of subtle switching in flagellin subunit packing<sup>42</sup>). It should also be noted that at late time points fibrils become increasingly difficult to observe in isolation on the substrate. This appears to be related to the incorporation of fibrils into large disordered clumps with increasing time and agitation.

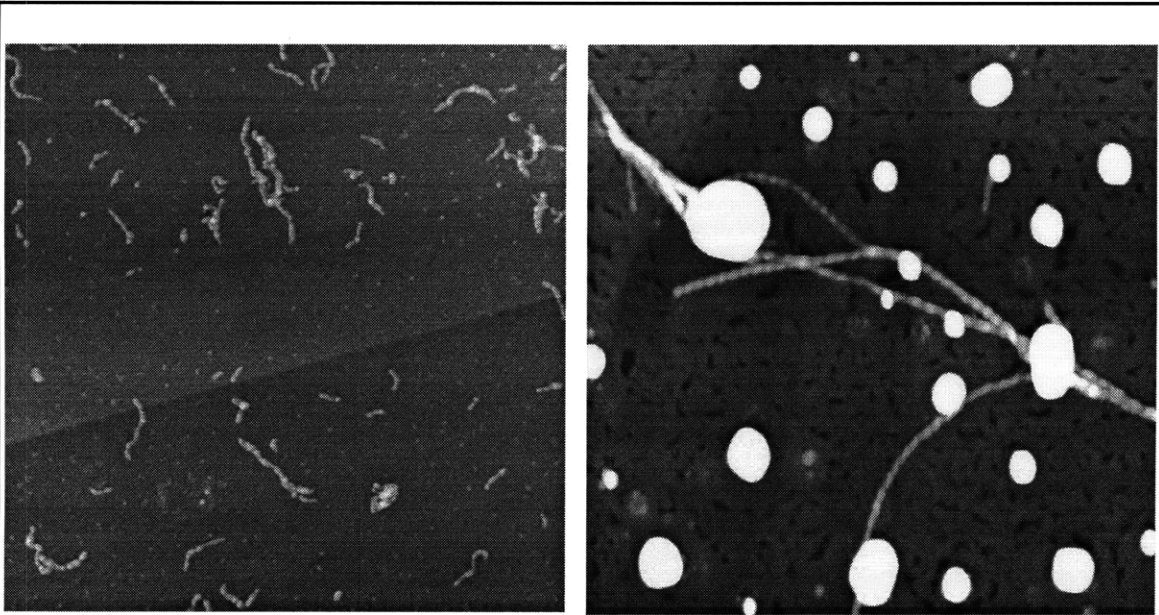


**Figure 2.9** A $\beta$ 1-40 Aggregate morphologies on HOPG. Images are 2  $\mu$ m square.

*Morphologies on a different substrate are similar*

Only the species that adsorb to the substrate are observed so it is impossible to rule out the existence of other species that might be very poorly adsorbed. In order to test the possibility that selective adsorption may bias our observations, we have performed initial experiments using sample preparation on freshly cleaved highly ordered pyrolytic graphite (HOPG) surfaces to look for different species that may adsorb to this hydrophobic surface which do not adhere to the hydrophilic surface of mica. There was occasionally an apparent



increase in the observation of large spherical species on this substrate (heights 25-40 nm, the hydrophobic surface HOPG is more prone to contamination so these could also represent non-A $\beta$  derived species) but no additional A $\beta$ 1-40 derived species were detected (Figure 2.9). The morphology of the protofibrils and type 1 fibrils observed on HOPG was indistinguishable from the observations made on mica, but type 2 fibrils were not observed.

#### *A $\beta$ 1-42 and A $\beta$ 1-40 aggregate morphologies have similar dimensions*

The A $\beta$ 1-42-derived species were very similar to the analogous A $\beta$ 1-40 species with respect to their measured diameter (not shown). The A $\beta$ 1-42 protofibrils had a diameter of  $4.2 \pm 0.58$  nm and a periodicity of  $22 \pm 3.1$  nm. Like A $\beta$ 1-40, two types of fibrils were detected: periodic type 1 fibrils (diameter =  $7.3 \pm 0.53$  nm, *ca.* 43 nm period) and type 2 fibrils (diameter =  $3.8 \pm 0.43$  nm, period of dislocations ranged between 100-200 nm).

### **Physical separation of aggregate morphologies**

#### *Filtration*

Filtration of A $\beta$  solutions/suspensions through 0.2  $\mu$ m filters has been commonly employed as a method for separating fibrillar A $\beta$  from “soluble” A $\beta$ . An A $\beta$ 1-40 solution (50  $\mu$ M) containing a mixture of protofibrils was partially filtered through a 0.2  $\mu$ m filter, and aliquots of the filtrate and retentate were used to prepare specimens on mica for AFM analysis (Figure 2.10). The retentate was observed to contain a mixture of protofibrils and fibrils, while only protofibrils and smaller features were observed in the filtrate. Although the presence of a small amount of fibrillar material in the filtrate cannot be ruled out, filtration appears to be a suitable method for qualitative removal of enough

fibrillar seed from A $\beta$  solutions so that a lag phase prior to fibril formation can be observed (since protofibrils do not seed fibril formation--Chap 4).

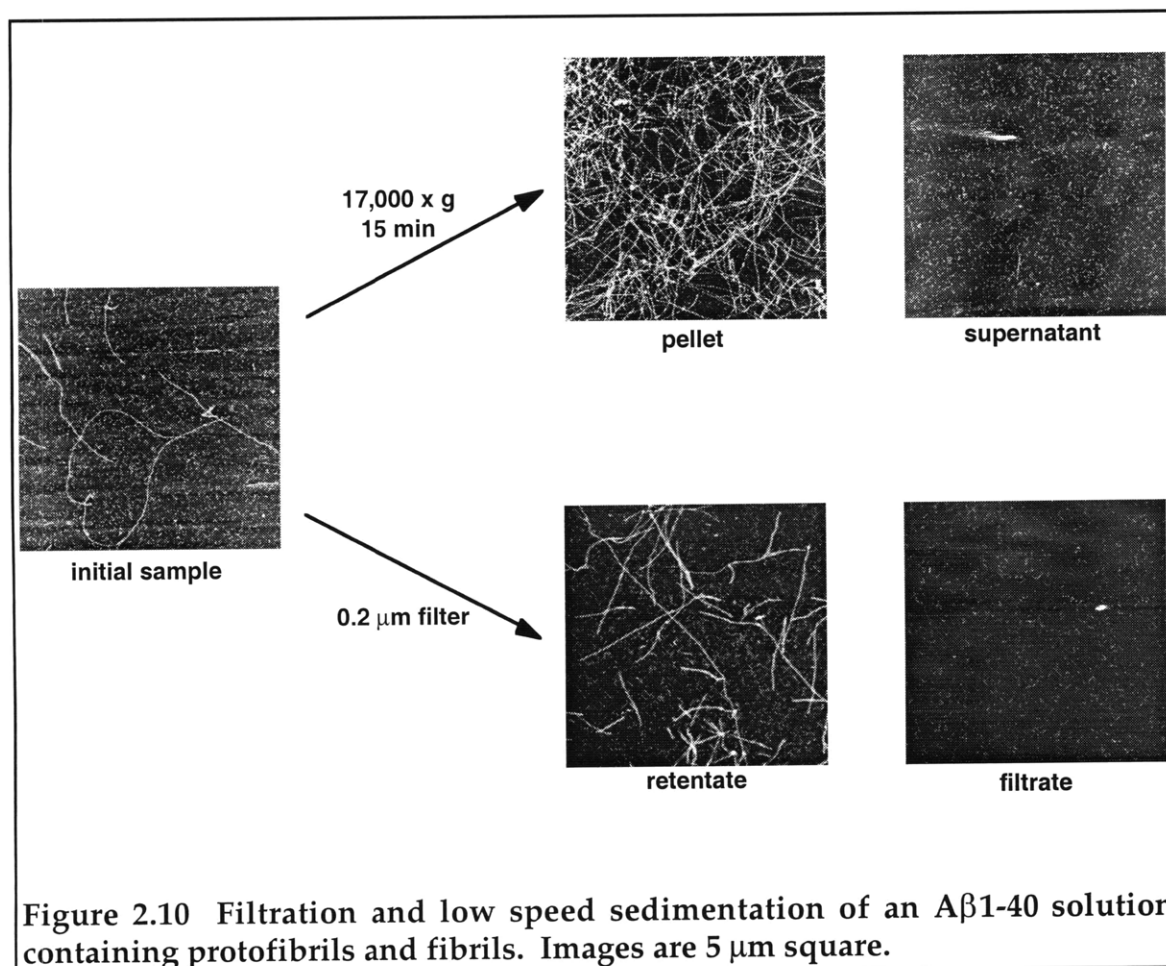
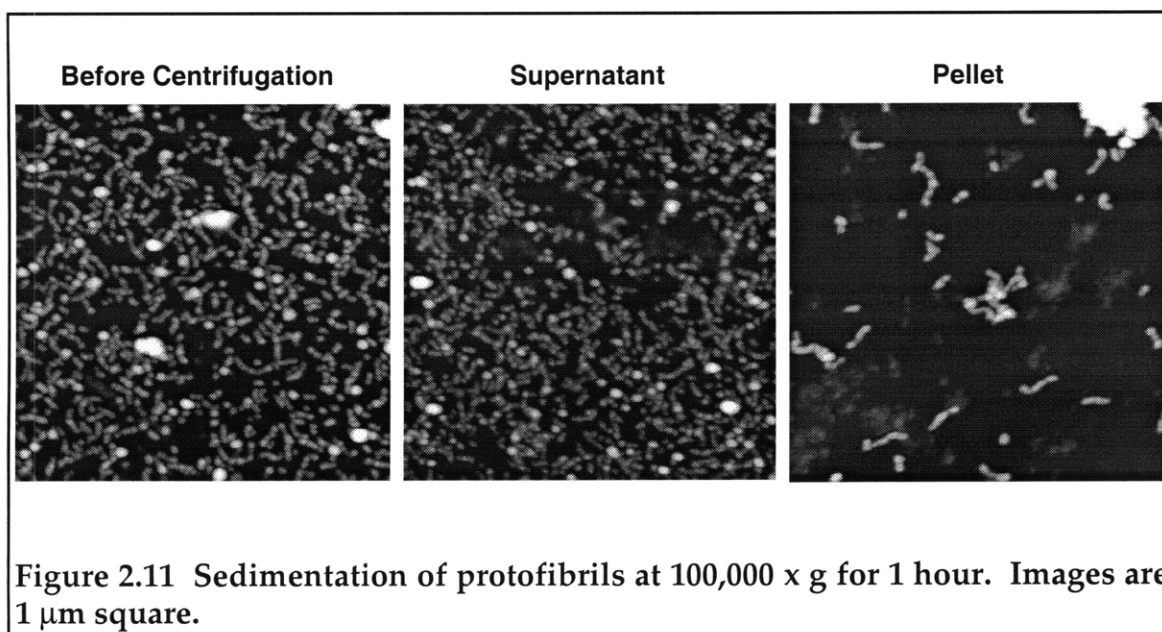


**Figure 2.10 Filtration and low speed sedimentation of an A $\beta$ 1-40 solution containing protofibrils and fibrils. Images are 5  $\mu$ m square.**

### *Sedimentation*

The same solution used in the filtration experiment described in the previous section was centrifuged for 15 minutes at  $\sim$ 17,000 g in a standard benchtop microfuge. The resulting separation is qualitatively similar to that achieved by filtration (0.2  $\mu$ m) with A $\beta$ 1-40 protofibrils and fibrils observed in the pellet while protofibrils and other smaller A $\beta$  species remain in the supernatant (occasional fibrils are observed, Figure 2.10). The presence of aggregated forms of A $\beta$  in the supernatant demonstrates that the use of similar

procedures to separate “soluble” and “insoluble” A $\beta$  would include the amount of A $\beta$  in protofibrillar form as soluble A $\beta$  and may significantly overestimate the amount of soluble A $\beta$  in a solution if protofibrils are present. Sedimentation at 100,000 g for 1 hour does selectively sediment longer protofibrils, but the small ~4 nm globular protofibrils are numerous in the supernatant along with occasional protofibrils as long as ~50 nm (Figure 2.11). The A $\beta$  in the supernatant is competent to go on to form protofibrils and fibrils (data not shown).



Preliminary equilibrium density ultracentrifugation experiments have also been done. Samples of A $\beta$ 1-40 (~25  $\mu$ g A $\beta$ 1-40 in each, [A $\beta$ 1-40] in solutions used was 40-45  $\mu$ M) in varying stages of fibril formation were adjusted to 40% sucrose, transferred to the bottom of a centrifuge tube, and overlaid with a 5-30% linear sucrose gradient. After equilibrium sedimentation in an ultracentrifuge, the tubes were fractionated and analyzed by SDS-PAGE/western blot analysis. AFM analysis of the aggregation state of each sample and the corresponding

sedimentation profile are shown in Figure 2.12. Samples containing pre-fibrillar aggregates and monomeric A $\beta$  (aggregation time = 4 h and 24 h) showed similar patterns with significant amounts of A $\beta$  migrating into lower density fractions.

A sample containing a mixture of protofibrils and fibrils showed a slight shift in the distribution toward higher density fractions. No detectable amounts of A $\beta$  in the sample containing fibrils alone migrated out of the highest density fraction. These results show that pre-fibrillar forms of A $\beta$  have lower densities compared to fibrillar A $\beta$ . However, we can not be certain that A $\beta$  protofibrils are included in these lower density species since the presence of sucrose prevented the preparation of suitable specimens for AFM analysis of the species present. Significant separation of pre-fibrillar and fibrillar A $\beta$ 1-40 was not achieved in these preliminary experiments, but may be possible with modifications in the sedimentation conditions used.

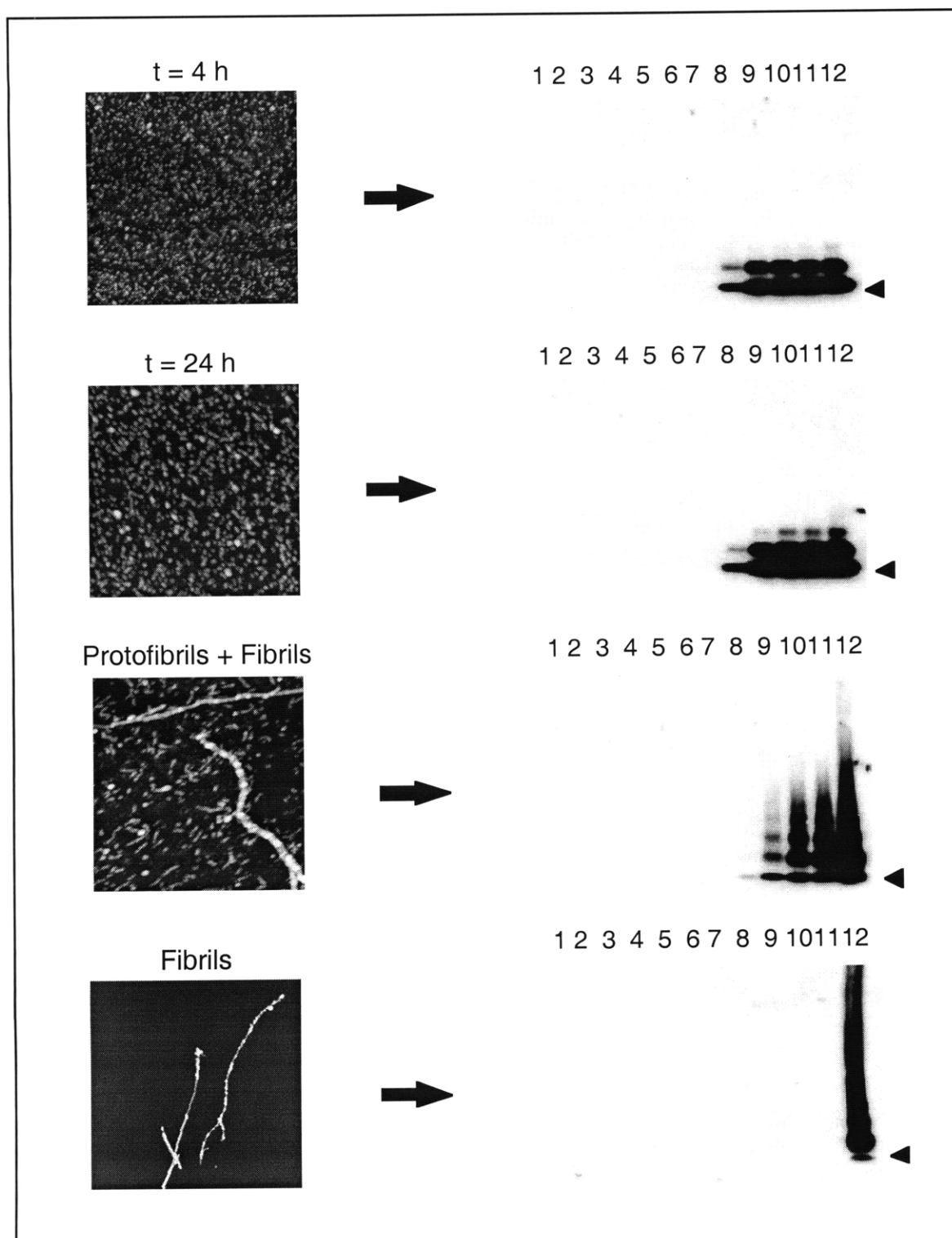


Figure 2.12 Equilibrium density ultracentrifugation of A $\beta$ 1-40 aggregates. AFM images of aggregates present are shown (left) and western blots (right, arrowheads indicate position of the 4 kDa A $\beta$ 1-40 monomer) showing the distribution of A $\beta$  with density. Density is lowest in fraction 1 and increases linearly to maximum density in fraction 12.

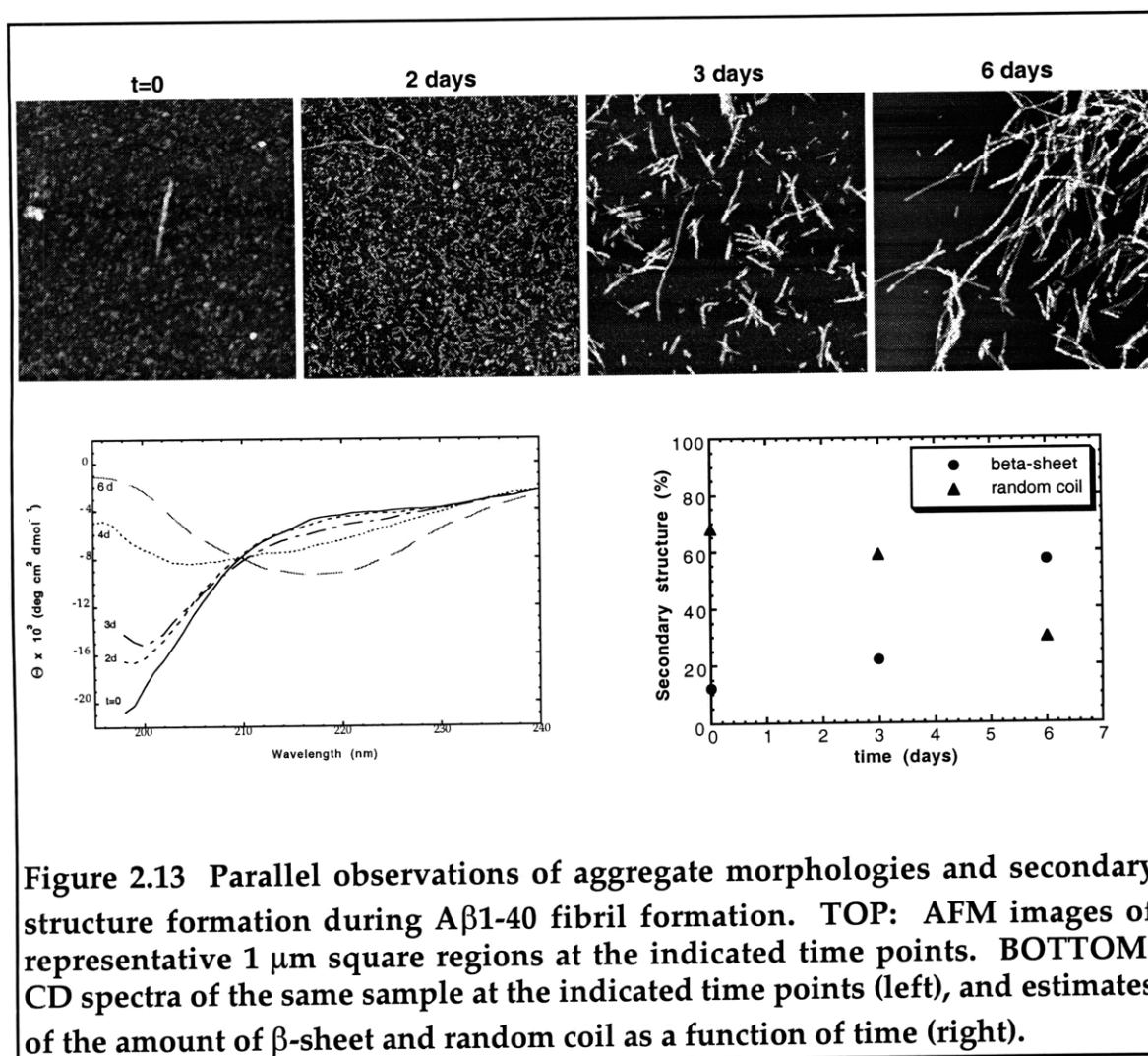
### **Time course for the formation of protein secondary structure**

To follow the time course for the formation of secondary structure in an unseeded solution with time by CD, it was first necessary to obtain a solution of A $\beta$ 1-40 that was as free of seed as possible without using DMSO (the strong absorbance of DMSO prevents CD analysis). Lyophilized peptide (HCl salt) was suspended in water and filtered through a 0.2  $\mu$ M microspin filter to remove any undissolved fibrillar material and concentrated buffer was added to the filtrate (an aliquot of the supernatant) yielding a solution containing 50  $\mu$ M A $\beta$ 1-40 in 5 mM phosphate, 100 mM NaF, pH 7.3. This solution was incubated at room temperature and the morphology and secondary structure of aggregates formed was monitored simultaneously by AFM and CD (Figure 2.13).

Immediately following dilution, rare short fibrils (lengths 500 nm - 1  $\mu$ m, about 1 per 100  $\mu$ m<sup>2</sup>) were observed among small globular features by AFM while the CD curve obtained showed little indication of the presence of ordered structure. After 2 days numerous protofibrils and occasional fibrils (lengths ~ 1  $\mu$ m) were observed by AFM in the presence of abundant spherical features in all size ranges, but there was little change from the original CD spectrum despite the observation by AFM of what appeared to be a significant population of structured aggregates. At three days changes in the CD spectrum indicated that detectable amounts of secondary structure were beginning to form. However, the CD curve still appeared to indicate the presence of a large proportion of non- $\beta$ -sheet structure even though fibrils appeared to be numerous at this point among a decreasing number of protofibrils and small spherical species. Only when protofibrils and smaller features had almost completely disappeared in favor of fibrils at day six did the CD spectrum indicate the formation of predominantly beta sheet structure in the A $\beta$ 1-40 solution. Estimates of the percent of A $\beta$  in  $\beta$ -sheet and random coil configurations at 0, 3 and 6 days were

made using the Lincomb program<sup>43</sup> and are shown in Figure 2.13 (bottom right). Similar results were obtained for solutions prepared in the same way using peptides from different sources and when seed material was removed by sedimentation (100,000 x g, 1 hour) rather than filtration (data not shown).

The delay between the observance of protofibrils and early fibrils and the appearance of a characteristic  $\beta$ -sheet CD curve is consistent with at least two interpretations-- 1) protofibrils do not have significant  $\beta$ -sheet structure, or 2) protofibrils do have significant secondary structural elements but only represent a small fraction of the total A $\beta$  in the sample at any time during fibril formation. Independent evidence from other studies supports the latter interpretation. Analysis of aggregating solutions of A $\beta$ 1-40 by Walsh et al. using size exclusion chromatography has also observed the transient formation of protofibrils (represented by the appearance of a peak in the void volume of the column). In these studies the relative amount of A $\beta$ 1-40 in the protofibril fraction (measured by relative UV intensity of peaks, recovery of <sup>125</sup>I-A $\beta$ 1-40 tracer, or radioimmunoassay) does accumulate to a significant amount but never appears to represent a majority of A $\beta$  in the samples.<sup>25</sup> Furthermore, CD analysis of protofibrils obtained in the size exclusion fraction that have been separated from unpolymerized forms of A $\beta$  produce spectra that are consistent with a protofibril structure containing a high percentage of  $\beta$ -sheet (Dominic Walsh, personal communication).



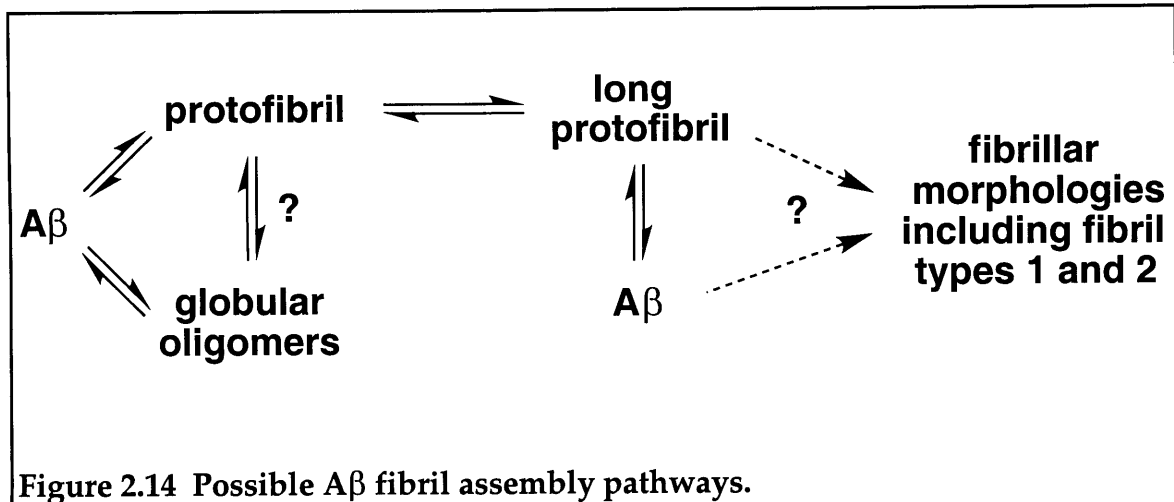
### A potential role for the protofibril as a fibril assembly intermediate.

A scenario in which A $\beta$  protofibrils are intermediates in the assembly of the A $\beta$  amyloid fibril (Figure 2.14) is supported by the fact that the disappearance of protofibrils occurs over a short time period compared to protofibril elongation and is concurrent with the appearance of fibrils. Several additional observations are pertinent to discussions of the probable mechanism. First, protofibril elongation is much slower than fibril elongation. The scarcity of small fibrils suggests that once fibrils are nucleated, their growth is rapid and favorable.<sup>1,2</sup> Second, A $\beta$  type 1 fibrils (formed by both A $\beta$ 1-40 and A $\beta$ 1-42) have



a maximum diameter that is roughly twice the diameter of the A $\beta$  protofibrils and appear to be helically twisted. The increased diameter precludes a simple end-to-end protofibril association mechanism and the apparent helicity suggests a lateral association and winding of protofibrils during fibril growth. Third, the significant lag period during which protofibrils grow in length and number in unseeded A $\beta$  solutions before fibrils appear suggests that a minimum number concentration of protofibrils or minimum inter-protofibril overlap may be required for the nucleation and/or growth of fibrils. Finally, an otherwise identical solution of A $\beta$ 1-40 (45  $\mu$ M) which was not agitated for eight weeks (solutions followed for the time course were agitated prior to sampling) contained only protofibrils, suggesting that an enhanced frequency of protofibril-protofibril encounters in agitated solutions promotes fibril formation. Thus, two or more protofibril or filament subunits appear to associate laterally and twist helically to form A $\beta$  type 1 fibrils.

Amyloid fibril formation from subunit filament precursors has been suggested at least as early as 1974 by Glenner and coworkers<sup>44</sup> based on the occasional observation of single filament extensions from the ends of multi-filament murine senile amyloid fibrils by negative-stain EM. More recently, morphological observations of fibrils formed by human calcitonin<sup>40</sup> and human amylin<sup>29</sup> have led to models for amyloid fibril formation closely resembling our own. Finally, Walsh et al. have also proposed a similar protofibril assembly model based on independent observations of the initial stages of A $\beta$  fibril formation as described above.<sup>25</sup>



Although the direct precursor mechanism is attractive, we have not ruled out the possibility that protofibrils are rapidly formed, but are in fast equilibrium with monomeric Aβ, which slowly assembles into the more stable type 1 and type 2 fibrils (Figure 2.14). In either scenario, the stabilization of protofibrils would inhibit fibril formation, either by blocking protofibril-protofibril interactions or by slowing the protofibril-monomer equilibrium. In addition, the relative stabilities of the multiple fibrillar morphologies cannot be determined from these experiments. It must be emphasized that species which do not adsorb onto mica are not seen by this method. However, preliminary experiments using a hydrophobic graphite surface (HOPG) show the same species and no additional ones. In addition, since the velocities of the individual steps may have different concentration-dependencies, it is conceivable that the lifetimes of these species may be altered at lower or higher concentrations of Aβ or that new species become apparent. The protofibril-to-fibril transition seems to be the best candidate for the nucleation-dependent step, since protofibrils apparently must reach a certain length and/or concentration before rapid fibril growth occurs. Growth of the fibrils, once nucleated, appears to have a first order dependence on the concentration of Aβ.<sup>12,45</sup>

Although there is no direct evidence presently available for the transient existence of A $\beta$  protofibrils *in vivo*, an apparently non-fibrillar form of deposited A $\beta$ , termed diffuse amyloid plaque, is prevalent in individuals known to be predisposed to AD, leading to the proposal that it represents an innocuous precursor to neuritic amyloid.<sup>46</sup> Diffuse plaque may contain protofibrillar A $\beta$ , not easily detected by electron microscopy. It will be important to study this material by AFM in the future. Significantly, A $\beta$  protofibrils, like diffuse amyloid plaques, are more difficult to sediment than amyloid fibrils. The work described in the remaining two chapters of this thesis describe our efforts to provide a more detailed characterization of the process of protofibril formation (Chapter 3) and clarification of the role of the protofibril in A $\beta$  amyloid fibril growth. We hope that the additional information gained will help provide the foundation necessary to address the possible relevance of the protofibril to the *in vivo* disease process.

## Experimental

### Materials

Synthetic A $\beta$ 1-40 (TFA salt, used in time course and morphology examinations) was purchased from Quality Controlled Biochemicals Inc. (Hopkinton, MA). Synthetic A $\beta$ 1-42 (TFA salt) and A $\beta$ 1-40 (HCl salt, used in CD/AFM study) was provided by Dr. David Teplow of the Center for Neurologic Diseases.

### In vitro fibril formation

*AFM experiments.* Stock solutions of A $\beta$ 1-40 and A $\beta$ 1-42 were made by dissolving each peptide in DMSO at 0.34 (A $\beta$ 1-42) or 0.84 mM (A $\beta$ 1-40) and, in the case of A $\beta$ 1-40, filtering through Millex-FG 0.22  $\mu$ m filters (Millipore), or 0.2  $\mu$ m microspin filtration units (Whatman). Final concentrations of the DMSO stocks were determined by quantitative amino acid analysis. Aliquots of the DMSO stock solutions (9 nmol in *ca.* 11  $\mu$ L for A $\beta$ 1-40, 4 nmol in *ca.* 11  $\mu$ L for A $\beta$ 1-42) were added to aqueous buffer (200  $\mu$ L total volume, 100 mM NaCl, 10 mM NaH<sub>2</sub>PO<sub>4</sub>, pH 7.4) and immediately vortexed to mix before allowing fibril formation to proceed at room temperature.

*CD/AFM time course experiments.* Lyophilized A $\beta$ 1-40 (HCl salt) was suspended in water, sonicated to dissolve the peptide, and filtered through a 0.02  $\mu$ m syringe filter to remove any undissolved fibrillar material. Concentrated buffer was added to the filtrate (an aliquot of the supernatant) yielding a solution containing 50  $\mu$ M A $\beta$ 1-40 (in 5 mM phosphate, 100 mM NaF, pH 7.3). This solution was incubated at room temperature and the morphology and secondary structure of aggregates formed was monitored simultaneously by AFM and CD.

## Atomic Force Microscopy

*Speciman preparation.* At the indicated time points, the aggregation mixtures were mixed by gentle tapping and samples were prepared for imaging by transferring 5  $\mu$ L of the suspension to the surface of freshly cleaved mica. After 1 min. the substrate was rinsed twice with 50  $\mu$ L water to remove salt and loosely bound peptide. Excess water was removed with a gentle stream of filtered compressed air and the sample was imaged immediately.

*AFM operation.* All images were obtained in ambient conditions in tapping mode using a Nanoscope IIIa force microscope (Digital Instruments, Santa Barbara, CA) operating in TappingMode<sup>TM</sup> with an etched silicon Nano Probe<sup>TM</sup> (model TESP: 125  $\mu$ m cantilever, spring constant = 20-100 N/m, tip radius = 5 - 10 nm, or model FESP: 125  $\mu$ m cantilever, spring constant = 1-5 N/m, tip radius = 5- 10 nm). Scanning parameters varied with individual tips and samples, but typical ranges were as follows: 1) TESP--starting RMS amplitude, 2.0-2.5 V; setpoint, 1.5 - 1.75 V; resonant frequency, 250-350 kHz; scan rate, 0.5-2 Hz. 2) FESP--starting RMS amplitude, 1.4-2.0 V; setpoint, 1.0-1.6 V; resonant frequency, 60-80 kHz; scan rate, 0.8-2 Hz.

*Measurements.* The diameters of features as described herein were obtained by averaging  $\geq 30$  peak height values obtained for the stated morphology using nanoscope section analysis software ( $\pm$  standard deviation). Periodicities were determined by averaging 30 peak-to-peak distances ( $\pm$  standard deviation) except for the case of the A $\beta$ 1-42 type 1 fibril, where only 12 values were available.

## Separation studies

*Filtration.* To a 0.2  $\mu\text{m}$  nylon microspin filter unit (Whatman) was added 100  $\mu\text{L}$  of an A $\beta$ 1-40 solution containing protofibrils and fibrils. The filter unit was spun for ~15 seconds @ 4,000 rpm in an Eppendorf model 5415C benchtop microcentrifuge with a fixed angle rotor. Aliquots (4 $\mu\text{L}$ ) were removed from the filtrate and retentate and used to prepare specimens for AFM analysis as described above.

*Low speed sedimentation.* To a microcentrifuge tube was added 100  $\mu\text{L}$  of an A $\beta$ 1-40 solution containing protofibrils and fibrils. The sample was centrifuged for 15 minutes at maximum speed (14,000 rpm, ~17,000  $\times$  g) in an Eppendorf model 5415C benchtop microcentrifuge with a fixed angle rotor. To examine the material in the supernatant, 4  $\mu\text{L}$  aliquot was carefully taken from the top 1/3 of the sample and used to prepare a specimen on mica for AFM analysis as described above. Since no visible pellet was generated in the sample, the sedimented material (pellet material in images) was analyzed after making the supernatant specimen by careful removal of an additional 4 $\mu\text{L}$  aliquot bottom of the tube and preparing a specimen on mica for AFM analysis as described above.

*High speed sedimentation.* An aliquot (200  $\mu\text{L}$ ) from an A $\beta$ 1-40 solution containing only pre-fibrillar A $\beta$ 1-40 aggregates (assessed by AFM prior to use) was centrifuged for 1 hour at 50,000 rpm in a Beckman TL-100 ultracentrifuge with a model 100.2 fixed angle rotor (~100,000  $\times$  g). 180  $\mu\text{L}$  of the supernatant was removed and an aliquot of this was used to prepare a specimen for AFM analysis. The remaining ~20  $\mu\text{L}$  of the sample containing the pellet was reconstituted to 200  $\mu\text{L}$  total volume with buffer (10 mM phosphate, 100 mM NaCl, pH 7.4). The pellet was gently homogenized by drawing the sample

repeatedly through a pipette, and an aliquot of this suspension (4  $\mu$ L) was used to prepare a specimen on mica for AFM analysis.

*Equilibrium density ultracentrifugation.* Aliquots of A $\beta$ 1-40 samples containing mixtures of morphologies as described in the text (~25  $\mu$ g total peptide in each sample) were adjusted to 40% sucrose (4 mL total volume) and transferred to the bottom of a 13 mL ultracentrifuge tube. The sample was overlaid with a 5-30% linear sucrose gradient (8 mL) and centrifuged for 20 hours at 39,000 rpm in a Beckman L8-55M ultracentrifuge with a SW 41 rotor. One mL fractions were collected from the top and 10  $\mu$ L aliquots from these fractions were boiled in Laemmli sample buffer for 5 minutes, separated using a 10-20% polyacrylamide tris-tricine gradient gel (Novex mini-gel), and transferred to a nitrocellulose membrane (pore size of 0.22  $\mu$ m, Schleicher and Schuell). The membrane was blocked with 5% non-fat dry milk in TBST (10 mM Tris, pH 7.4, 150 mM NaCl, 0.05% Tween-20) for 1 hour at room temp, probed with anti-A $\beta$  mouse monoclonal 2G3 in TBST containing 1% bovine serum albumin for 1 hour at room temp, washed, and incubated with goat anti-mouse IgG conjugated to horseradish peroxidase. Bound antibodies were visualized by chemiluminescent substrate as described by the manufacturer (NEN life science products).

### **Circular Dichroism**

CD spectra were obtained using an AVIV model 62A DS spectrophotometer. The sample was scanned four times at 23°C in a quartz cell (0.1 cm pathlength) at 1 nm intervals over the wavelength range 198-240 nm. Buffer and cell backgrounds were subtracted from each spectrum. Results are expressed in units of deg cm<sup>2</sup> dmol<sup>-1</sup>. The percent of  $\beta$ -sheet and random coil

structures present was estimated with the Lincomb program<sup>43</sup> using spectra fit to the basis spectra set of Yang et al.<sup>47</sup>



## References for Chapter 2

1. Jarrett, J.T., Berger, E.P., and Lansbury, P.T., Jr. The carboxy terminus of the beta amyloid protein is critical for the seeding of amyloid formation: implications for the pathogenesis of Alzheimer's disease. *Biochemistry* **1993**, *32*, 4693-4697.
2. Jarrett, J.T. and Lansbury, P.T., Jr. Seeding "one-dimensional crystallization" of amyloid: a pathogenic mechanism in Alzheimer's disease and scrapie? *Cell* **1993**, *73*, 1055-1058.
3. Lansbury, P.T., Jr. A Reductionist view of Alzheimer's disease. *Acc. Chem. Res.* **1996**, *29*, 317-321.
4. Bustamante, C. and Keller, D. Scanning force microscopy in biology. *Physics Today* **1995**, *48*, 32-38.
5. Colton, R.J., Baselt, D.R., Dufrene, Y.F., Green, J.-B., and Lee, G.U. Scanning probe microscopy. *Curr. Opin. Chem. Biol.* **1997**, *1*, 370-377.
6. Oda, T., Wals, P., Osterburg, H.H., Johnson, S.A., Pasinetti, G.M., Morgan, T.E., Rozovsky, I., Stine, W.B., Snyder, S.W., Holzman, T.F., and et al. Clusterin (apoJ) alters the aggregation of amyloid beta-peptide (A beta 1-42) and forms slowly sedimenting A beta complexes that cause oxidative stress. *Exp. Neurol.* **1995**, *136*, 22-31.
7. Roher, A.E., Chaney, M.O., Kuo, Y.M., Webster, S.D., Stine, W.B., Haverkamp, L.J., Woods, A.S., Cotter, R.J., Tuohy, J.M., Krafft, G.A., Bonnell, B.S., and Emmerling, M.R. Morphology and toxicity of Abeta-(1-42) dimer derived from neuritic and vascular amyloid deposits of Alzheimer's disease. *J. Biol. Chem.* **1996**, *271*, 20631-20635.
8. Stine, W.B., Jr., Snyder, S.W., Ladrone, U.S., Wade, W.S., Miller, M.F., Perun, T.J., Holzman, T.F., and Krafft, G.A. The nanometer-scale structure of amyloid-beta visualized by atomic force microscopy. *J. Prot. Chem.* **1996**, *15*, 193-203.
9. Shivji, A.P., Davies, M.C., Roberts, C.J., Tendler, S.J.B., and Wilkinson, M.J. Molecular surface morphology studies of beta-amyloid self-assembly: Effect of pH on fibril formation. *Prot. Pept. Lett.* **1996**, *3*, 407-414.
10. Seelig, J., Lehrmann, R., and Terzi, E. Domain formation induced by lipid-ion and lipid-peptide interactions. *Mol. Membr. Biol.* **1995**, *12*, 51-57.
11. Evans, K.C., Berger, E.P., Cho, C.G., Weisgraber, K.H., and Lansbury, P.T., Jr. Apolipoprotein E is a kinetic but not a thermodynamic inhibitor of amyloid formation: implications for the pathogenesis and treatment of Alzheimer disease. *Proc. Natl. Acad. Sci. U S A* **1995**, *92*, 763-767.
12. Naiki, H. and Nakakuki, K. First-order kinetic model of Alzheimer's beta-amyloid fibril extension in vitro. *Lab. Invest.* **1996**, *74*, 374-383.
13. Janciauskiene, S., Garcia de Frutos, P., Carlemalm, E., Dahlback, B., and Eriksson, S. Inhibition of Alzheimer beta-peptide fibril formation by serum amyloid P component. *J. Biol. Chem.* **1995**, *270*, 26041-26044.
14. Han, H., Weinreb, P.H., and Lansbury, P.T., Jr. The core Alzheimer's peptide NAC forms amyloid fibrils which seed and are seeded by beta-

- amyloid: is NAC a common trigger or target in neurodegenerative disease? *Chem. Biol.* **1995**, *2*, 163-169.
15. Scheuner, D., Eckman, C., Jensen, M., Song, X., Citron, M., Suzuki, N., Bird, T.D., Hardy, J., Hutton, M., Kukull, W., Larson, E., Levy-Lahad, E., Viitanen, M., Peskind, E., Poorkaj, P., Schellenberg, G., Tanzi, R., Wasco, W., Lannfelt, L., Selkoe, D., and Younkin, S. Secreted amyloid beta-protein similar to that in the senile plaques of Alzheimer's disease is increased in vivo by the presenilin 1 and 2 and APP mutations linked to familial Alzheimer's disease *Nat. Med.* **1996**, *2*, 864-870.
  16. Cai, X.D., Golde, T.E., and Younkin, S.G. Release of excess amyloid beta protein from a mutant amyloid beta protein precursor. *Science* **1993**, *259*, 514-516.
  17. Iwatsubo, T., Odaka, A., Suzuki, N., Mizusawa, H., Nukina, N., and Ihara, Y. Visualization of A beta 42(43) and A beta 40 in senile plaques with end-specific A beta monoclonals: evidence that an initially deposited species is A beta 42(43). *Neuron* **1994**, *13*, 45-53.
  18. Lemere, C.A., Lopera, F., Kosik, K.S., Lendon, C.L., Ossa, J., Saido, T.C., Yamaguchi, H., Ruiz, A., Martinez, A., Madrigal, L., Hincapie, L., Arango, J.C., Anthony, D.C., Koo, E.H., Goate, A.M., Selkoe, D.J., and Arango, J.C. The E280A presenilin 1 Alzheimer mutation produces increased A beta 42 deposition and severe cerebellar pathology. *Nat. Med.* **1996**, *2*, 1146-11450.
  19. Suzuki, N., Cheung, T.T., Cai, X.D., Odaka, A., Otvos, L., Jr., Eckman, C., Golde, T.E., and Younkin, S.G. An increased percentage of long amyloid beta protein secreted by familial amyloid beta protein precursor (beta APP717) mutants. *Science* **1994**, *264*, 1336-13340.
  20. Borchelt, D.R., Thinakaran, G., Eckman, C.B., Lee, M.K., Davenport, F., Ratovitsky, T., Prada, C.M., Kim, G., Seekins, S., Yager, D., Slunt, H.H., Wang, R., Seeger, M., Levey, A.I., Gandy, S.E., Copeland, N.G., Jenkins, N.A., Price, D.L., Younkin, S.G., and Sisodia, S.S. Familial Alzheimer's disease-linked presenilin 1 variants elevate Abeta1-42/1-40 ratio in vitro and in vivo. *Neuron* **1996**, *17*, 1005-1013.
  21. Citron, M., Westaway, D., Xia, W., Carlson, G., Diehl, T., Levesque, G., Johnson-Wood, K., Lee, M., Seubert, P., Davis, A., Kholodenko, D., Motter, R., Sherrington, R., Perry, B., Yao, H., Strome, R., Lieberburg, I., Rommens, J., Kim, S., Schenk, D., Fraser, P., St George Hyslop, P., and Selkoe, D.J. Mutant presenilins of Alzheimer's disease increase production of 42-residue amyloid beta-protein in both transfected cells and transgenic mice. *Nat. Med.* **1997**, *3*, 67-72.
  22. Selkoe, D.J. Alzheimer's disease: genotypes, phenotypes, and treatments. *Science* **1997**, *275*, 630-631.
  23. Snyder, S.W., Ladror, U.S., Wade, W.S., Wang, G.T., Barrett, L.W., Matayoshi, E.D., Huffaker, H.J., Krafft, G.A., and Holzman, T.F. Amyloid-beta aggregation: selective inhibition of aggregation in mixtures of amyloid with different chain lengths. *Biophys. J.* **1994**, *67*, 1216-1228.
  24. Lomakin, A., Chung, D.S., Benedek, G.B., Kirschner, D.A., and Teplow, D.B. On the nucleation and growth of amyloid beta-protein fibrils:

- detection of nuclei and quantitation of rate constants. *Proc. Natl. Acad. Sci. U S A* **1996**, 93, 1125-1129.
25. Walsh, D.M., Lomakin, A., Benedek, G.B., Condron, M.M., and Teplow, D.B. Amyloid beta-protein fibrillogenesis. Detection of a protofibrillar intermediate. *J. Biol. Chem.* **1997**, 272, 22364-22372.
  26. Wong, S.S., Harper, J.D., Lansbury, P.T. Jr., and Lieber, C.M. Carbon nanotubes tips: High resolution probes for imaging biological systems. *J. Am. Chem. Soc.* **1998**, 120, 603-604.
  27. Wood, S.J., Maleeff, B., Hart, T., and Wetzel, R. Physical, morphological and functional differences between pH 5.8 and 7.4 aggregates of the Alzheimer's amyloid peptide Abeta. *J. Mol. Biol.* **1996**, 256, 870-867.
  28. Wood, S.J., Chan, W., and Wetzel, R. An ApoE-Abeta inhibition complex in Abeta fibril extension. *Chem. Biol.* **1996**, 3, 949-956.
  29. Goldsbury, C.S., Cooper, G.J., Goldie, K.N., Muller, S.A., Saafi, E.L., Gruijters, W.T., Misur, M.P., Engel, A., Aebi, U., and Kistler, J. Polymorphic fibrillar assembly of human amylin. *J. Struct. Biol.* **1997**, 119, 17-27.
  30. Lansbury, P.T., Jr., Costa, P.R., Griffiths, J.M., Simon, E.J., Auger, M., Halverson, K.J., Kocisko, D.A., Hendsch, Z.S., Ashburn, T.T., Spencer, R.G., and et al. Structural model for the beta-amyloid fibril based on interstrand alignment of an antiparallel-sheet comprising a C-terminal peptide. *Nat. Struct. Biol.* **1995**, 2, 990-998.
  31. Narang, H.K. High-resolution electron microscopic analysis of the amyloid fibril in Alzheimer's disease. *J. Neuropathol. Exp. Neurol.* **1980**, 39, 621-631.
  32. Merz, P.A., Wisniewski, H.M., Somerville, R.A., Bobin, S.A., Masters, C.L., and Iqbal, K. Ultrastructural morphology of amyloid fibrils from neuritic and amyloid plaques. *Acta Neuropathol. (Berl)* **1983**, 60, 113-124.
  33. Roher, A.E., Palmer, K.C., Yurewicz, E.C., Ball, M.J., and Greenberg, B.D. Morphological and biochemical analyses of amyloid plaque core proteins purified from Alzheimer disease brain tissue. *J. Neurochem.* **1993**, 61, 1916-1926.
  34. Fraser, P.E., Nguyen, J.T., Inouye, H., Surewicz, W.K., Selkoe, D.J., Podlisny, M.B., and Kirschner, D.A. Fibril formation by primate, rodent, and Dutch-hemorrhagic analogues of Alzheimer amyloid beta-protein. *Biochemistry* **1992**, 31, 10716-10723.
  35. Howlett, D.R., Jennings, K.H., Lee, D.C., Clark, M.S., Brown, F., Wetzel, R., Wood, S.J., Camilleri, P., and Roberts, G.W. Aggregation state and neurotoxic properties of Alzheimer beta-amyloid peptide. *Neurodegeneration* **1995**, 4, 23-32.
  36. Malinchik, S.B., Inouye, H., Szumowski, K.E., and Kirschner, D.A. Structural analysis of Alzheimer's beta(1-40) amyloid: protofilament assembly of tubular fibrils. *Biophys. J.* **1998**, 74, 537-545.
  37. Serpell, L.C., Sunde, M., Fraser, P.E., Luther, P.K., Morris, E.P., Sangren, O., Lundgren, E., and Blake, C.C. Examination of the structure of the

- transthyretin amyloid fibril by image reconstruction from electron micrographs. *J. Mol. Biol.* **1995**, 254, 113-118.
38. Blake, C.C., Serpell, L.C., Sunde, M., Sandgren, O., and Lundgren, E. A molecular model of the amyloid fibril. *Ciba Found. Symp.* **1996**, 199, 6-15; discussion 15-21, 40-6.
  39. Blake, C. and Serpell, L. Synchrotron X-ray studies suggest that the core of the transthyretin amyloid fibril is a continuous beta-sheet helix. *Structure* **1996**, 4, 989-98.
  40. Bauer, H.H., Aebi, U., Haner, M., Hermann, R., Muller, M., and Merkle, H.P. Architecture and polymorphism of fibrillar supramolecular assemblies produced by in vitro aggregation of human calcitonin. *J. Struct. Biol.* **1995**, 115, 1-15.
  41. Seilheimer, B., Bohrmann, B., Bondolfi, L., Muller, F., Stuber, D., and Dobeli, H. The toxicity of the Alzheimer's beta-amyloid peptide correlates with a distinct fiber morphology. *J. Struct. Biol.* **1997**, 119, 59-71.
  42. Hasegawa, K., Yamashita, I., and Namba, K. Quasi- and nonequivalence in the structure of bacterial flagellar filament. *Biophys. J.* **1998**, 74, 569-575.
  43. Perczel, A., Park, K., and Fasman, G.D. Deconvolution of the circular dichroism spectra of proteins: the circular dichroism spectra of the antiparallel beta-sheet in proteins. *Proteins. Struct. Funct. Genet.* **1992**, 13, 57-69.
  44. Glenner, G.G., Eanes, E.D., Bladen, H.A., Linke, R.P., and Termine, J.D.  $\beta$ -pleated sheet fibrils: a comparison of native amyloid with synthetic protein fibrils. *J. Histochem. Cytochem.* **1974**, 12, 1141-1158.
  45. Esler, W.P., Stimson, E.R., Ghilardi, J.R., Vinters, H.V., Lee, J.P., Mantyh, P.W., and Maggio, J.E. In vitro growth of Alzheimer's disease beta-amyloid plaques displays first-order kinetics. *Biochemistry* **1996**, 35, 749-757.
  46. Selkoe, D.J. Normal and abnormal biology of the beta-amyloid precursor protein. *Annu. Rev. Neurosci.* **1994**, 17, 489-517.
  47. Yang, J.T., Wu, C.S., and Martinez, H.M. Calculation of protein conformation from circular dichroism. *Methods. Enzymol.* **1986**, 130, 208-269.

## Chapter 3

### **AFM Measurements of A $\beta$ 1-40 Protofibril Growth**

In the previous chapter, AFM experiments were described which identified and characterized several distinct aggregate species which form during fibril formation by synthetic A $\beta$ 1-40 and A $\beta$ 1-42 *in vitro*. The first-detected species was not the amyloid fibril as predicted by the simplest interpretation of the nucleation dependent polymerization mechanism. Instead, a number of smaller oligomeric A $\beta$  assemblies including the A $\beta$  protofibril were observed for extended periods prior to the formation of prototypical amyloid fibrils by both peptides. Since very little was known about the behavior of these pre-fibrillar species and the events preceding the onset of fibril formation, we decided to more closely examine the time course of A $\beta$  protofibril formation. For these initial studies we chose to use A $\beta$ 1-40 instead of A $\beta$ 1-42 since its slower onset of fibril formation allows greater opportunity to observe protofibril formation and growth.

This chapter describes our efforts to develop an AFM-based method for comparing protofibril growth under a variety of conditions. Changes in the measured lengths of protofibrils with time are used as the basis for comparing the rate of of protofibril formation. After briefly discussing the basic features of the detection methods used and a series of experiments designed to test the reproducibility of the measurements, this chapter will present data that

indicates that protofibril formation increases with time, A $\beta$ 1-40 concentration, temperature, and ionic strength. These observations expand the range of conditions where protofibril formation is observed and indicate the usefulness of AFM as a tool for comparing protofibril growth.

### **AFM-based methods for monitoring protofibril growth**

Although AFM examination cannot provide quantitative information about changes in the amount of protofibrils with time, it can very accurately measure the dimensions of individual protofibrils in a specimen. We believed that measurements of protofibril length could provide the basis for quantitative comparisons of protofibril growth since the qualitative observations from the time course of fibril formation discussed in Chapter 2 suggest that protofibril lengths, like the amount of protofibrils,<sup>1</sup> increase with time during protofibril formation. Two methods used to compare the lengths of protofibrils among different specimens are described below.

#### *Measuring average protofibril length*

For determinations of the average protofibril length, regions containing > 50 protofibrils were selected from suitable specimens (see below) and the lengths of all protofibrils in that region were measured and used to calculate the average. The ~4 nm globular species present in the scan were included in the length average as protofibrils with lengths 4.5 nm (approximately equal to their diameter). Error in the average length

measurements is estimated to be  $\pm 5$  nm. The error is difficult to determine empirically, but the digital nature of the image data, and imprecision when approximating the curvature of the protofibrils will contribute to measurement error. Variation in specimen preparation conditions needed to optimize protofibril density could also influence the value of protofibril length and were controlled for experimentally (results discussed below).

While using the average protofibril length to represent changes in protofibril growth with time provides a good way to compare changes in the protofibril population as a whole, it may provide deceptive information if used to estimate elongation rates for protofibrils. Increases in average protofibril length only provide an accurate representation of the protofibril elongation rates if the number of protofibrils remains constant during the measurement period. If new (shorter) protofibrils form between measurements then the growth rate would be underestimated by the increase in average length.

#### *Measuring the length of the longest protofibril observed*

By extension of the same argument, the longest protofibrils should have formed closest to  $t = 0$  and continued to grow during the period prior to sampling. Therefore, the length of the longest protofibril in a specimen could provide an estimate of elongation rate which might more closely represent the actual elongation rate for protofibrils. This method will be used to provide an alternate estimate for the average growth rate in A $\beta$ 1-40 samples.

To obtain this value we take the same scan containing the region used for average length measurements, divide it into quadrants and then find and measure the longest protofibril present in each quadrant. We then use the average of these lengths  $\pm$  the standard deviation of the values to represent the length of the longest protofibril. We use this averaging method instead of relying on the length of a single protofibril to improve confidence that the value obtained is an accurate representation of the longest protofibrils present and to provide some sense of the variability of this measurement. The elongation rate is obtained by dividing this length by the time elapsed prior to sampling. It is important to realize that elongation rates measured this way (and estimates based on the longest protofibril method) represent average elongation rates, and could significantly underestimate actual elongation rates if protofibrils are prone to disassembly episodes during growth (as is the case for microtubules)<sup>2,3</sup> or a population of protofibrils becomes dormant while other protofibrils in the sample continue to grow (a similar scenario has been described for *in vitro* elongation of *salmonella* flagella).<sup>4</sup>

### **Effects of specimen preparation conditions on measurements**

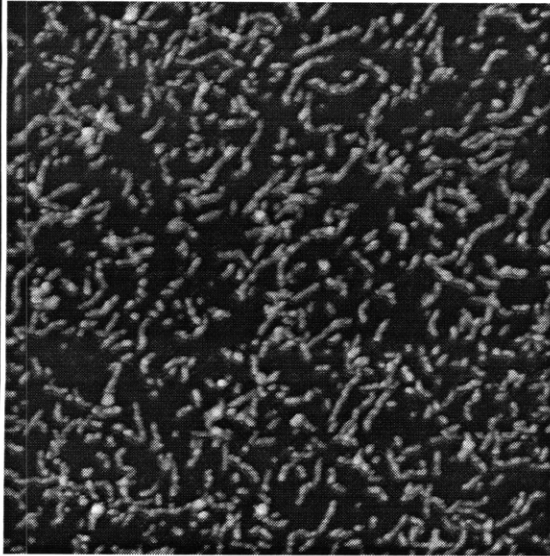
To reliably determine the lengths of protofibrils in a specimen required that the protofibrils be evenly dispersed on the mica substrate so that individual protofibrils could be distinguished and measured. Alterations in the incubation time on mica and the A $\beta$ 1-40 concentration in the aliquot applied to the substrate can be used to achieve protofibril adsorption densities



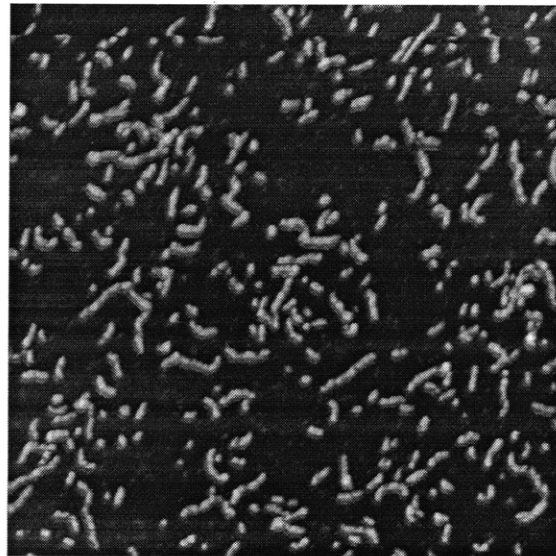
from most samples that allow accurate length determinations. Reducing incubation times for undiluted aliquots on mica from 1 min (used in time course experiments in Chapter 2) to 30 seconds generally produced suitable specimens from solutions with A $\beta$ 1-40 concentrations  $\leq 40 \mu\text{M}$ . Solutions with A $\beta$ 1-40 concentrations  $> 40 \mu\text{M}$  required brief dilution of aliquots to concentrations  $\leq 40 \mu\text{M}$  before specimen preparation to produce suitable specimens for length measurements (example images shown in figure 3.1) Because it was possible that these alterations to the specimen preparation procedure could change the lengths of protofibrils which adsorb to the mica surface, their effects on protofibril length measurements were investigated to test the reproducibility and accuracy of length measurements made using this method.

*Controlling for the effect of brief dilution.*

After 7 days and 22 days of incubation at room temperature (average temperature = 18°C), aliquots of an A $\beta$ 1-40 solution (32  $\mu\text{M}$ ) were used to make specimens either without dilution or following brief ( $\leq 30$  seconds) dilution to 16  $\mu\text{M}$ . Representative images of these specimens are shown in Figure 3.1 and the average protofibril length and the length of the longest protofibril was determined for each sample and the results are summarized in Table 3.1.



**32  $\mu$ M A $\beta$ 1-40, Undiluted**



**32  $\mu$ M A $\beta$ 1-40, Diluted to 16  $\mu$ M**

**Figure 3.1** Typical protofibril distributions used for measuring protofibril lengths. Both specimens were prepared from the same suspension of A $\beta$ 1-40 protofibrils that had been growing for 22 days at room temperature (18°C). Images are 1  $\mu$ m square.

**Table 3.1** Protofibril lengths measured with and without dilution. After 7 days and 22 days of incubation at room temperature, aliquots of an A $\beta$ 1-40 solution (32  $\mu$ M) were used to make specimens either without dilution or following brief ( $\leq$  30 seconds) dilution to 16  $\mu$ M.

Incubation time prior to analysis	Dilution	Average Length	Longest Protofibril
7 days	no	24.4 $\pm$ 5 nm	130 $\pm$ 10 nm
	yes	23.6 $\pm$ 5 nm	121 $\pm$ 7 nm
22 days	no	29.4 $\pm$ 5 nm	136 $\pm$ 16 nm
	yes	34.5 $\pm$ 5 nm	157 $\pm$ 49 nm

For both time points, the average protofibril length and longest protofibril length for specimens prepared either with or without dilution were within the error of the measurements. Although it is not possible to test the effect of dilution in this way for dilution from higher A $\beta$ 1-40 concentrations (since the protofibril density is too great for accurate length measurements in undiluted samples above  $\sim 40 \mu\text{M}$ ), these results suggest that dilution of protofibrils briefly (less than 30 seconds in all cases) prior to measurement does not significantly alter the lengths of protofibrils observed using this method.

*The effect of extended dilution.*

A solution of A $\beta$ 1-40 ( $160 \mu\text{M}$ ) was diluted to  $8 \mu\text{M}$  after aggregation at  $18^\circ\text{C}$  for 4 hours and imaged immediately, 25 minutes, 3 days, and 7 days following dilution (Figure 3.2).

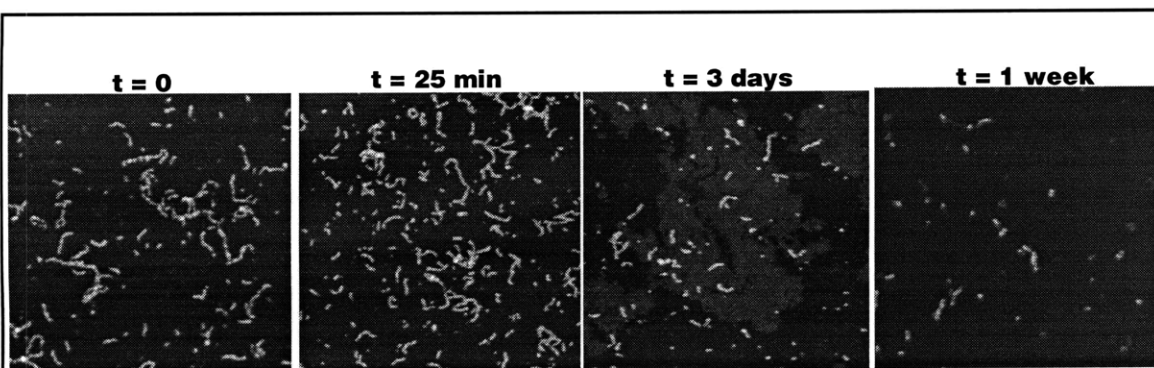


**Figure 3.2** Images of protofibrils following dilution. After 4 hours of incubation at  $18^\circ\text{C}$  an A $\beta$ 1-40 ( $160 \mu\text{M}$ ) solution was diluted to  $8 \mu\text{M}$  and imaged at the indicated times following dilution. Images are  $1 \mu\text{m}$  square.

The values for the average protofibril length and longest protofibril measurements at each time point are shown in Table 3.2. No significant change in the average protofibril length or the average length of the longest protofibril was observed during the first 25 minutes of dilution. Dilution for 3 days did result in significant reductions in both length measurements and also appeared to reduce the overall amount of protofibrils adsorbed to the mica surface. After 7 days, protofibrils numbers were reduced even further, but the additional decreases observed for the average length and longest protofibril measurements were within the error of the measurements. The reduction in the length and number of protofibrils during extended dilution may reflect protofibril disassembly caused by dilution. However, the change is too slow to cause protofibril lengths to be significantly underestimated in these experiments where the dilution prior to specimen preparation and AFM analysis never exceeds 1 minute.

**Table 3.2 Effect of extended dilution on protofibril lengths. An A $\beta$ 1-40 solution (160  $\mu$ M, t = 4 hours) containing protofibrils was diluted to 8  $\mu$ M and protofibril lengths were analyzed at the indicated times following dilution.**

Dilution time	t = 0	25 min	3 days	7 days
<b>Average Length</b>	30.6 $\pm$ 5 nm	30.5 $\pm$ 5 nm	17.0 $\pm$ 5 nm	14.0 $\pm$ 5 nm
<b>Longest Protofibril</b>	177 $\pm$ 21 nm	193 $\pm$ 34 nm	106 $\pm$ 24 nm	86 $\pm$ 13 nm

*Controlling for the effect of incubation time on the mica substrate.*

Aliquots from an A $\beta$ 1-40 protofibril suspension (32  $\mu$ M briefly diluted to 16  $\mu$ M after 7 days at 18°C) were placed on mica for 30 seconds or 1 minute before rinsing away unbound material and imaging. The average protofibril length was  $23.6 \pm 5$  nm for the 30 second specimen and  $22.2 \pm 5$  nm for the 1 minute specimen. The longest protofibril measured  $122 \pm 7$  nm in the 30 second specimen, and  $110 \pm 16$  nm in the 1 minute specimen. In another comparison, 30 second and 2 minute incubations on mica were used to prepare specimens from a different A $\beta$ 1-40 solution (200  $\mu$ M briefly diluted to 20  $\mu$ M after 14 hours at 18°C). The average protofibril length was  $45.4 \pm 5$  nm in the 30 second specimen and  $49.8 \pm 5$  nm in the 2 minute specimen. From the same images the longest protofibril measured  $131 \pm 6$  nm in the 30 second specimen, and  $148 \pm 19$  nm in the 2 minute specimen. No significant changes in protofibril length measurements resulted from variations in the incubation time on mica between 30 seconds and 2 minutes. The incubation time on mica was kept as constant as possible among specimens that were used for comparisons of protofibril lengths in the following discussions, but the actual times may differ by up to 5 seconds. Based on these observations, such small variations are unlikely to significantly alter the length of protofibrils observed.

## Measurements of protofibril growth

### *Time-dependent elongation of protofibrils.*

Images of specimens prepared from a 100  $\mu\text{M}$  suspension of A $\beta$ 1-40 after 2 days, 7 days, and 18 days incubation at room temperature are shown in Figure 3.3. Comparison of protofibril lengths in these images indicated that protofibrils longer than 100 nm are observed with greater frequency over time (1% of protofibrils at 2 days, 8% after 7 days and 20% after 18 days) while protofibrils  $\leq$  40 nm long remain common (Figure 3.3-Histograms).

The number of protofibrils observed in a 1  $\mu\text{m}^2$  region started at 440 in the 2 day specimen, decreased to 256 at 7 days and was 218 after 18 days. The trend toward decreasing numbers of protofibrils on specimens over time was a general trend among the specimens described in this chapter with more rapid decreases generally associated with more rapid protofibril elongation. If this trend reflects actual differences in protofibril number in solution, it could be an indication that smaller protofibrils (for example the 4.5 nm globular species) combine to form longer protofibrils. The average protofibril length was 22.4 nm at 2 days, increased to 37.5 nm at 7 days and reached 58.8 nm at 18 days (Figure 3.4). A similar trend toward increasing length with time is observed for the longest protofibrils in solution (Figure 3.4). The average diameter of the protofibrils does not change significantly with time as the lengths increase (Figure 3.4) indicating that growth occurs primarily, if not entirely, by addition of A $\beta$  onto the ends of protofibrils.

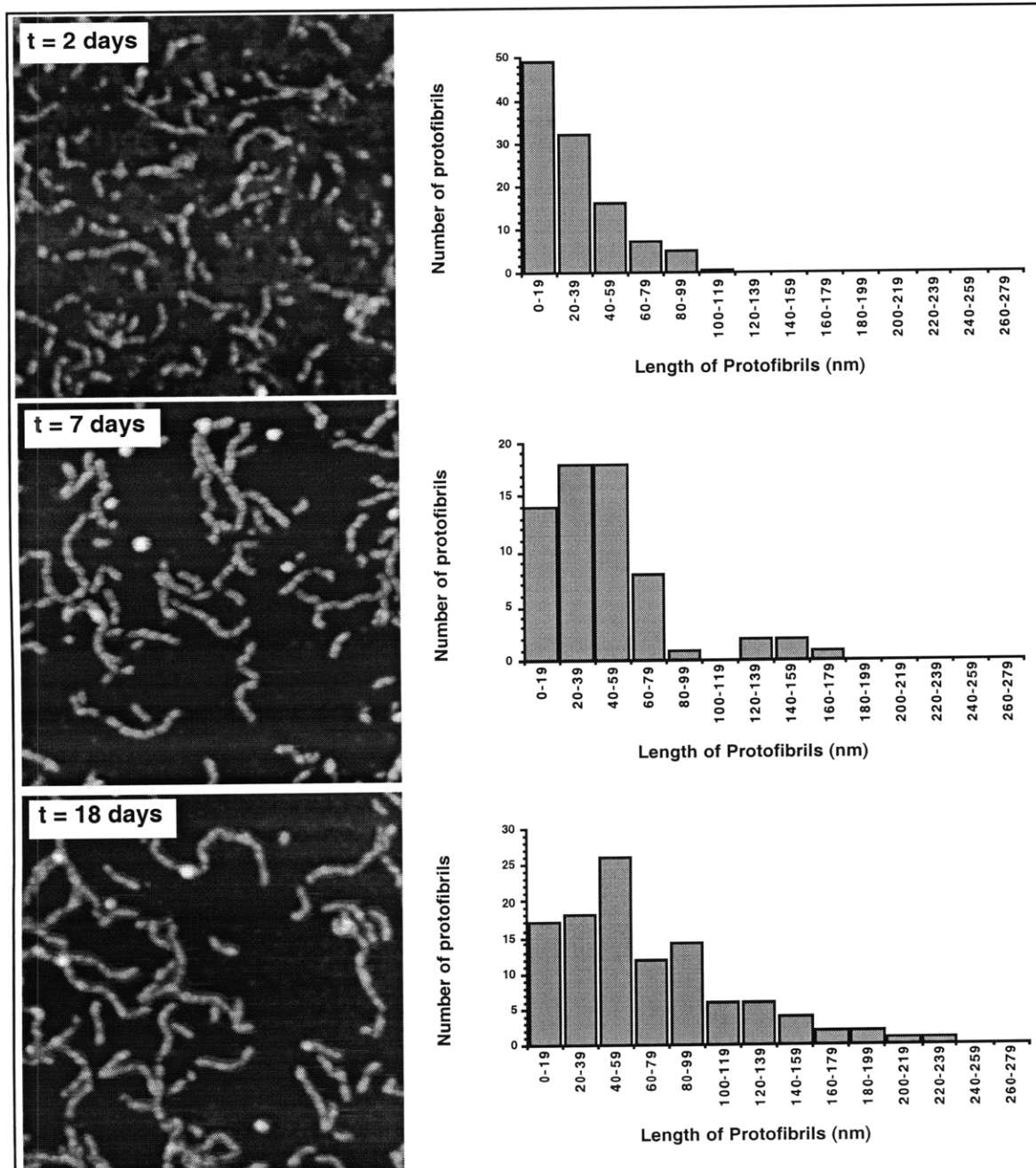
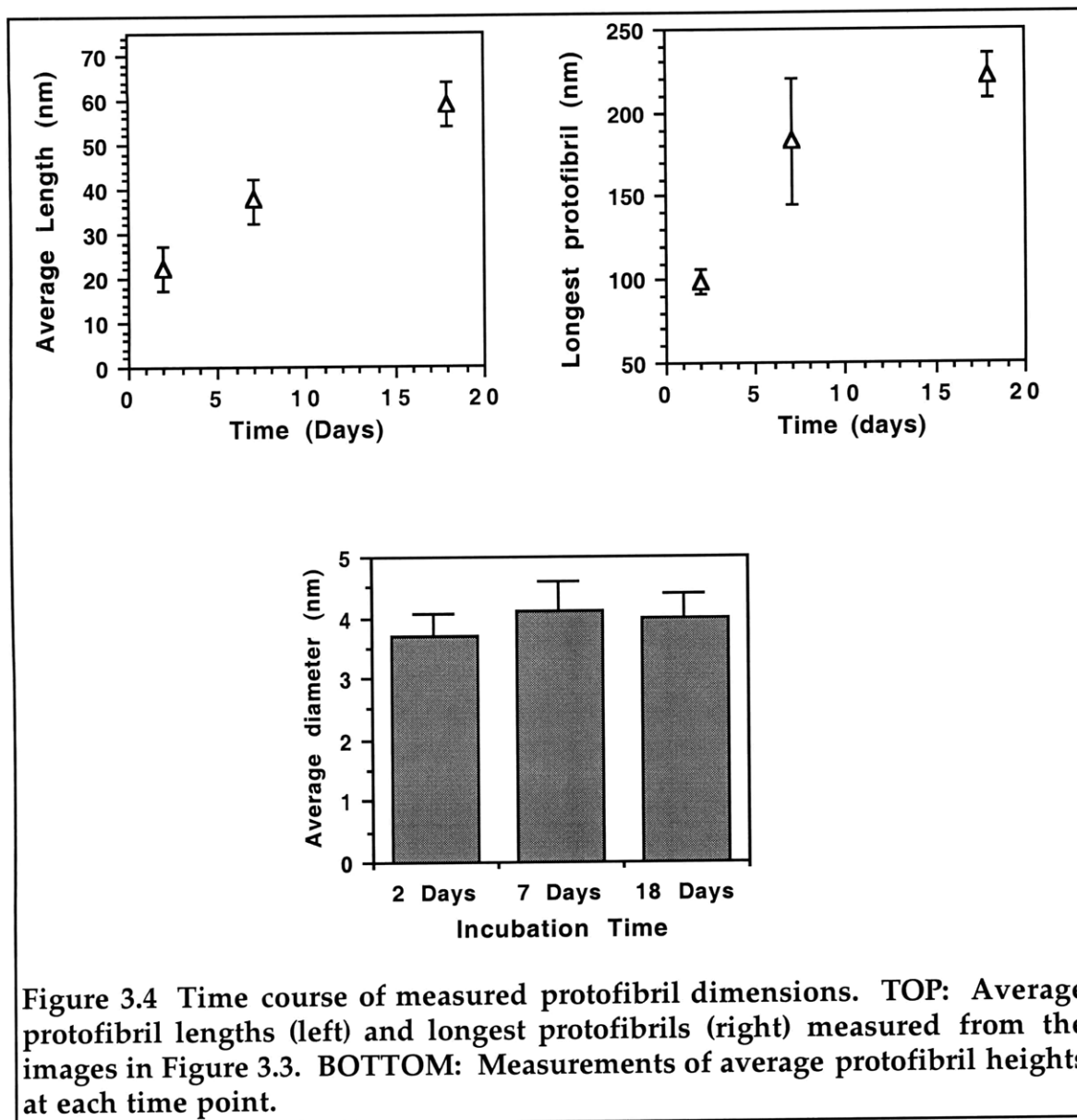


Figure 3.3 Images and histograms of protofibril growth.  $1 \mu\text{m}$  square images on left and histograms on right showing  $\text{A}\beta_{1-40}$  protofibril lengths increasing with time. Total protofibril numbers in histograms were 110 (in  $0.25 \mu\text{m}^2$ ) at day 2, 64 (in  $0.25 \mu\text{m}^2$ ) at day 7, and 109 (in  $0.50 \mu\text{m}^2$ ) at day 18.



*Concentration-dependent elongation of protofibrils.*

The elongation of protofibrils was followed in solutions with different A $\beta$ 1-40 concentrations (16  $\mu$ M, 32  $\mu$ M, 80  $\mu$ M and 160  $\mu$ M) but otherwise identical incubation conditions. After incubating for 4 hours at room temperature, only rare protofibrils showing no evidence of elongation were observed in the 16  $\mu$ M sample while protofibrils were readily observed at the



higher concentrations (Figure 3.5). At 2 days and all later time points, protofibrils were present in all samples (no fibrils observed). Protofibrils from the 160  $\mu\text{M}$  sample were less evenly distributed on the substrate, and often appeared to be closely associated into clumps on the surface. Since the length of protofibrils in these clumps could not be accurately determined, only the isolated protofibrils were used for length determination in specimens from this sample.

The average lengths of the protofibrils in each sample were determined and plotted as a function of time in Figure 3.5. Average lengths generally increased with A $\beta$ 1-40 concentration, although the differences were within experimental error in some cases (especially at lower time points). For the 160  $\mu\text{M}$  sample, an initial increase in average length was seen over the course of the first week, but a significant decrease occurred between 7 and 22 days. The reason for this decrease is not clear, but it could be related to the increased tendency of the protofibrils in this sample to associate if longer protofibrils are selectively incorporated into these larger aggregates.

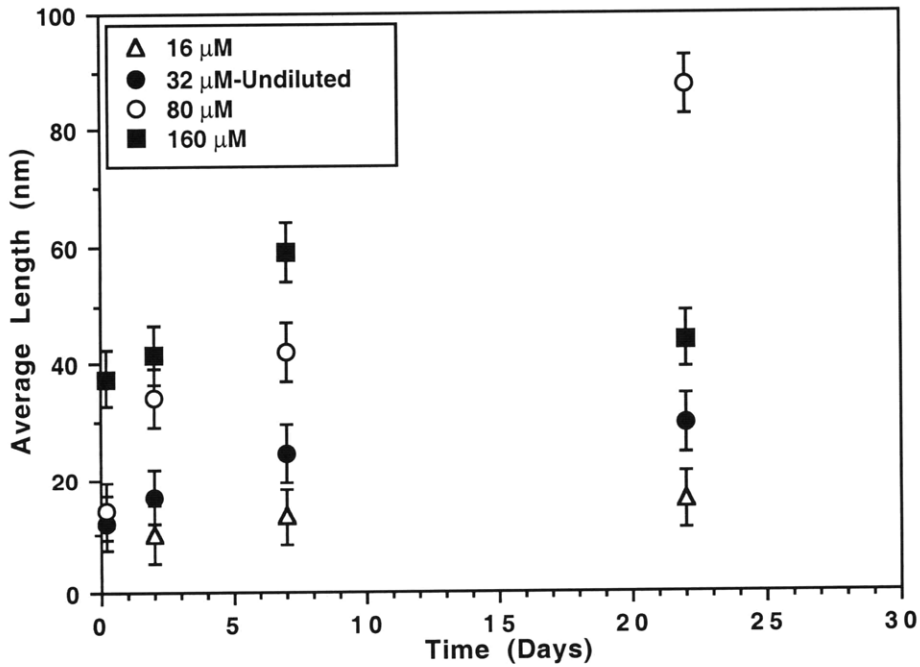
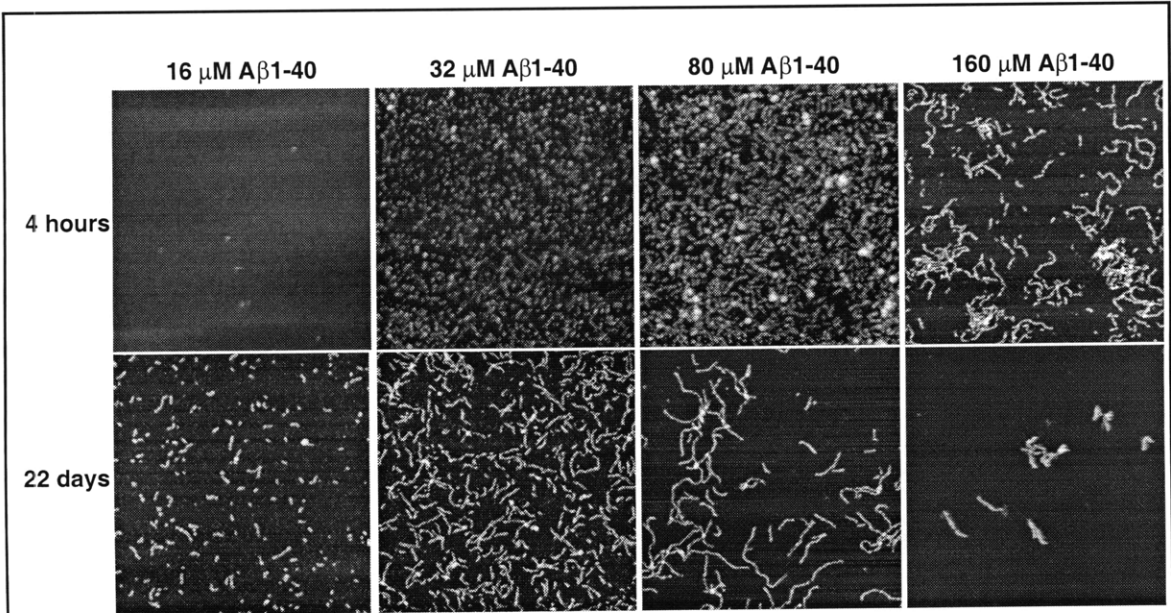
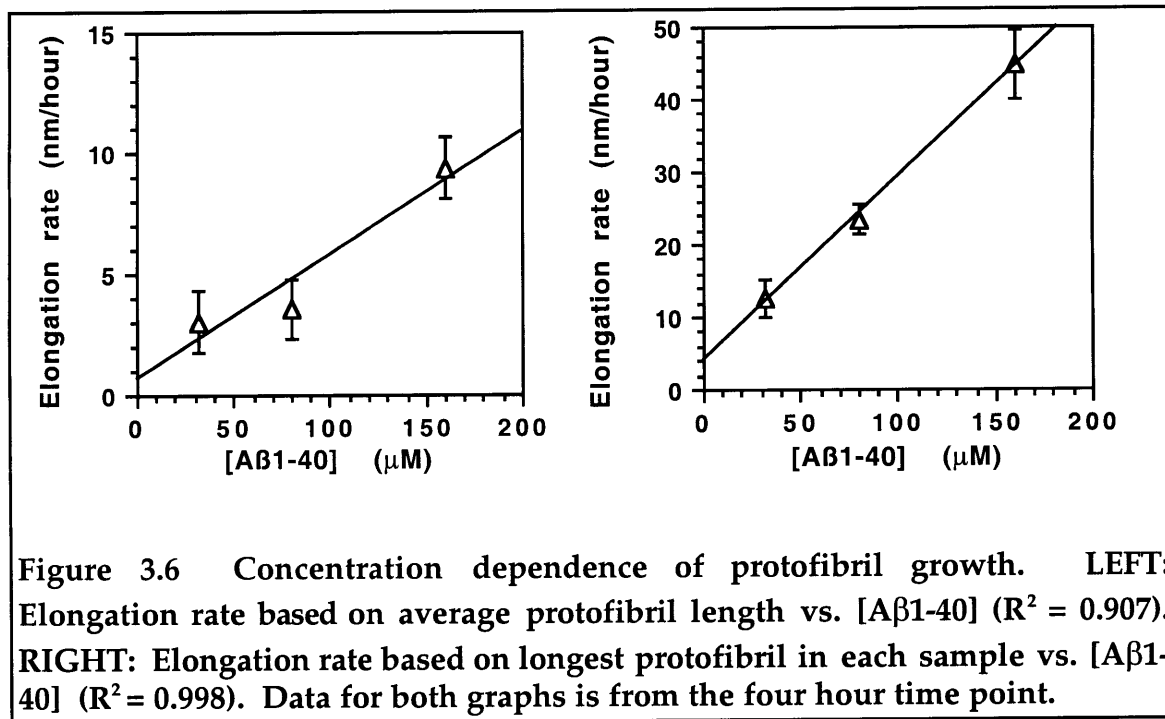


Figure 3.5 Time course of protofibril growth at different Aβ1-40 concentrations. TOP: AFM images of protofibrils formed at the indicated times and Aβ1-40 concentrations. The 80 μM and 160 μM samples were diluted to 16 μM for specimen preparation, and the 16 μM and 32 μM samples were used without dilution. All images are 1 μm square. BOTTOM: The average protofibril length as a function of time for each concentration.

To obtain estimates of elongation rates based on the average protofibril length, we used the earliest 4 hour time point and assumed a protofibril length of 0 nm at  $t = 0$ . We then divided the average length of protofibrils for each concentration by 4 to give the estimated elongation rate in nm/hour (the errors represent the estimated  $\pm 5$  nm error of the average protofibril length divided by 4). Since protofibrils were not numerous enough to accurately determine an average length in the 16  $\mu\text{M}$  sample at 4 hours the calculation was only made for the three remaining samples and yielded values of  $3.0 \pm 1.3$  nm/h at 32  $\mu\text{M}$ ,  $3.5 \pm 1.3$  nm/h at 80  $\mu\text{M}$ , and  $9.4 \pm 1.3$  nm/h at 160  $\mu\text{M}$ . Only the 160  $\mu\text{M}$  sample showed a significant increase in elongation rate using these methods. These values are plotted as a function of A $\beta$ 1-40 concentration in Figure 3.6.

The longest protofibril present in these samples at 4 hours was  $50 \pm 10.6$  nm for the 32  $\mu\text{M}$  sample,  $94 \pm 7.9$  nm for the 80  $\mu\text{M}$  sample and  $179 \pm 19.2$  nm for the 160  $\mu\text{M}$  sample. These values are much higher than would be predicted by the estimated elongation rates based on the average protofibril length, and as discussed previously, may be more accurate representations of the protofibril elongation rate since they are not biased by the presence of shorter protofibrils which may be continuously formed during the measurement period. Plotting the elongation rate calculated based on these values as a function of A $\beta$ 1-40 concentration (Figure 3.6) shows a linear ( $R^2 = 0.998$ ) relationship between elongation rate based on the longest protofibril and the A $\beta$ 1-40 concentration. The linear dependence of protofibril growth

rates (based on the longest protofibril measurements) on the initial A $\beta$ 1-40 concentration suggests that protofibril growth does occur by sequential addition of an A $\beta$  species.

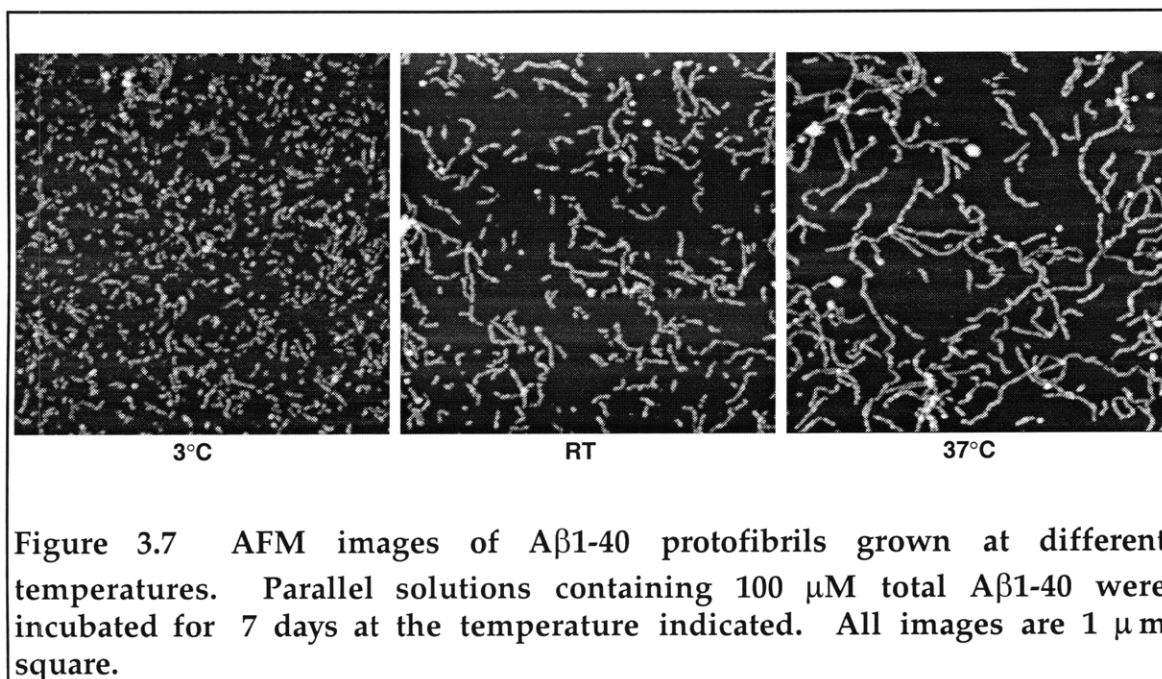


The concentration-dependence of seeded A $\beta$  aggregate (presumably fibril) growth *in vitro*, has been measured by following increases in thioflavine T fluorescence<sup>5</sup>, and incorporation of radiolabeled A $\beta$ 1-40 into brain-derived<sup>6</sup> and synthetic<sup>7</sup> amyloid. In each of these studies, a linear relationship was observed between the A $\beta$ 1-40 concentration and the rate of growth leading the authors to propose that seeded fibril growth occurs via sequential incorporation of monomeric A $\beta$  to growing fibril ends.<sup>5-7</sup> Our results are consistent with a similar first order mechanism for protofibril

elongation, but it is not clear whether monomeric A $\beta$  is the assembly substrate. Because multiple distinct small globular species are observed in these solutions by AFM (which may represent A $\beta$ 1-40 monomer and/or small oligomers), monitoring growth rate alone without the ability to measure changes in the quantity of each possible assembly species cannot establish the identity of the assembly substrate. Although this analysis is not possible using AFM analysis of protofibril growth, it may be possible with other techniques including analytical ultracentrifugation analysis which have the potential to separate and quantitate the species present in aggregating solutions of A $\beta$ .

*Temperature-dependent elongation of protofibrils.*

Protofibril growth was monitored in identical solutions of A $\beta$ 1-40 (100  $\mu$ M) which were incubated at 3°C, room temperature (averaging 18°C), and 37°C to probe the effect of temperature on the process. AFM images of these samples reveal obvious increases in protofibril lengths with increasing temperature at each time point examined (representative time point shown in Figure 3.7).



The average length of protofibrils from each of these images is plotted as a function of time in Figure 3.8. Both the average length at each time point and the rate of increase of the average length with time were found to depend on temperature as follows:  $37^{\circ}\text{C} > 18^{\circ}\text{C} > 3^{\circ}\text{C}$ . Incubation of protofibrils ( $40\ \mu\text{M}$   $\text{A}\beta 1\text{-}40$ ,  $t = 9$  days) grown at room temperature for 15 minutes at  $3^{\circ}\text{C}$ , or  $37^{\circ}\text{C}$  just prior to specimen preparation did not significantly change the average protofibril lengths for these samples (38.2 nm for the  $4^{\circ}\text{C}$  specimen, 44.6 nm for the RT specimen, and 39.0 nm for the  $37^{\circ}\text{C}$  specimen). Therefore, the differences in average length most likely reflect differences in assembly rate and were not caused by temperature dependent adsorption effects on the observation of average protofibril length.

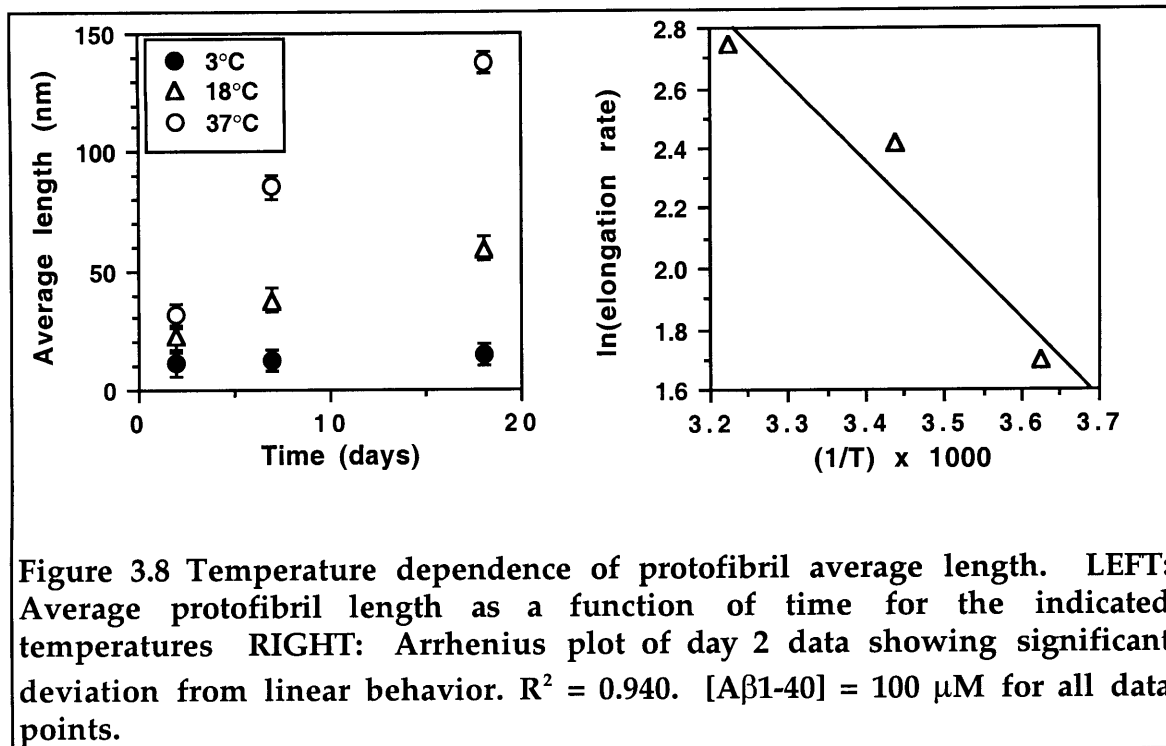
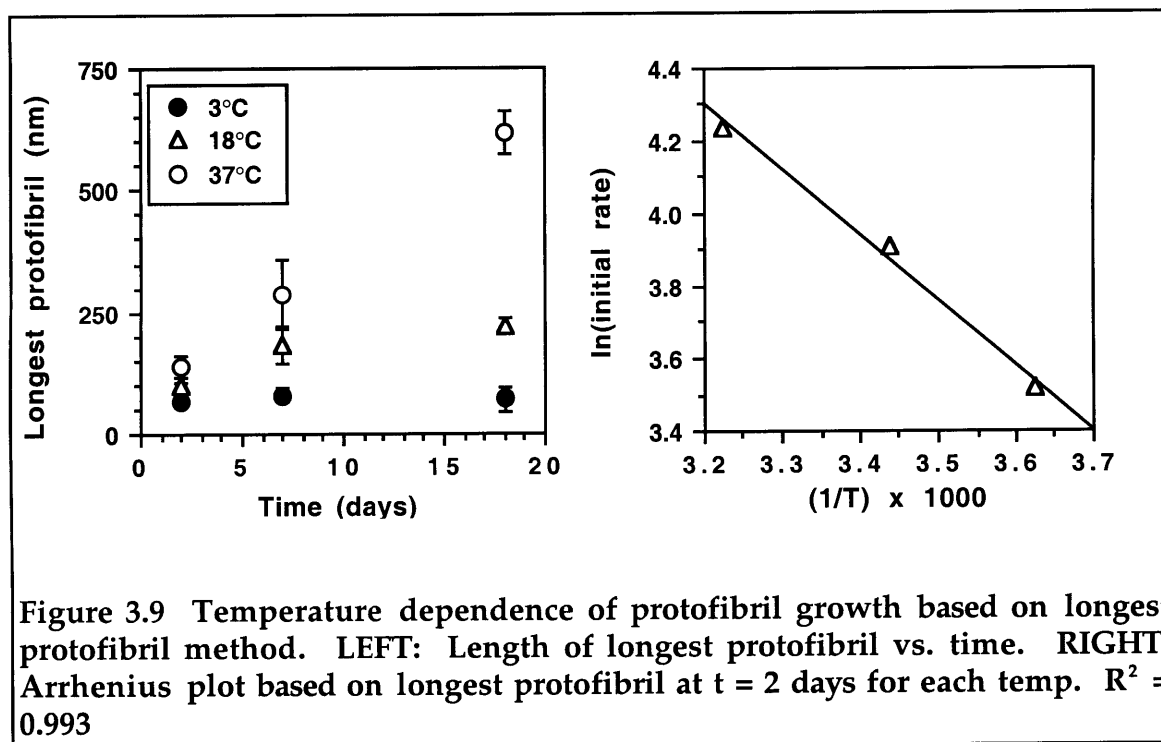


Figure 3.9 shows the lengths of the longest protofibrils found in the specimens and an Arrhenius plot of the natural log of the average growth rates based on these values versus the reciprocal of the absolute incubation temperature (the elongation rate was based on the longest protofibrils in the specimens after 2 days and calculated as described above except that values and errors are divided by 2 and represented in units of nm/day). The data from the previously mentioned control experiment for temperature dependent effects on protofibril average length was re-examined to test whether temperature changes just prior to adsorption altered the length of the longest protofibril observed. The longest protofibril lengths found were;  $140 \pm 8\text{nm}$  at  $3^\circ\text{C}$  ,  $152 \pm 21\text{ nm}$  at  $18^\circ\text{C}$ , and  $148 \pm 8\text{ nm}$  at  $37^\circ\text{C}$ . As was the case for average protofibril length, the temperature of the sample at the time it is

applied to mica does not significantly alter the length of the longest protofibril observed.



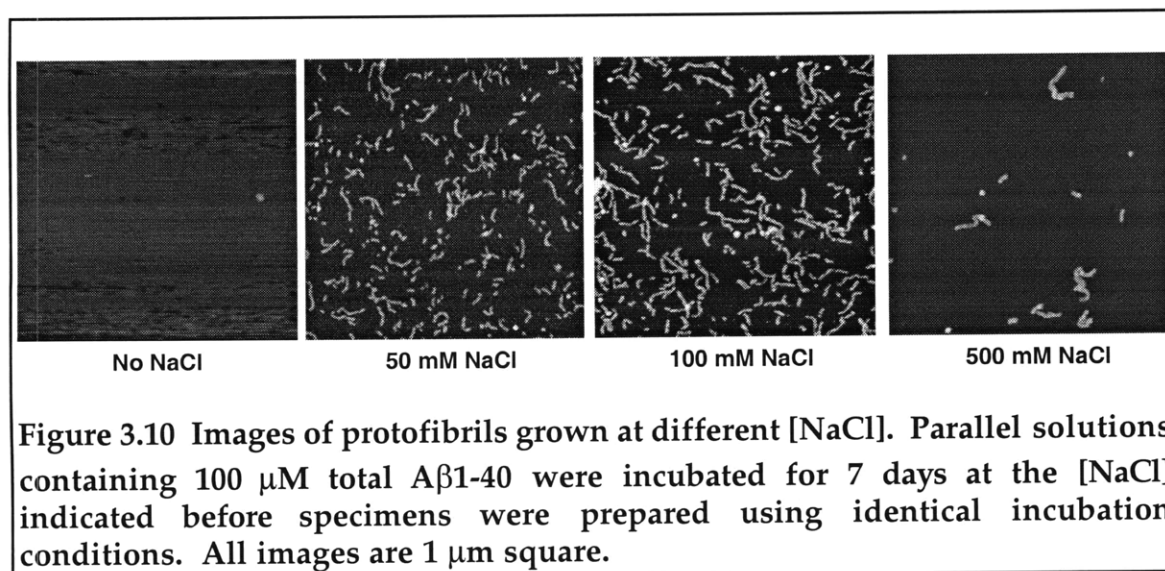
The Arrhenius plot based on the longest protofibril length shows good linearity over the temperature range examined and is a better fit than that obtained from the average length data. Although Arrhenius behavior for protofibril growth in the temperature range we investigated has not been confirmed by other methods, the improved fit for the longest protofibril derived rate data provides another indication that measuring average protofibril lengths provides less reliable rate data. Since we do not know the number of A $\beta$  molecules in a given length of protofibril, the observation of

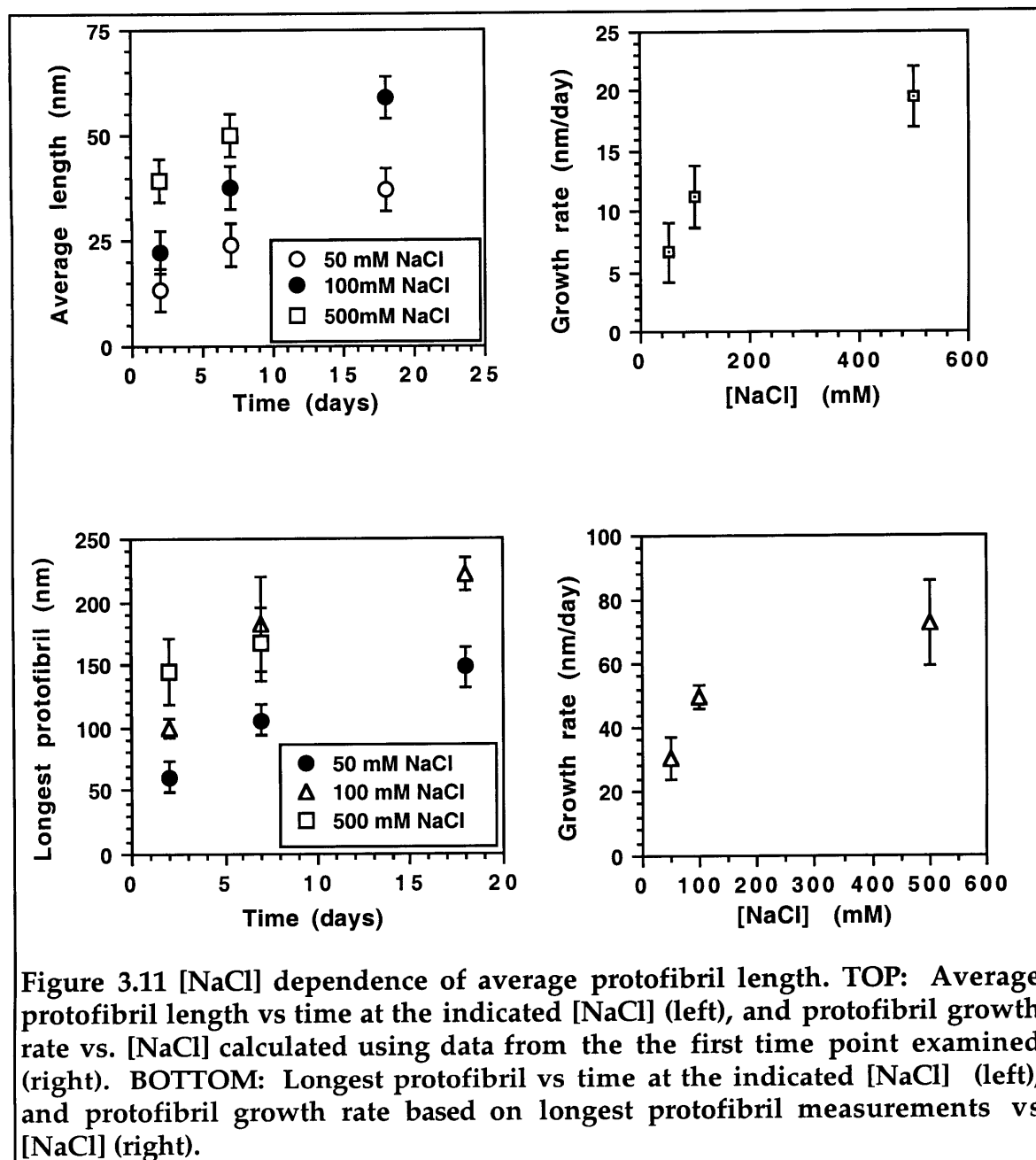


Arrhenius behavior does not allow us to make a meaningful estimate of the activation energy of protofibril growth.

*Ionic strength-dependent protofibril growth.*

Aggregation of 100  $\mu\text{M}$  A $\beta$ 1-40 at room temperature was followed in 100 mM phosphate buffer (pH 7.4) containing varying amounts of NaCl (no added NaCl and 50, 100, or 500  $\mu\text{M}$  added NaCl). Representative images of these samples are shown in Figure 3.10. For the sample without NaCl, there was very little evidence of aggregation--protofibrils were observed only observed at incubation times  $\geq 7$  days and then only occasionally ( $\sim 5$  protofibrils per  $\mu\text{m}^2$ , lengths  $\leq 50$  nm).





Protofibrils were common and well dispersed at all time points examined for the samples containing 50 and 100 mM NaCl. However, at 500 mM [NaCl] protofibrils were observed at early time points to form large disordered mats. Possibly as a result of this clumping, isolated individual protofibrils were observed less frequently with time making it impossible to

determine length averages by day 18. Where sufficient protofibrils were observed to determine the average protofibril length and the length of the longest protofibril possible, the data indicated that average protofibril lengths increased significantly with NaCl concentration and time (Figure 3.11). Growth rates calculated from both sets of data at 2 days also increased significantly with [NaCl].

Abundant literature precedent exists for ionic strength being of critical importance for biological specimen adsorption on mica (See for example Hansma et al.,<sup>8</sup> and Muller et al.<sup>9</sup>). As a result, the absence of protofibrils on the specimens made from samples without added NaCl in the buffer does not necessarily indicate that protofibrils are not forming in those solutions. To test whether NaCl concentration influences the length of protofibrils adsorbed to mica, protofibrils from the same 100  $\mu\text{M}$  A $\beta$ 1-40 solution were diluted into buffer containing 50, 100, and 500 mM NaCl (final A $\beta$ 1-40 = 25  $\mu\text{M}$ ) for 30 seconds before preparing specimens for AFM analysis. The average length of protofibrils and the length of the longest protofibril was determined for each specimen and the results are summarized in table 3.3 below. The NaCl concentration during specimen preparation did not cause significant differences in the average protofibril length or the length of the longest protofibril.

**Table 3.3 The effect of NaCl concentration on protofibril adsorption. Aliquots containing protofibrils from the same 100  $\mu$ M A $\beta$ 1-40 solution were diluted into buffer containing 50, 100, and 500 mM NaCl (final A $\beta$ 1-40 = 25  $\mu$ M) for 30 seconds before preparing specimens for AFM analysis of protofibril lengths.**

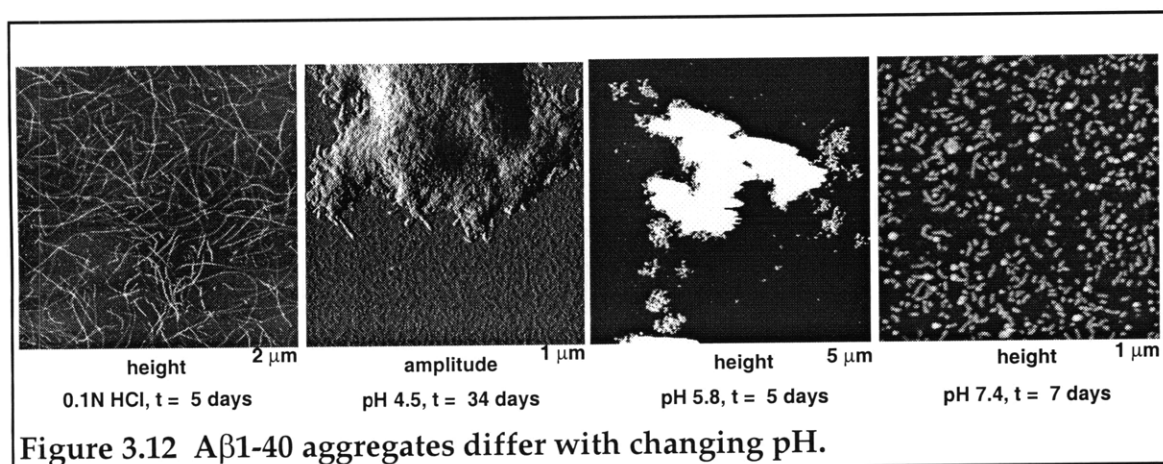
[NaCl]	50 mM	100 mM	500 mM
<b>Average Length</b>	38.4 $\pm$ 5 nm	47.4 $\pm$ 5 nm	39.2 $\pm$ 5 nm
<b>Longest Protofibril</b>	180 $\pm$ 50 nm	167 $\pm$ 32 nm	154 $\pm$ 21 nm

*Protofibril growth at acidic pH.*

We compared the aggregation of 50  $\mu$ M A $\beta$ 1-40 at pH 1.0 (0.1 N HCl, used previously in dynamic light scattering investigations of fibril growth kinetics)<sup>10</sup> pH 4.5 (10 mM acetate-buffered saline), pH 5.8 (10 mM MES-buffered saline),<sup>11</sup> and pH 7.4 (10 mM phosphate-buffered saline) (saline = 137 mM NaCl, 27 mM KCl). Within 5 days following dilution there were visible differences in the solutions with the solutions at pH 4.5 and 5.8 containing flocculent precipitate while the at pH 1.0 and pH 7.4 remained clear (similar observations have also been reported by Wood et al. for pH 5.8 solutions).<sup>11</sup> AFM images of specimens prepared from these samples are shown in Figure 3.12.

The pH 1.0 sample contained long filaments (lengths commonly  $\geq$  1 $\mu$ m) that showed little evidence of association/clumping and had significantly smaller diameters than fibrils formed at pH 7.4 (3-4 nm at pH 1, compared to 8-9 nm at pH 7.4). In contrast, the samples at pH 4.5 and pH 5.8 both produced specimens characterized by very large masses of material (often

as large as 5  $\mu\text{m}$ ) that displayed features closely resembling protofibrils extending from their periphery. In all cases the appearance of the aggregates formed differed significantly from those formed in phosphate buffered saline at pH 7.4. Because of the rapid formation of very long aggregates at pH 1 and the association of protofibrils into large masses at pH 4.5 and 5.8, it was not possible to compare elongation rates using length measurements.



Previous investigations of A $\beta$  aggregation as a function of pH have indicated that maximal aggregation in unseeded A $\beta$ 1-40 solutions (as determined by detection of beta sheet,<sup>12,13</sup> turbidity,<sup>14</sup> Congo red binding,<sup>11</sup> and thioflavine T binding<sup>5,11</sup>) occurs between pH 5 and pH 6. Wetzel and coworkers have demonstrated that aggregates formed at pH 5.8, in contrast to fibrillar pH 7.4 aggregates, were much more amorphous but sometimes appeared in electron micrographs as large (widths in the 100 nm range) bundles of small filaments.<sup>11</sup> Interestingly, according to Wetzel et al., the

non-fibrillar pH 5.8 aggregate was unable to seed fibril formation at pH 7.4 or convert to fibrils when the sample was adjusted to pH 7.4.<sup>11</sup>

## SUMMARY

The temporal increases in protofibril lengths reported here are in good agreement with the time-dependent increase in the amount of protofibrils observed using size exclusion chromatography.<sup>1</sup> In addition to providing complementary information about the progress of protofibril formation, AFM analysis provides the ability to directly detect changes in aggregate morphology that could result from changing aggregation conditions.<sup>11</sup> This additional capability ensures that comparisons made between protofibril formation over a variety of conditions are based solely on changes in the formation of protofibrils and not other assemblies with similar physical behavior.

We have also observed significant increases in the rate of protofibril elongation with increasing A $\beta$ 1-40 concentration, temperature, and ionic strength. These observations increase the range of conditions where protofibril formation is observed and provide further support for the involvement of this species in unseeded A $\beta$ 1-40 aggregation *in vitro*. We have also observed that the morphology of A $\beta$ 1-40 aggregates depends on the pH at which they were formed as previously reported.<sup>11</sup>

These AFM analyses do not by themselves provide conclusive evidence to support detailed interpretations of the molecular mechanism for protofibril formation and growth. Determination of the molecular events involved in amyloid formation will require both qualitative demonstration of the structure and assembly relationship of the various species present during fibril formation and quantitative understanding of the changing population of each distinct species present during the formation and growth of protofibrils and fibrils. The ability of AFM to observe RNA polymerase activity in real time<sup>15</sup> suggests that it may be possible to obtain useful information by following the growth of single protofibrils and fibrils on a substrate in an aqueous environment if current limitations in lateral resolution and substrate binding in fluid for A $\beta$  can be overcome. This analysis could distinguish between steady elongation expected for sequential incorporation of monomeric A $\beta$  and quantized increases in length that should result from incorporation of discrete oligomeric intermediates. Recently, we have achieved significant improvements in resolution for AFM imaging of biological specimens using carbon nanotube tips in collaboration with Stanislaus Wong and Charles Lieber,<sup>16</sup> and progress toward achieving stable adhesion in fluids is being made in our lab. Analytical ultracentrifugation methods for analyzing the association state of small peptides<sup>17</sup> have been described which may be able to provide information about the changing populations of the species we have observed by AFM.

## **Experimental**

### **Protein substrate**

Synthetic A $\beta$ 1-40 was purchased from Quality controlled Biochemicals Inc. (Hopkinton, MA).

### **Preparation of seed-free A $\beta$ 1-40 stock solutions**

Stock solutions of A $\beta$ 1-40 in dimethyl sulfoxide (DMSO) were prepared at concentrations of 12 to 15 mg/ml. The peptide solution was then sonicated for 5 - 10 min and filtered through a 0.2  $\mu$ m nylon micro-spin filter (Whatman Inc., Clifton, NJ) to remove any undissolved seed. Final peptide concentrations of the DMSO stock solutions, as determined by quantitative amino analysis, were typically 2-2.5 mM.

### ***In vitro* aggregation of A $\beta$ 1-40.**

A $\beta$  aggregation was initiated by adding an aliquot of a concentrated DMSO stock of A $\beta$ 1-40 to aqueous buffer (10 mM phosphate, 137 mM NaCl, 27 mM KCl, pH 7.4, unless otherwise specified) followed by immediate vortexing to mix thoroughly. For experiments investigating the concentration dependence of protofibril elongation, DMSO in the aggregation buffer was kept constant ( $\leq$  5% by volume) by adding DMSO to the sample buffer of the less concentrated A $\beta$ 1-40 solutions to make sure that any effect of DMSO on



the rate of assembly would be the same in each sample. After initial mixing the solutions were incubated at room temperature without further agitation except for the minimal disturbance caused by removing aliquots for AFM analysis.

### **General methods for AFM analysis**

*Specimen preparation.* AFM specimens were prepared by removing 3-5  $\mu\text{L}$  aliquots from peptide suspensions and placing them on freshly cleaved mica (Ted Pella Inc., Redding, CA). After incubating for between 30 seconds and 2 minutes, the remaining suspension was removed by rinsing twice with 50  $\mu\text{L}$  water to remove salt and loosely bound peptide that can interfere with image quality. Excess water was removed with a gentle stream of difluoroethane (Dust-Off Plus, Falcon Safety Products Inc.) and the samples were stored in a covered container to protect them from contamination until they were imaged (within 1-2 hours).

*Optimization of protofibril adsorption density.* For accurate measurements of the lengths of protofibrils adsorbed to mica, specimens with well dispersed protofibrils are necessary to minimize uncertainty when determining the beginning and end of individual protofibrils for measurements. Protofibril distributions were controlled by diluting the samples immediately prior to specimen preparation and by adjusting the time that the protein suspension was incubated on the mica surface prior to rinsing. Typically, incubating A $\beta$ 1-

40 aggregate suspensions at 15-25  $\mu\text{M}$  for between 30 seconds and 2 minutes produced specimens with protofibril distributions suitable for determining length averages. The amount of dilution and the incubation time were adjusted for each set of samples at the initial time point and were kept constant for all subsequent analyses within that series. Whenever high concentrations of peptide were studied, specimens for AFM were prepared immediately after dilution to the desired concentration (typically 15-25  $\mu\text{M}$ ). Keeping dilution times as brief as possible minimized the possible effects of dilution on protofibril lengths

*Atomic force microscopy.* All images were obtained under ambient conditions with a Nanoscope IIIa Multimode scanning probe workstation (Digital Instruments, Santa Barbara, CA) operating in TappingMode™ using etched silicon NanoProbes™ (probe model FESP, Digital Instruments). Scanning parameters varied with individual tips and samples, but typical ranges were as follows: initial root mean square (RMS) amplitude, 1.6 V; setpoint, 1.1-1.4 V; tapping frequency 70-90 kHz; scan rate 1.5-2 Hz. Consecutive scans were monitored until distortion due to creep or shifts in the slow scan direction were negligible before collecting scans at sizes of 1  $\mu\text{m}$  with the maximum 512 x 512 pixel resolution (occasionally 2  $\mu\text{M}$  scan sizes were used when protofibril adsorption density was too low to find 50 protofibrils in a 1  $\mu\text{M}$  square region).

## **Protofibril length measurements**

*Average protofibril length.* An area containing 50-100 protofibrils was chosen from the original image, and all protofibrils within this region were measured by summing the lengths of short line segments (in top view mode in the Nanoscope software) approximating the curvature of the protofibrils. Globular aggregates measuring  $\leq 20$  nm and showing no evidence of elongation were counted in each region and included in the calculation of average protofibril length as described below. Protofibrils which were not entirely within scanned area were excluded from the measurements unless they extended into an adjacent region where data was collected and could be traced for accurate determination of their lengths. In some instances groups of protofibrils were too intertwined for all of the individual species to be distinguished, so only protofibrils that could clearly be distinguished were included in the average.

Before calculating the average we subtracted 8.5 nm from each measured protofibril length to remove the contribution of tip related broadening artifacts from the measurements. The 8.5 nm adjustment value was obtained experimentally by measuring the average protofibril width at half height ( $12.8 \pm 2.5$  nm) in representative scans from these experiments and subtracting the approximate value for protofibril diameter in the same scans (4.3 nm, Figure 3.3). Each  $\sim 4$  nm globular feature (no evidence of elongation & widths  $< 20$  nm) in the region was listed as a protofibril with length = 4.3 nm. This list was divided by the number of protofibrils +

globular features to yield the average protofibril length. Typical scans used for these measurements were 1  $\mu\text{m}$  square scans captured at highest resolution (512 x 512 pixels), giving a pixel size is  $\sim 2$  nm. The estimated error of  $\pm 5$  nm listed for protofibril average length measurements is based in part on the  $\pm 2$  pixel error of each protofibril measurement ( $\pm 1$  at each protofibril end =  $\pm 4$  nm) and on the variability in repeated length average measurements from the same sample which generally fell within a 5 nm range.

*Length of longest protofibril.* Using the same scans containing the region used for average length measurements, we divided each scan into quadrants and then found and measured the longest protofibril present in each quadrant. We then calculated the average of these lengths and used this value ( $\pm$  the standard deviation of the individual measurements included in the average) to represent the length of the longest protofibril. The averaging method was used instead of relying on the length of a single protofibril to improve confidence that the value obtained is an accurate representation of the longest protofibrils present and to provide some sense of the variability of this measurement.

### References for Chapter 3

1. Walsh, D.M., Lomakin, A., Benedek, G.B., Condron, M.M., and Teplow, D.B. Amyloid beta-protein fibrillogenesis. Detection of a protofibrillar intermediate. *J. Biol. Chem.* **1997**, *272*, 22364-22372.
2. Mitchison, T. and Kirschner, M. Dynamic instability of microtubule growth. *Nature* **1984**, *312*, 237-242.
3. Walker, R.A., O'Brien, E.T., Pryer, N.K., Soboeiero, M.F., Voter, W.A., Erickson, H.P., and Salmon, E.D. Dynamic instability of individual microtubules analyzed by video light microscopy: Rate constants and transition frequencies. *J. Cell. Biol.* **1988**, *107*, 1437-1448.
4. Hotani, H. and Asakura, S. Growth saturation *in vitro* of salmonella flagella. *J. Mol. Biol.* **1974**, *86*, 285-300.
5. Naiki, H. and Nakakuki, K. First-order kinetic model of Alzheimer's beta-amyloid fibril extension *in vitro*. *Lab. Invest.* **1996**, *74*, 374-383.
6. Esler, W.P., Stimson, E.R., Ghilardi, J.R., Vinters, H.V., Lee, J.P., Mantyh, P.W., and Maggio, J.E. *In vitro* growth of Alzheimer's disease beta-amyloid plaques displays first-order kinetics. *Biochemistry* **1996**, *35*, 749-757.
7. Esler, W.P., Stimson, E.R., Ghilardi, J.R., Felix, A.M., Lu, Y.A., Vinters, H.V., Mantyh, P.W., and Maggio, J.E. A beta deposition inhibitor screen using synthetic amyloid. *Nat. Biotechnol.* **1997**, *15*, 258-263.
8. Hansma, H.G. and Laney, D.E. DNA binding to mica correlates with cationic radius: Assay by atomic force microscopy. *Biophys. J.* **1996**, *70*, 1933-1939.
9. Müller, D.J., Amrein, M., and Engel, A. Adsorption of biological molecules to a solid support for scanning probe microscopy. *J. Struct. Biol* **1997**, *119*, 172-188.
10. Lomakin, A., Chung, D.S., Benedek, G.B., Kirschner, D.A., and Teplow, D.B. On the nucleation and growth of amyloid beta-protein fibrils: detection of nuclei and quantitation of rate constants. *Proc. Natl. Acad. Sci. U S A* **1996**, *93*, 1125-1129.
11. Wood, S.J., Maleeff, B., Hart, T., and Wetzel, R. Physical, morphological and functional differences between pH 5.8 and 7.4 aggregates of the Alzheimer's amyloid peptide A $\beta$ . *J. Mol. Biol.* **1996**, *256*, 870-877.
12. Barrow, C.J. and Zagorski, M.G. Solution structures of b peptide and its constituent fragments: Relation to amyloid deposition. *Science* **1991**, *253*, 179-182.
13. Barrow, C.J., Yasuda, A., Kenny, P.T., and Zagorski, M.G. Solution conformations and aggregational properties of synthetic amyloid beta-peptides of Alzheimer's disease. Analysis of circular dichroism spectra. *J. Mol. Biol.* **1992**, *225*, 1075-1093.
14. Snyder, S.W., Lador, U.S., Wade, W.S., Wang, G.T., Barrett, L.W., Matayoshi, E.D., Huffaker, H.J., Krafft, G.A., and Holzman, T.F. Amyloid-beta aggregation: selective inhibition of aggregation in

- mixtures of amyloid with different chain lengths. *Biophys. J.* **1994**, *67*, 1216-1228.
15. Kasas, S., Thompson, N.H., Smith, B., Hansma, H.G., Zhu, X., Guthold, M., Bustamante, C., Kool, E., Kashlev, M., and Hansma, P.K. *Escherichia coli* RNA polymerase activity observed using atomic force microscopy. *Biochemistry* **1997**, *36*, 461-468.
  16. Wong, S.S., Harper, J.D., Lansbury, P.T. Jr., and Lieber, C.M. Carbon nanotubes tips: High resolution probes for imaging biological systems. *J. Am. Chem. Soc.* **1998**, *120*, 603-604.
  17. Schuck, P., MacPhee, C.E., and Howlett, G.J. Determination of sedimentation coefficients for small peptides. *Biophys. J.* **1998**, *74*, 466-474.

## Chapter 4

### **Seeding Behavior and Morphological Clues Lead to an Expanded Model for the A $\beta$ Fibril Assembly Process**

AFM images of early *in vitro* A $\beta$  amyloid fibril formation reveal the existence of a family of elongated A $\beta$  oligomers, of heterogeneous length, which differ from the much longer product fibrils with respect to their height and surface morphology. These oligomers, collectively designated protofibrils, appear well before fibrils are observed, grow over a period of weeks in the absence of agitation and then disappear rapidly as fibrils grow. The protofibril is approximately 3-4 nm in height and has a periodicity of *ca.* 20 nm, as compared to the type 1 fibril which has a height of 7-8 nm and a periodicity of *ca.* 40 nm. Two explanations for the transient appearance of the protofibril were put forward; the protofibril could be an off-pathway "reservoir phase", in rapid equilibrium with monomeric A $\beta$ , or an on-pathway assembly intermediate, from which fibrils are constructed.<sup>1,2</sup> In the latter case, the protofibril would also be expected to be the preferred substrate for fibril growth.

This chapter discusses AFM observations of the seeded polymerization of A $\beta$ 1-40 which provide insight into the role of the protofibril in *in vitro* fibril formation. Analysis of the effect of preassembly on the efficiency of seeded fibril formation and careful examination of fibrillar structures

indicates that the protofibril is likely to be an assembly substrate for fibrils. In addition, decreases in filament flexibility following protofibril incorporation into fibrils and associated increases in filament resistance to denaturation imply that a conformational change may be a driving force in fibril formation. These observations combined with results discussed in the preceding chapters form the basis of a new testable model of *in vitro* fibril formation which may provide insight into amyloid formation *in vivo*.

### **Protofibril elongation and fibril elongation may be distinct processes.**

A $\beta$ 1-40 and A $\beta$ 1-42 follow analogous pathways to the fibril, including the early appearance of protofibrils which elongate and eventually disappear as fibrils grow. Since agitation accelerates fibril formation (Chapter 2), the studies reported herein were performed with as little agitation as possible to maximize our chances of observing the more rapid seeded fibril growth process. In addition, the A $\beta$  variant A $\beta$ 1-40, rather than A $\beta$ 1-42, was used because it forms fibrils after a longer lag phase (Chapter 1, 2), making it easier to observe transient protofibrils and reducing the likelihood that spontaneous nucleation would contribute to our observations.

Although A $\beta$ 1-42 seems to be the pathogenic species in early-onset FAD based on accumulating genetic evidence,<sup>3</sup> pathological observations of the AD brain suggest that A $\beta$ 1-40 also plays a critical role in AD.<sup>4</sup> First, the



increased deposition of A $\beta$ 1-40 is characteristic of late-onset AD patients bearing the apoE4 allele which is a susceptibility factor for AD.<sup>5</sup> The postmortem examination of brains of individuals with Down syndrome (DS) also points to the importance of A $\beta$ 1-40 in AD. The brains of DS patients show numerous non-fibrillar A $\beta$ 1-42 containing diffuse plaques as early as 12 years of age.<sup>6</sup> However, pathological evidence of neurodegeneration (dystrophic neurites, activated microglia) did not appear until around age 30, when mature A $\beta$ 1-40 containing plaques also began to appear.<sup>6</sup> Therefore, although A $\beta$ 1-42 appears to be an important initiating factor in early onset forms of AD, the accumulation of A $\beta$ 1-40 may also contribute significantly to the development of neurodegeneration in AD.

### **Evidence from seeding behavior**

Addition of A $\beta$ 1-40 amyloid fibrils to a supersaturated solution of A $\beta$ 1-40 reduces or eliminates the lag phase prior to aggregation (as detected by turbidity).<sup>7-9</sup> AFM analysis shows that the conversion of a freshly diluted supersaturated A $\beta$ 1-40 solution (100  $\mu$ M) to amyloid fibrils at room temperature was similarly accelerated (Figure 4.1) by the addition of an aliquot from an A $\beta$ 1-40 solution containing a mixture of fibrillar morphologies but no protofibrils (Figure 4.1). The total amount of A $\beta$ 1-40 in the seed aliquot was *ca.* 1% the amount present in the supersaturated

solution. No fibrils were observed when the same amount of fibrils was diluted into buffer alone and used to produce specimens, so the appearance of fibrils can be attributed to new fibril growth and not just the detection of the seed material. In the seeded conversion, fibrils were clearly visible after 3 days; in the absence of seed, fibrils generally did not appear until at least 15 and usually > 21 days had elapsed. Protofibrils were no longer present in specimens prepared from the seeded conversion by 14 days; in the absence of seed, protofibrils were still present along with fibrils after 30 days.

In a separate experiment, starting with a similar solution of A $\beta$ 1-40 (100 $\mu$ M, freshly diluted), addition of an aliquot (also containing *ca.* 1% the amount present in the supersaturated solution) from a solution containing protofibrils, but no fibrils (by AFM), resulted in no observable fibril growth by 4 days following the addition of the protofibrillar seed (Figure 4.2, center). A parallel sample seeded with the same amount of A $\beta$ 1-40 in the form of fibrils contained growing fibrils by day 4 (Figure 4.2, right).

Not all fibrillar preparations of A $\beta$ 1-40 were equally effective as seeds in similar experiments. This suggests that either certain fibrillar morphologies are more effective seeds, or that the seeding and incubation conditions used for these room temperature experiments are not optimal for promoting fibril growth. Similar considerations may also explain why the observation of heterogeneous seeding of A $\beta$ 1-40 fibril growth by A $\beta$ 1-42 fibrils has been observed to be very inconsistent (data not shown).

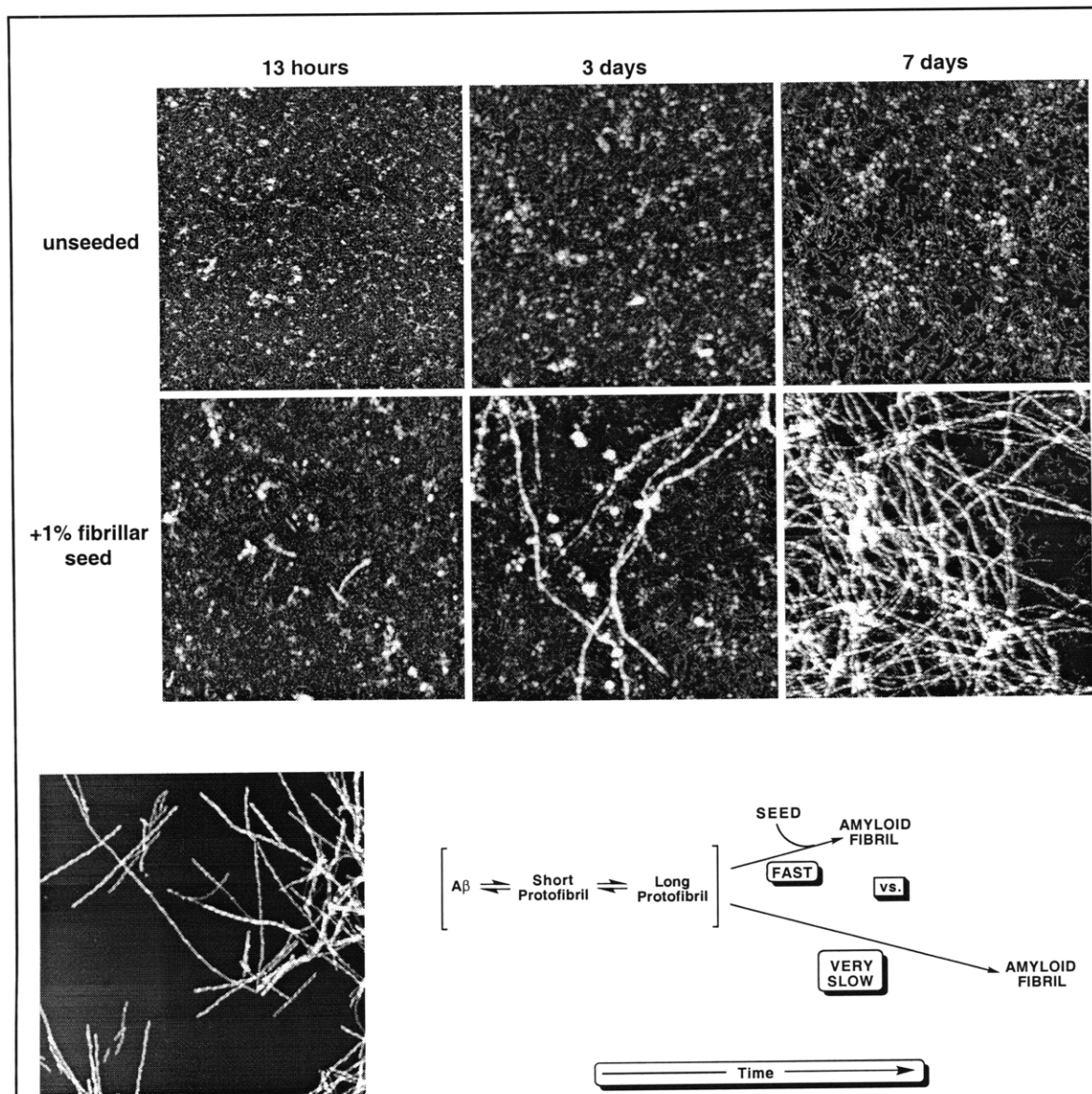
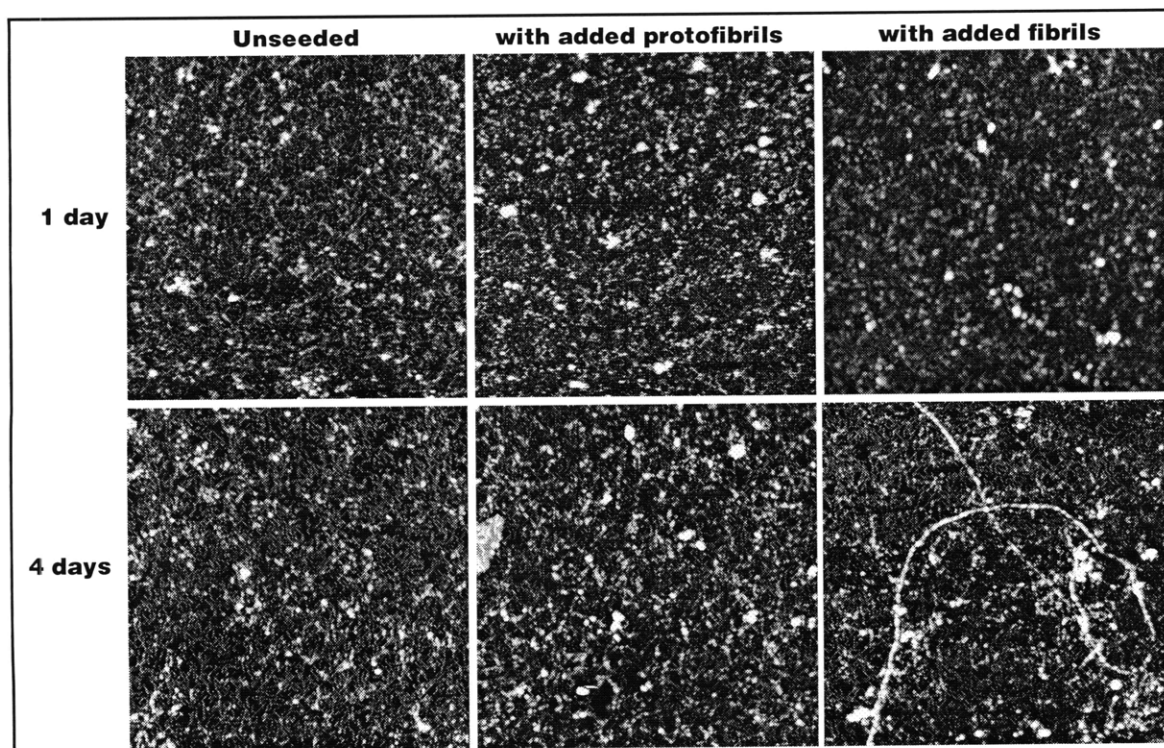


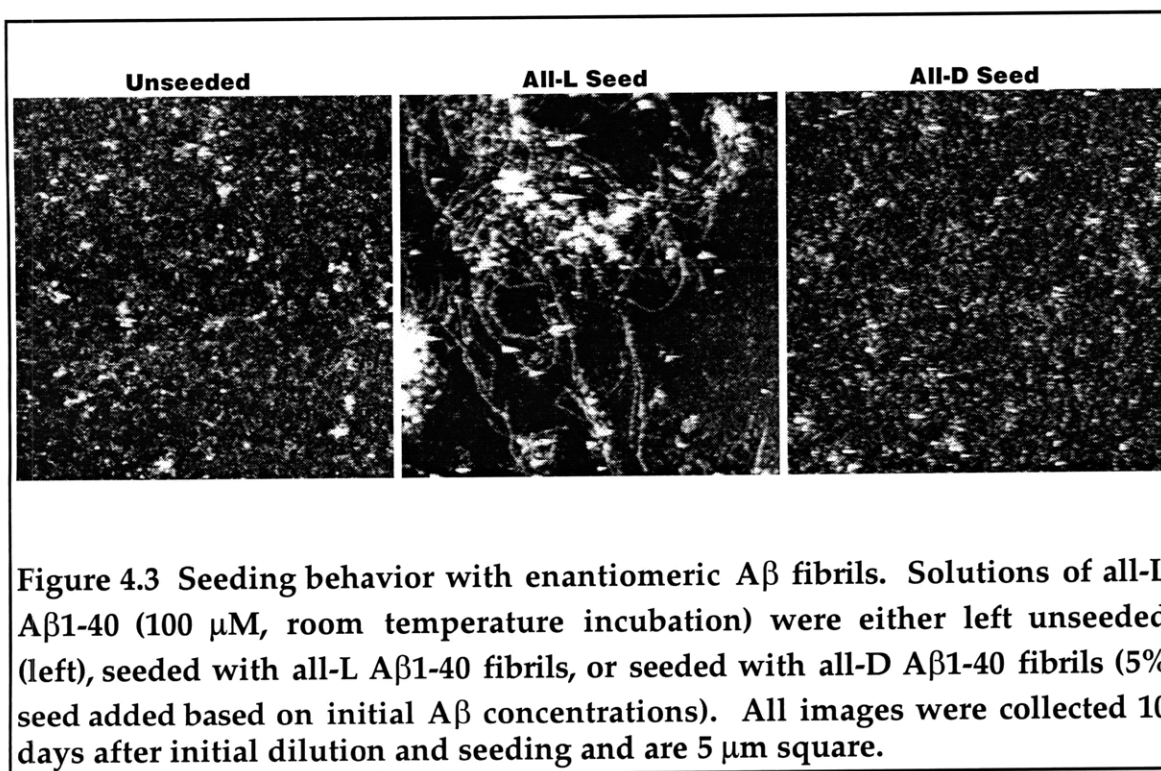
Figure 4.1: Images of unseeded samples and samples seeded with preformed fibrils. TOP ROW: Three AFM images showing snapshots of an unseeded 100  $\mu$ M  $A\beta$ 1-40 at the indicated times after dilution. SECOND ROW: Snapshots at the same times of an identical parallel sample of  $A\beta$ 1-40 that was seeded immediately following dilution with a suspension containing preformed  $A\beta$ 1-40 fibrils but no protofibrils. BOTTOM: An image of a specimen prepared with the seed material used (left), and a mechanistic model (right) showing the key finding--preformed fibrils greatly accelerate the conversion of protofibrils to fibrils. All images are 2  $\mu$ m square.



**Figure 4.2** The effect of adding preformed protofibrils or protofibrils to freshly diluted A $\beta$  solutions. A $\beta$ 1-40 solutions (100  $\mu$ M) were seeded with aliquots of preformed protofibrils (center) or fibrils (right) (the amount of A $\beta$  in the aliquots represented  $\sim$ 1% of the amount in the supersaturated solution). Images are 2  $\mu$ m square.

The seeding behavior of the enantiomeric fibrils was also examined as a control for the specificity of the seeding event. Aliquots of protofibrils formed by each A $\beta$ 1-40 enantiomer (100  $\mu$ M) were separately seeded by adding fibril suspensions (5% of the initial A $\beta$  concentration) formed by either the same or the opposite enantiomer and compared to unseeded control solutions. Acceleration of fibril formation was observed when all-L fibrillar seed material was added to the freshly diluted solution of all-L A $\beta$ 1-40 (Figure

4.3, center). Addition of the same amount of preformed all-D fibrils had no effect. Similarly, for supersaturated solutions of all-D A $\beta$ 1-40 only addition of preformed fibrils made from all-D A $\beta$ 1-40 accelerated fibril formation, while fibrils formed by all-L A $\beta$ 1-40 had no effect (not shown). This is consistent with previous observations of amyloid seeding specificity.<sup>10</sup>



The observation by AFM that the transition of A $\beta$ 1-40 to fibrils can be accelerated by adding preformed fibrillar A $\beta$  aggregates is consistent with previous observations using turbidity of a reduced lag time or nucleation phase for A $\beta$ 1-40 aggregation following addition of preformed fibrillar seed material. Accelerated fibril growth is not observed following the addition of

protofibrils but is only observed when the added material contains filaments and fibrils. This suggests that the rate limiting step or nucleation event in fibril formation is not the formation of protofibrils, but is the process that results in the formation of the first fibril in the supersaturated solution. Furthermore, the ability to selectively accelerate fibril formation implies that the process responsible for fibril formation is fundamentally different from the process responsible for protofibril elongation.

### **Evidence from growth rate estimates**

As described in Chapter 3, an estimate of the elongation rate for a growing filament species can be made by finding the longest filament on a specimen and dividing the change in length by the time elapsed since dilution. A rough estimate of the protofibril elongation rate can be obtained in this way by examining an A $\beta$ 1-40 solution (100  $\mu$ M) incubated for 2.5 days at room temperature before analysis by AFM (left image in Figure 4.4). The maximum protofibril length observed on the specimen was 242 nm. Assuming an initial length for that protofibril of 4 nm (approximately equal to the protofibril diameter), then the estimated protofibril elongation rate under these conditions was 95 nm per day. A similar estimate of the maximum rate of fibril elongation can be made from the observation of fibril lengths in a supersaturated solution of A $\beta$ 1-40 (100  $\mu$ M, pre-incubated 8 days prior to seeding) two days following the addition of fibrillar seed (1% based on initial A $\beta$ 1-40 concentration). Fibrils can frequently be observed to cross an

entire 10  $\mu\text{m}$  square region of the specimen prepared from this sample (right image in Figure 4.4). Assuming an initial fibril length of 5  $\mu\text{m}$  (compare to image of similar seed material shown in Figure 4.1) and limiting the maximum fibril length to the 10  $\mu\text{m}$  scan size provides a conservative estimate for the rate of fibril elongation of 2500 nm per day--a value an order of magnitude greater than the maximum protofibril elongation rate.

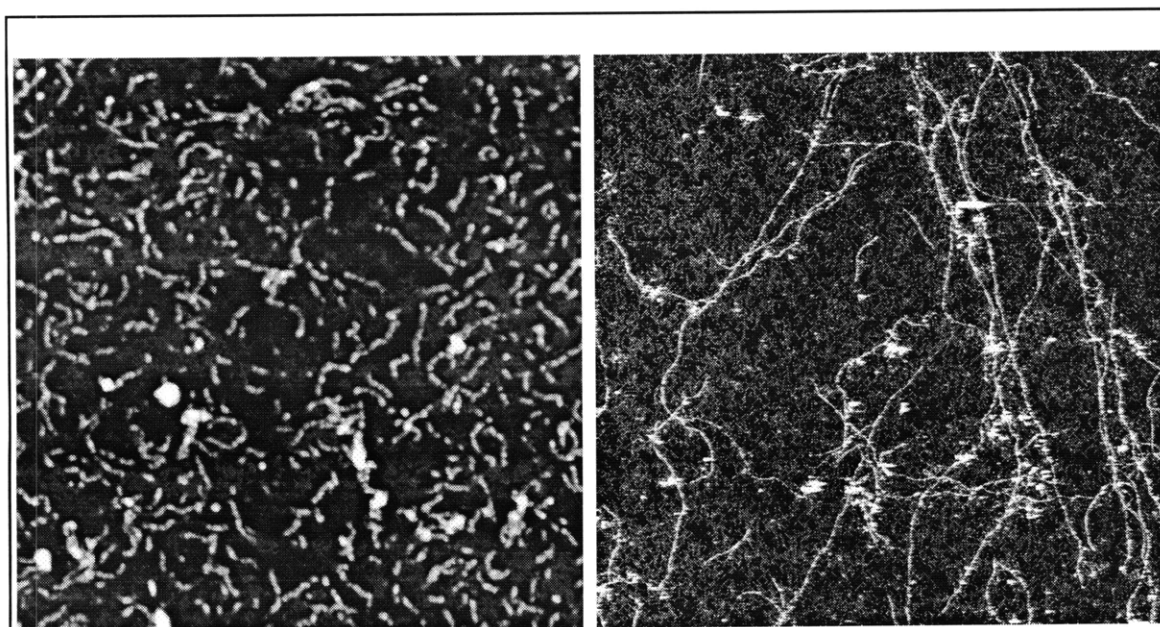


**Figure 4.4** Images used for estimating protofibril and fibril elongation rates. The 2  $\mu\text{m}$  square image on the left shows protofibrils grown by A $\beta$ 1-40 after 2.5 days. The 10  $\mu\text{m}$  square image on the right shows fibrils grown over 2 days following seeding (with 1% preformed fibrils) a solution of A $\beta$ 1-40 (100  $\mu\text{M}$ , preincubated for 8 days prior to seeding).

This dramatic difference in the apparent elongation rate for protofibrils and fibrils, like the seeding behavior discussed above, supports the hypothesis that the growth mechanisms for protofibrils and fibrils are different under these conditions. One possible explanation is that protofibril growth may

occur primarily by addition of monomers or small oligomers of A $\beta$  to the growing protofibril ends while fibril formation may involve direct incorporation of pre-formed protofibrils in addition to monomer and small oligomer incorporation.

## **Evidence that fibrils grow by incorporation of protofibrils**

### **Evidence from the effects of pre-incubation on seeding efficiency**

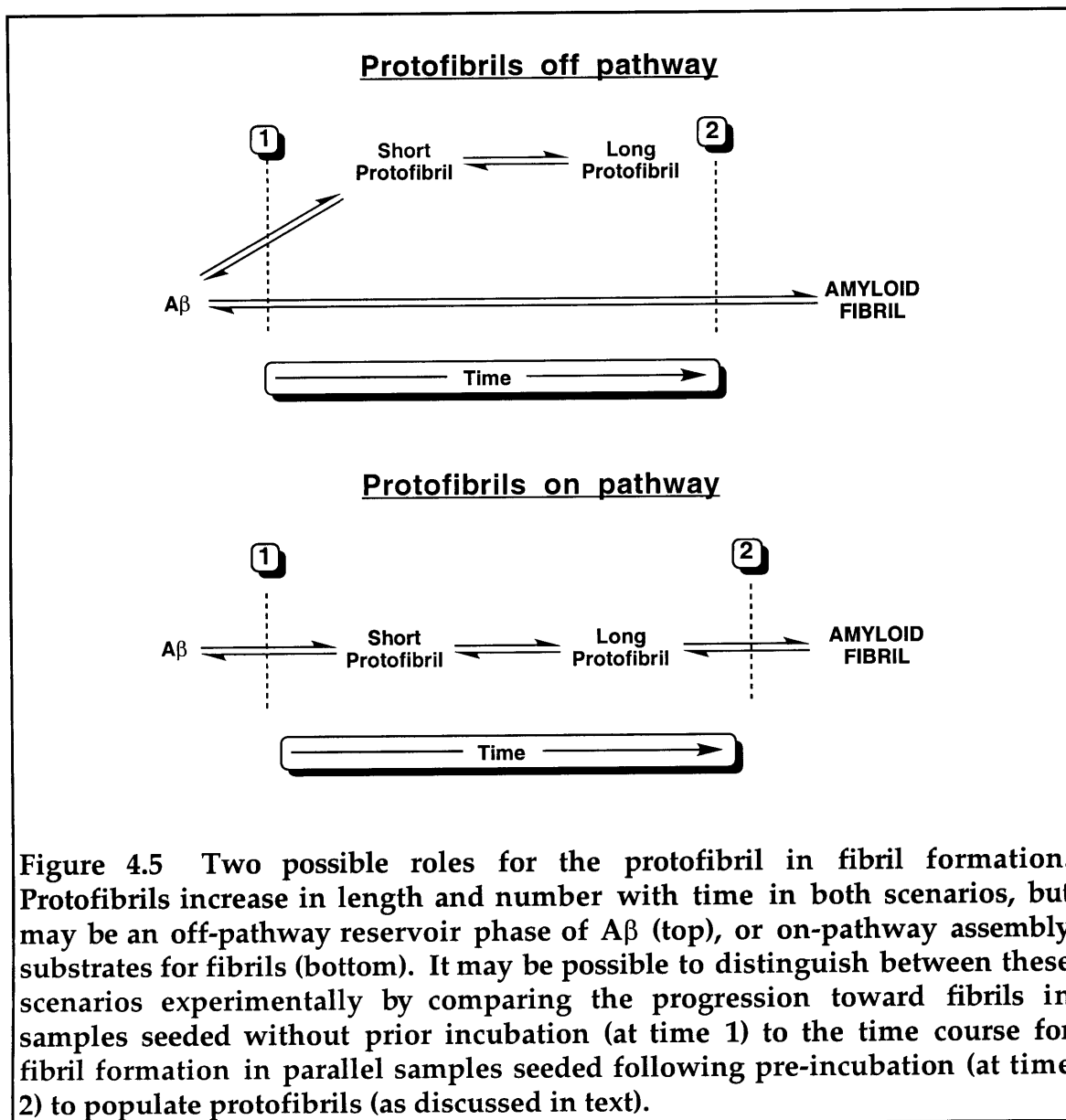
The observation of seeded protofibril-to-fibril conversion (Figure 4.1) does not prove that protofibrils are on-pathway intermediates in fibril formation. Protofibrils could also merely serve as an off-pathway reservoir phase for A $\beta$ . To try to distinguish between these alternatives, we sought to investigate the relationship between protofibril formation/growth and the time course of the seeded conversion (Figure 4.5). Our methodology does not allow us to measure the amount of protofibrils directly (Chapter 3). Therefore, to compare the extent of protofibril formation we instead refer to the relative length of protofibrils, which, like the amount of protofibrillar A $\beta$ <sub>1-40</sub>,<sup>(12)</sup> increases over time (also Chapter 3).

For the off-pathway scenario, the seeded fibril formation rate should show no dependence on the extent of pre-assembly/pre-population (no difference between seeding at time 1 or time 2 in Figure 4.5) if the exchange rate between protofibrillar and monomeric A $\beta$  (or the species responsible for



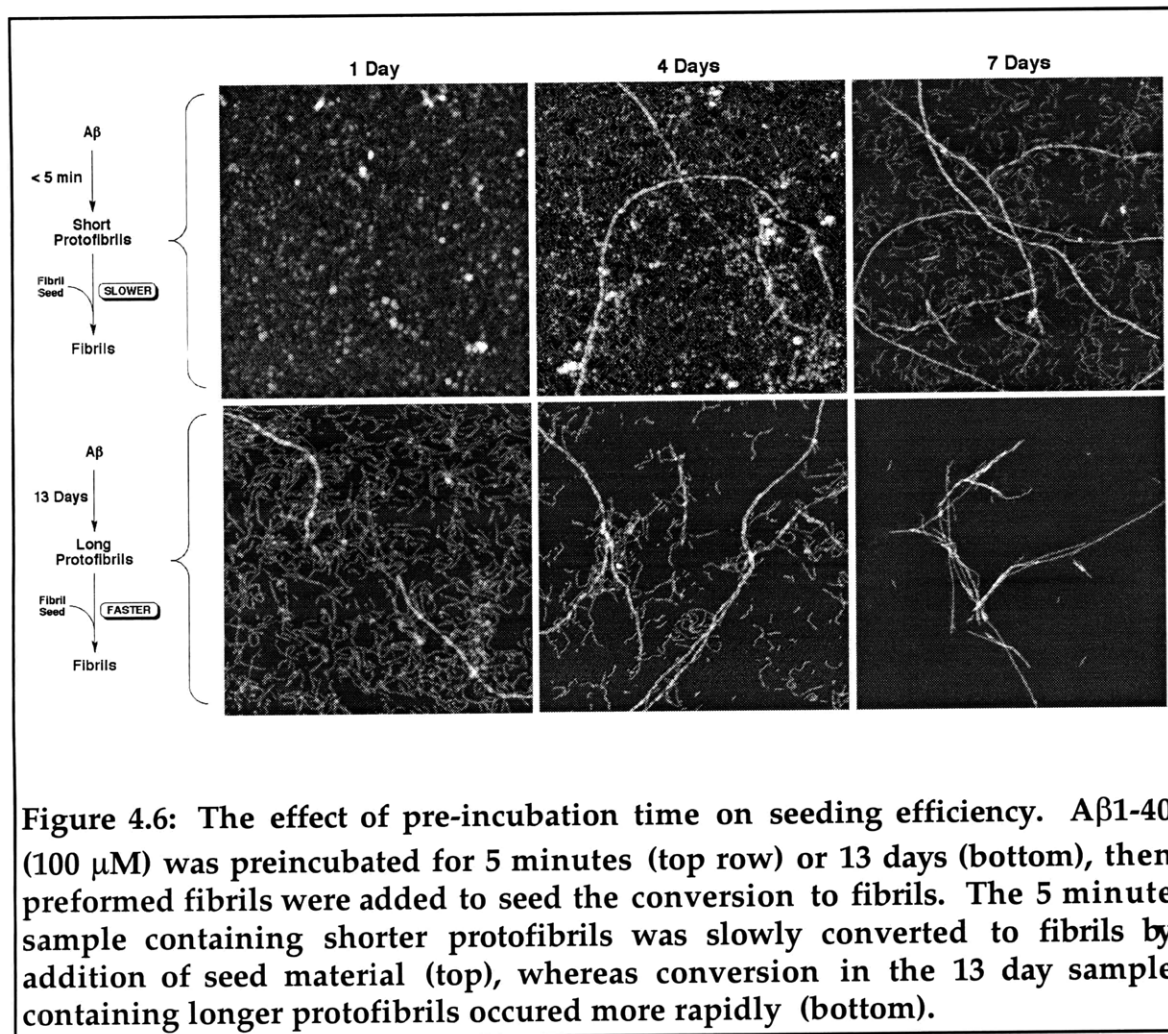
fibril growth) is faster than the rate of incorporation of A $\beta$  into fibrils. Circumstantial evidence suggests, however, that the exchange rate may be relatively slow. When A $\beta$ 1-40 protofibrils are isolated from low molecular weight precursors using size exclusion chromatography and dialyzed against buffer without A $\beta$  using membranes which allow monomeric A $\beta$  but not protofibrils to pass through, fibrils can form inside the dialysis membrane (observed by negative stain EM, Dominic Walsh and David Teplow--unpublished observations). The ability of fibrils to form before the protofibrils disassemble in this dialysis experiment suggests that the protofibril to fibril transition is faster than protofibril dissolution.

For the off-pathway model, slower conversion of preincubated A $\beta$  solutions to fibrils following seeding would be expected if exchange between the protofibrils and the assembly substrate is slow compared to association of the assembly substrate to growing fibrils. However, if protofibrils are assembly substrates in the pathway leading to A $\beta$  fibrils, the effect of preassembly may be reversed. In the on-pathway scenario, pre-incubation would pre-populate a substrate for fibril growth. Therefore, pre-incubation should accelerate the seeded transition to fibrils if growth by incorporation of protofibrils is more productive growth by incorporation of smaller forms of A $\beta$ . However, if all of the species on the pathway (monomers, oligomers(?), protofibrils, etc.) are equally productive substrates for fibril growth, then pre-incubation may have little effect.



As shown in Figure 4.6, the seeded conversion of protofibrils to fibrils occurred much more rapidly from an incubation containing longer protofibrils (Figure 2, bottom panels;  $A\beta$ 1-40 (100  $\mu$ M) was preincubated for 13 days before seeding) as compared to an incubation containing short protofibrils but an equal total  $A\beta$ 1-40 concentration (top panels,  $A\beta$ 1-40 (100

$\mu\text{M}$  was preincubated less than 5 minutes before seeding). In the absence of added seed, fibrils were not observed in the incubation containing short protofibrils after 7 days. One day after seeding the non-pre-incubated solution, no evidence of fibril formation was seen, and only isolated fibrils were seen among protofibrils at 4 days. By 7 days, long fibrils had become more common, but the presence of numerous protofibrils indicated that fibril formation was still not complete (Figure 4.6, top panels).



In contrast, long ( $> 5 \mu\text{m}$ ) fibrils were commonly observed in the pre-incubated solution one day after seeding. The amount of protofibrils on the substrate decreased noticeably by day 4 as fibrils became more numerous. After 7 days, protofibrils were rare and fibril formation appeared to be almost complete (Figure 4.6, bottom panels). Comparing these observations to the hypothetical seeding scenarios discussed above suggests that the accelerated seeded transition to fibrils in preincubated A $\beta$ 1-40 solutions (compared to otherwise identical freshly diluted A $\beta$ 1-40 solutions) is consistent with fibril growth by protofibril incorporation.

Given the clear effect of temperature on protofibril growth (Chapter 3), it is possible that temperature may also have an important effects on the progress of seeded fibril growth as well. We are currently investigating the effects of pre-incubation on seeding behavior at 37°C to see if similar effects are observed at temperatures approximating those found in the body.

**Morphological observations are also consistent with fibril growth by protofibril incorporation**

*Fibrils have an inherent helical twist.*

Images of the type 1 fibril at high magnification clearly show a left-handed helical orientation to the periodic height increases (period =  $\sim 43 \text{ nm}$ ) along the length of type 1 fibrils formed from all-L A $\beta$ 1-40. The top two images of Figure 4.7 show details of a type 1 fibril formed by all-L A $\beta$ 1-40. The helical nature of the periodic height increases along the length of the fibril is

apparent in the height image on the top left. The left-handed orientation of the helix is more clearly resolved in the image on the right generated by plotting simultaneously acquired cantilever oscillation amplitude data which emphasizes rapid changes in height (bright areas correspond to decreases and dark areas to increases in cantilever oscillation amplitude during the scan).

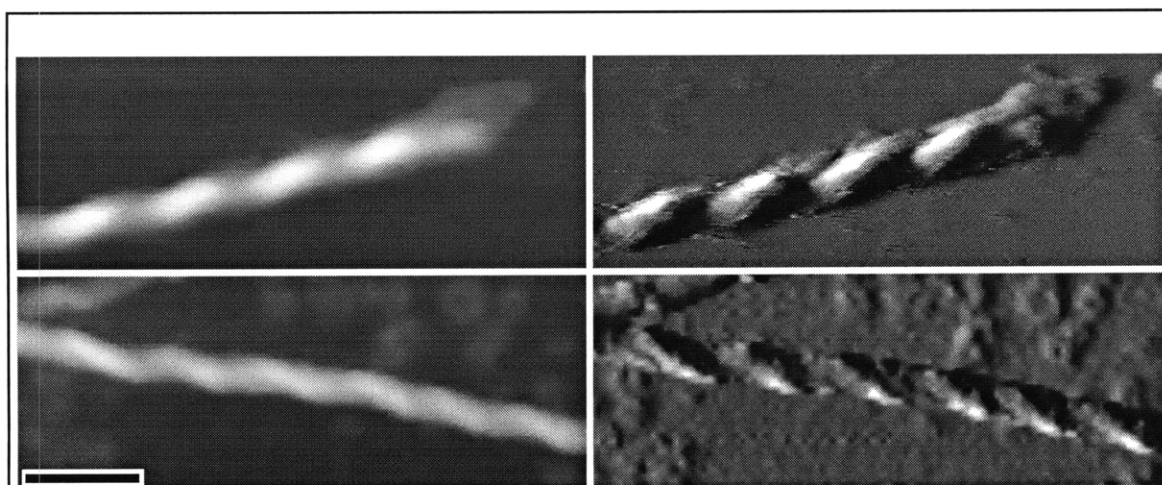


**Figure 4.7 Helicity of A $\beta$ 1-40 type 1 fibrils. Top: Type 1 fibrils formed by all-L A $\beta$ 1-40 imaged in height mode (left) and amplitude mode (right). Bottom: Type 1 fibrils formed by all-D A $\beta$ 1-40 imaged in height mode (left) and amplitude mode (right). Scale bar = 50 nm.**

It is possible that simple beaded objects could have a helical appearance if the tip used to scan them was irregularly shaped, but two separate observations rule out this possibility. First, the observed helicity is the same regardless of orientation of the fibrils in the image (data not shown). Furthermore, type 1 fibrils formed by all-D A $\beta$ 1-40 showed identical periodicity of the height increases and were also clearly helical (Figure 4.7, bottom), but the twist direction was always observed to be right handed

(Figure 4.7, bottom right). Although the fibrils appear to have different widths, the heights of adsorbed type 1 fibrils formed by each peptide are indistinguishable, and width differences of this magnitude are consistent with variations in broadening artifacts caused by differences in tip shape.

The observed helicity is consistent with fibril formation by lateral association and winding of protofibrils or filaments to form the fibril. Dependence of helical handedness on the enantiomer of A $\beta$  forming the fibril indicates that the orientation of winding is not determined randomly, but may arise from specific filament contact orientations or from the structure of the filaments themselves.

*Observation of staggered filaments at type 1 fibril ends.*

As protofibrils disappeared in seeded A $\beta$ 1-40 solutions, type 1 fibrils became the predominant morphology. Images of the ends of type 1 fibrils produced with standard silicon AFM probes were sometimes characterized by what appeared to be staggered termination of filaments (Figure 4.8). Single filament extensions have been observed with lengths of tens of nanometers to a micron or more (some longer examples can be seen in Figure 4.10). These staggered ends could result from imperfect alignment of two protofibrils or filaments during assembly. As filament contacts are maximized during winding, imperfectly aligned filaments would form a type 1 fibril with a single filament extending beyond the end of the shorter protofibril/filament.

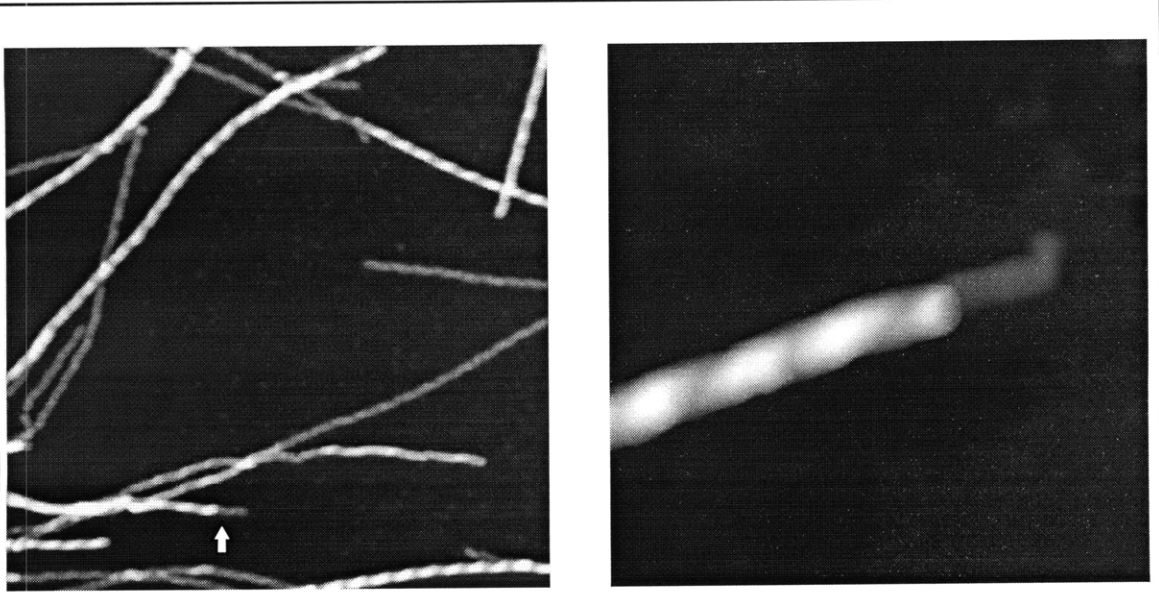


**Figure 4.8 Images of staggered filaments at the end of type 1 fibrils. LEFT: A 1  $\mu\text{m}$  image generated with a standard silicon probe resolves a single filament extending from the end of a type 1 fibril (arrow). RIGHT: A 250 nm image generated using a carbon nanotube tip clearly resolving a short single filament extension and the termination of the shorter filament.**

Utilization of newly developed nanotube probes<sup>11</sup> made by Stan Wong from Professor Charles Lieber's group at Harvard, provides significantly improved resolution of A $\beta$  fibrils.<sup>12</sup> These tips are made by attaching carbon nanotube bundles to the tips of standard silicon AFM probes.<sup>11,12</sup> Imaging with nanotube probes provides improved resolution by decreasing the radius of curvature and increasing the aspect ratio of the tip thereby minimizing the broadening effects caused by tip-sample interactions.<sup>12</sup> The improved resolution made possible with these nanotube tips provides a much clearer image of this feature and clearly shows the terminus of the shorter filament as well as the short extension of the longer filament (Figure 4.8, right).

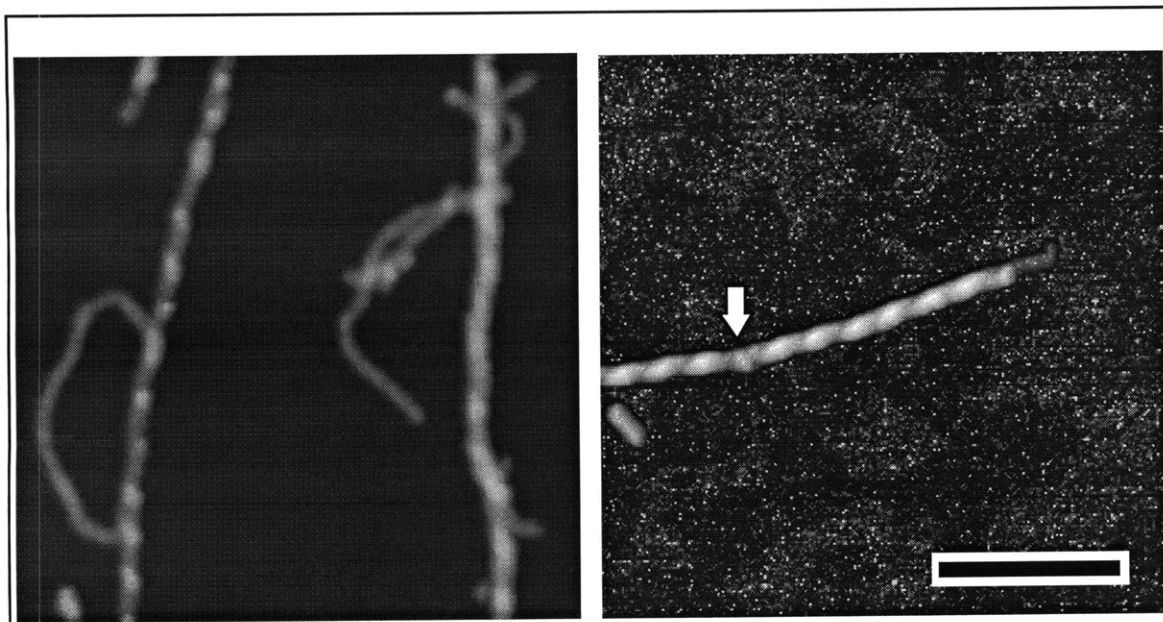


**Figure 4.9 Imperfect winding in type 1 fibrils. LEFT: A 500 nm square image of fibrils generated using a standard silicon probe. RIGHT: Image generated using a nanotube probe--arrow indicates imperfection (scale bar = 200 nm).**

#### *Imperfections in type 1 fibrils*

Type 1 fibrils with closely associated protofibrils commonly appear at intermediate stages of fibril formation when protofibrils are still numerous (for example, see the 4 day image of the pre-incubated sample in figure 4.6). The overall appearance of these features resembles what one would expect to see if protofibrils in the process of winding to form type 1 fibrils were trapped by adsorption to the substrate. However, since protofibrils are still relatively abundant at these time points, one would expect a number of protofibrils to adsorb near fibrils regardless of whether they were actually associated in solution. Sometimes, however, features appearing to be type 1 fibrils trapped in the process of winding can also be seen at much later time points when isolated protofibrils are not observed (Figure 4.9, left image). Protofibrils



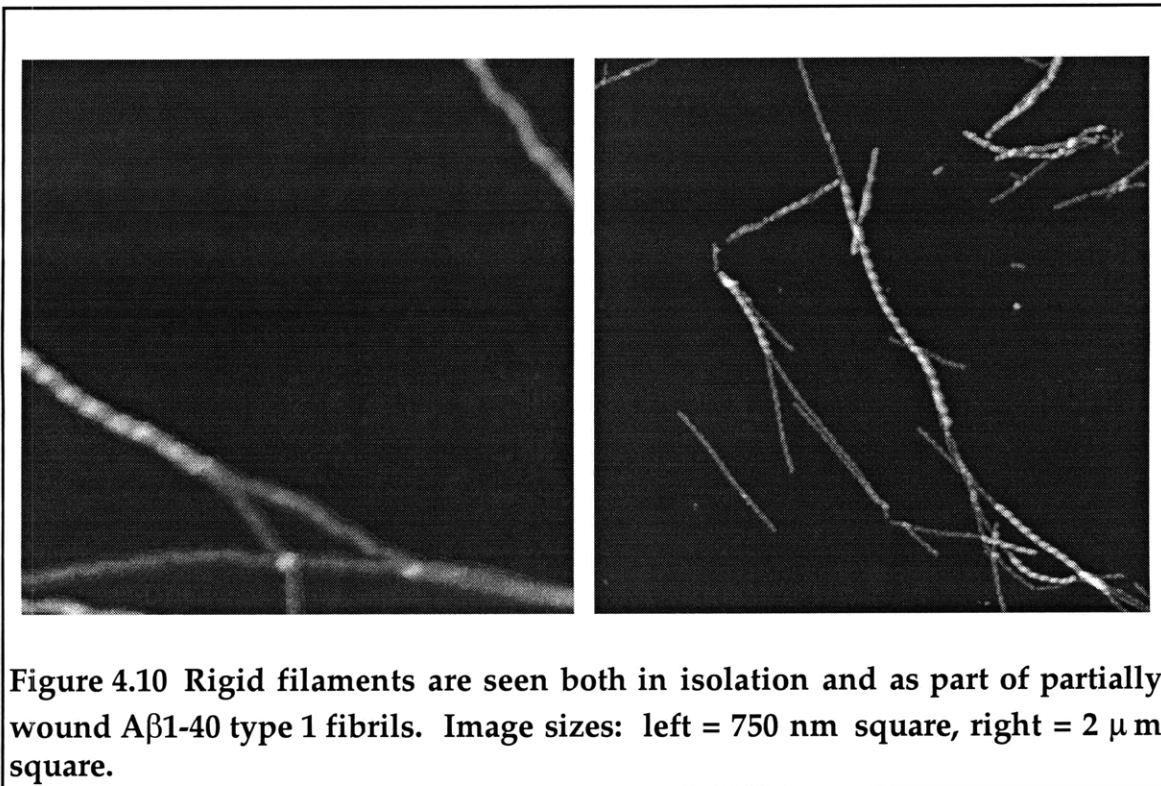
associated to fibrils in features such as this one (from a seeded A $\beta$ 1-40 solution,  $t = 40$  days), are more likely to represent protofibrils that have been trapped in the process of winding.

Less striking disruptions in the periodic helical substructure of type 1 fibrils can also be clearly observed using nanotube tips. The right image in Figure 4.9 shows examples of this disruption in the middle of the type 1 fibril. Imperfections such as this one may represent gaps in one of the strands forming the fibril caused by failed ligation of protofibrils/filaments during the assembly process. This failed ligation could be explained either by association of protofibrils or filaments in an orientation such that the adjacent ends are not close enough to be ligated, but are too close for incorporation of an additional protofibril. Alternatively, the formation of very small overlaps during assembly could interfere with proper ligation of filaments but produce extensions that are too short to support association and incorporation of further protofibrils to produce a branched structure (see discussion on branched structures below).

#### *Observations of partially wound type 1 fibrils and isolated filaments*

At late time points in the A $\beta$ 1-40 fibril formation process, after protofibrils have disappeared, junctions between type 1 fibrils and two filaments with smaller diameters can sometimes be observed (Figure 4.10). These structures appear to be partially wound type 1 fibrils and suggest a two filament architecture for type 1 fibrils. The average diameter of the filaments

was  $3.6 \pm 0.4$  nm (within the range of protofibril diameters observed previously), and type 1 fibrils in the same image had a diameter of  $9.2 \pm 0.2$  nm. These filaments had regular increases in diameter along their axes with a period of  $38 \pm 4.4$  nm that was very similar to the periodicity of type 1 fibril diameter increases (see section in figure 4.11). Isolated filaments with the same diameter and periodicity were also seen (again, only after the complete disappearance of fibrils) and may result from complete unwinding of type 1 fibrils, or from single filament extensions becoming detached from type 1 fibrils as a result of shearing forces generated during the sample preparation process. The lengths of the filaments observed both in isolation and as part of type 1 fibrils were often greater than  $1 \mu\text{m}$ .



Junctions between type 1 fibrils and two long filaments with smaller diameters apparently represent partially wound or unwound type 1 fibrils that exist at least transiently in solution and become trapped by adsorption to the mica substrate. An on-pathway role for protofibrils in fibril formation would suggest that these long filaments are the result of simple ligation of protofibrils following lateral association and winding of protofibrils to form type 1 fibrils. This idea is supported by the similar diameters of the protofibril and filament and by the observation of single filaments that are an order of magnitude longer than the longest protofibrils observed during fibril growth in the sample. However, subtle differences in the apparent structure of these two morphologies provide evidence that the process of filament formation may involve more than ligation of protofibril ends in the context of a growing fibril (see below).

**Branched type 1 fibrils were observed.**

Branched type 1 fibrils were commonly observed during fibril formation while protofibrils were still abundant (examples in Figure 4.6) and also following the apparent completion of fibril formation (Figure 4.11). At some branch points, all of the diverging fibrils resembled type 1 fibrils (top of left panel). At others, one of the branches was a long single filament extension of one of the type 1 fibrils (Figure 4.11, right panel).

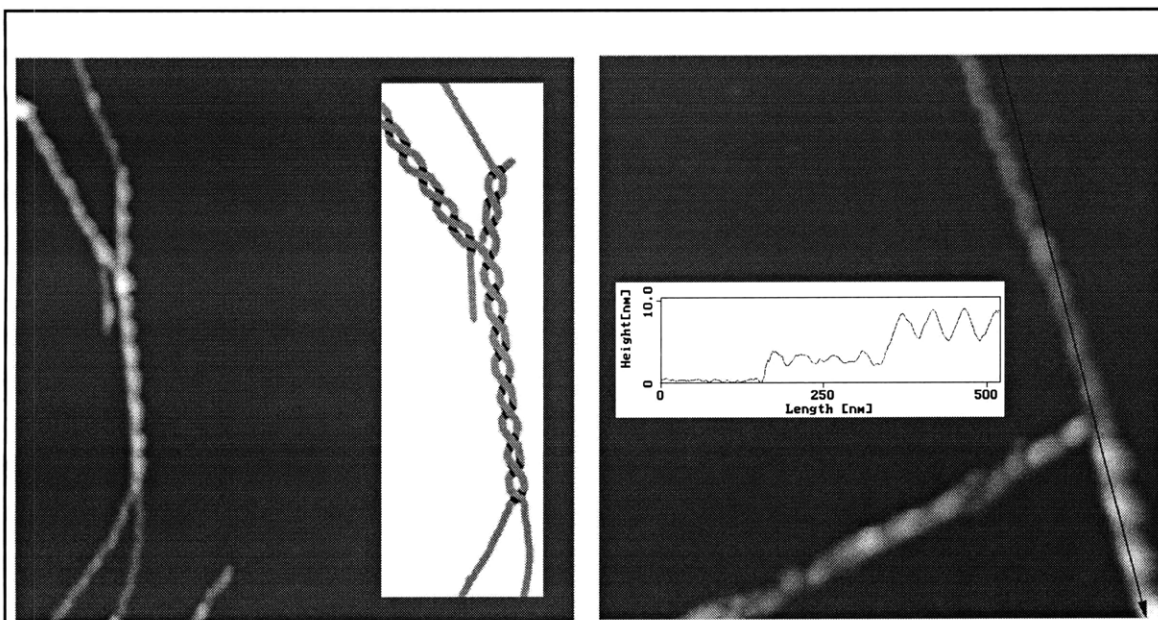


**Figure 4.11. Images of branched type 1 fibrils. The left image (1  $\mu\text{m}$  square) shows a fibril that is partially wound at one end and branched at the other. The inset shows a schematic interpretation of the morphology. The right image shows a 500 nm square image showing branching in more detail. The inset shows a cross section along the indicated plane (arrow) that shows the transition from 8-9 nm type 1 fibril to 3-4 nm single filament and shows the 40 nm periodicity of height increases along the length of both the filament and the fibril.**

Branched fibrils are a reasonable product in a fibril formation process involving association and winding of protofibrils. During assembly, improperly staggered protofibrils could associate with the growing fibril and leave exposed single filament extensions protruding from the side of the fibril at points of overlap. Association and incorporation of a protofibril with the protruding filament could then produce a new fibril extending from the existing fibril at the original overlap site. Partially wound type 1 fibrils appear to exist at least transiently in solution (above), and could also result in branched fibrils by a similar mechanism. Branching increases the number of

fibril growth sites, and could lead to geometric amplification of the overall rate of incorporation of A $\beta$  into fibrils with time if repeated branching occurs. This amplification effect would be similar to the autocatalysis that is observed during fibril formation by sickle cell hemoglobin *in vitro* that has been explained in terms of a double-nucleation model.<sup>13</sup> In the double nucleation model the sides of existing fibrils promote the formation of new oligomeric nuclei at a rate related to the surface area of the fibrils present. Since the available surface is continuously increasing as fibril growth proceeds the rate of side-nucleation also increases and provides a scenario which can explain the autocatalysis of hemoglobin fibril growth.<sup>13</sup>

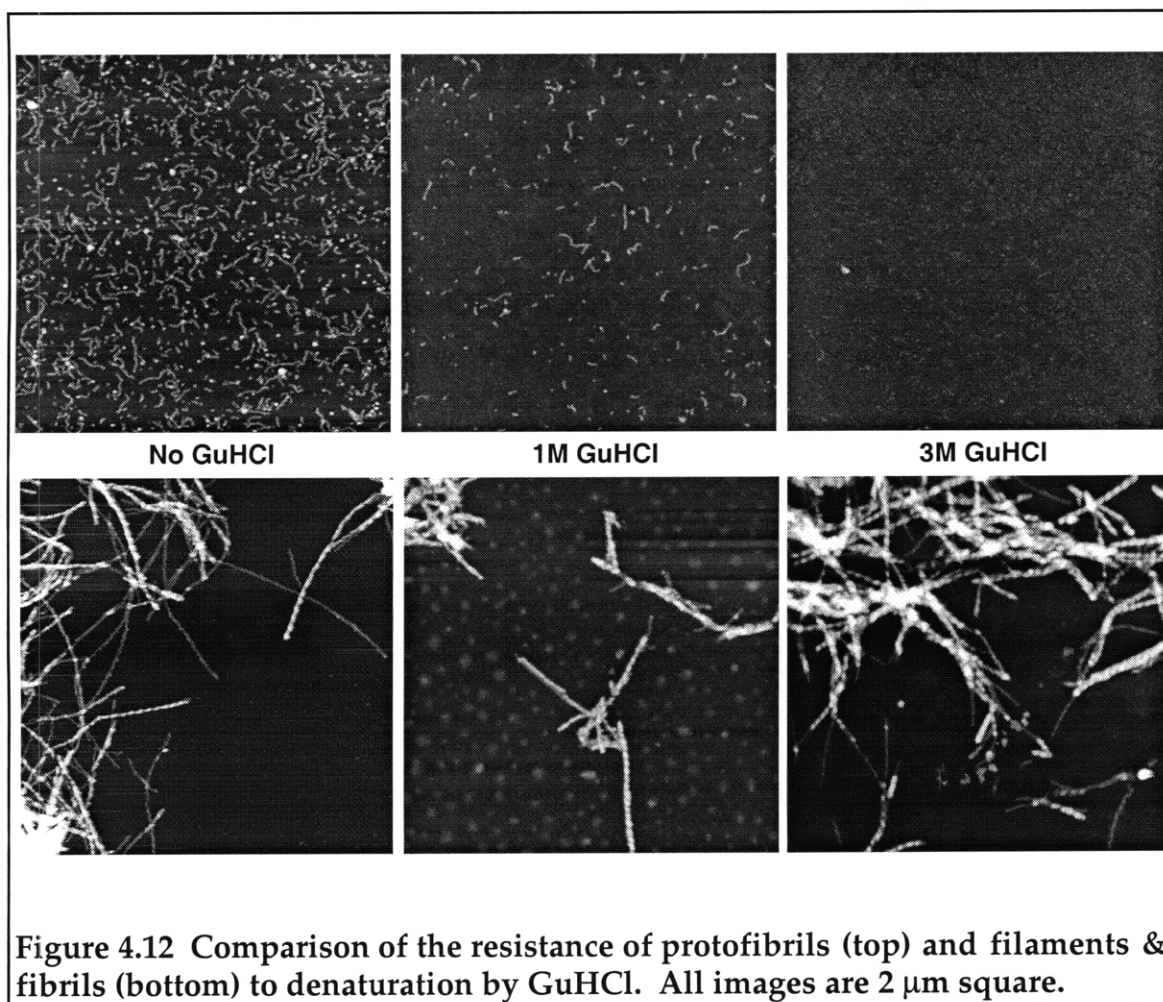
Although amyloid fibrils are typically described as unbranched in the literature, our observations of branching are not entirely unprecedented. Light scattering data from *in vitro* fibril formation has been interpreted to reflect a low degree of A $\beta$ 1-40 fibril branching under certain conditions.<sup>14</sup> In addition, branched A $\beta$ 1-40 fibrils formed *in vitro* have also been visualized previously by EM of rotary-shadowed specimens<sup>15</sup> and AFM imaging under isopropanol.<sup>16</sup>

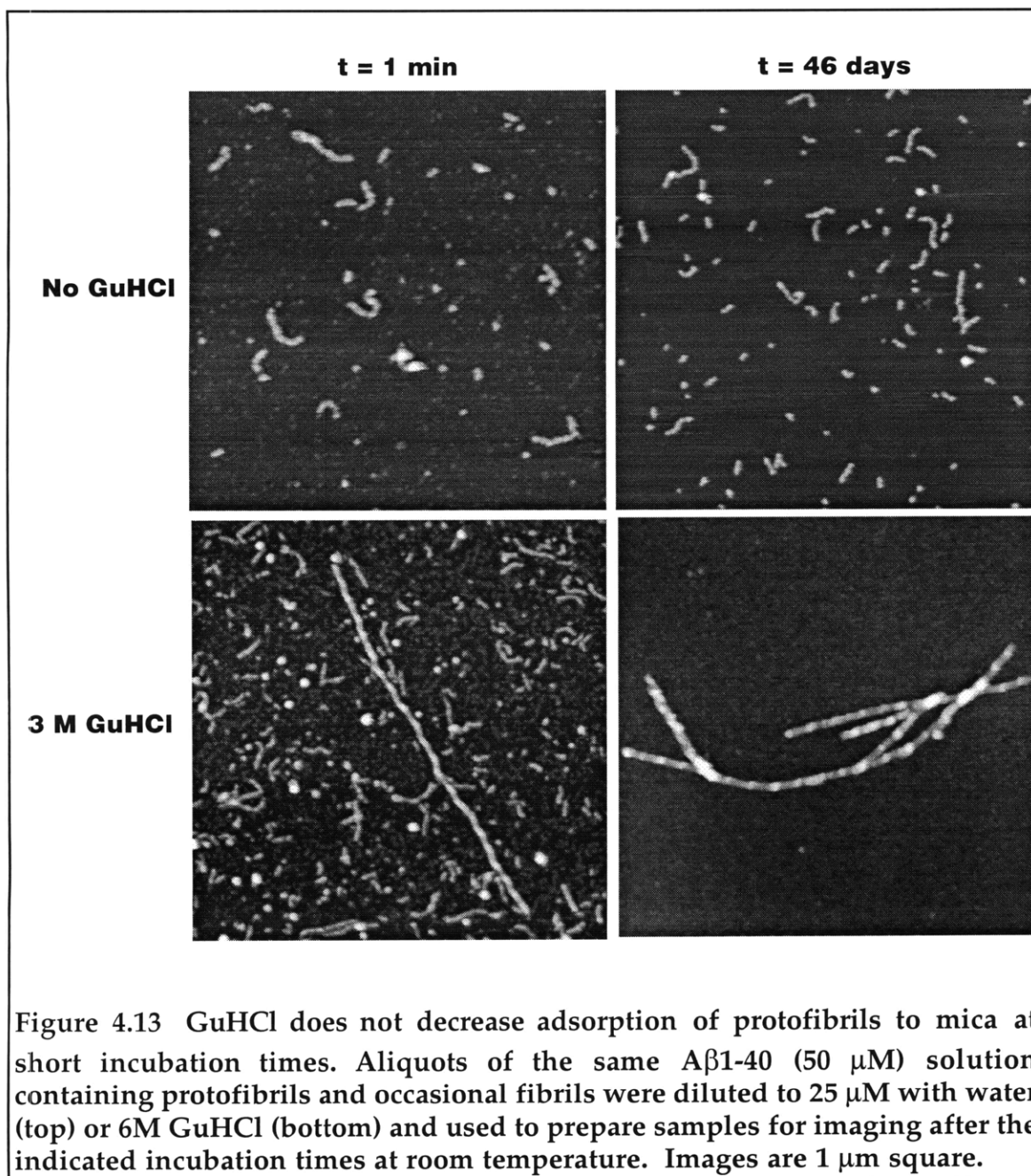
## **A conformational change may occur during fibril formation.**

### **Indications from denaturation studies.**

Evidence for a conformational change during fibril and filament formation can be seen in experiments which investigate the relative

resistance of protofibrils vs. filaments and fibrils to disassembly following exposure to guanidine hydrochloride (GuHCl). In the first experiment, aliquots containing 50  $\mu\text{M}$  A $\beta$ 1-40 (either containing protofibrils and other small oligomers present prior to fibril formation, or containing fibril and filament morphologies but no protofibrils) were diluted to a final A $\beta$ 1-40 concentration of 25  $\mu\text{M}$  in buffer containing no GuHCl, 1 M GuHCl, or 3 M GuHCl. Following incubation for 24 hours at room temperature, the samples were used to prepare specimens on mica for analysis by AFM.





The images in Figure 4.12 show that after 24 hours of incubation protofibrils are abundant in the dilution without GuHCl, are seen with reduced frequency on the mica surface prepared from the suspension in 1 M GuHCl, and are entirely absent on the substrate prepared from the suspension in 3 M GuHCl (Figure 4.12, TOP). In contrast, fibrils can be observed for all

concentrations of GuHCl examined (Figure 4.12, BOTTOM). It is also clear that single filaments are more stable than protofibrils since several single filament extensions of type 1 fibrils can be seen in the 3 M GuHCl treated fibril sample (Figure 4.12, bottom right).

The disappearance of protofibrils in the images prepared from GuHCl containing samples suggested that protofibrils have been disaggregated in these suspensions. However, since the effects of GuHCl on the adsorption process were not known, it was also possible that GuHCl caused the disappearance of protofibrils by selectively interfering with their adsorption to mica. To control for this possibility, aliquots from a 50  $\mu$ M A $\beta$ 1-40 suspension which produced specimens on mica with mostly protofibrils and only widely scattered fibrils were diluted to 25  $\mu$ M with water or 6 M GuHCl to produce suspensions without GuHCl or with 3 M GuHCl. Specimens prepared from these suspensions 1 minute after dilution clearly showed the presence of numerous protofibrils in the sample containing 3 M GuHCl as well as the sample diluted with water (Figure 4.13, left).

Imaging specimens prepared from the same suspensions after incubation at room temperature for 46 days confirms the previous observation that protofibrils are stable upon dilution to 25  $\mu$ M, but are destroyed by prolonged exposure to 3 M GuHCl (Figure 4.13, right). In addition, the persistence of fibrils, but not protofibrils, after 46 days in the 3 M GuHCl sample provides another demonstration (this time from a single sample) that protofibrils are more sensitive to denaturation by GuHCl



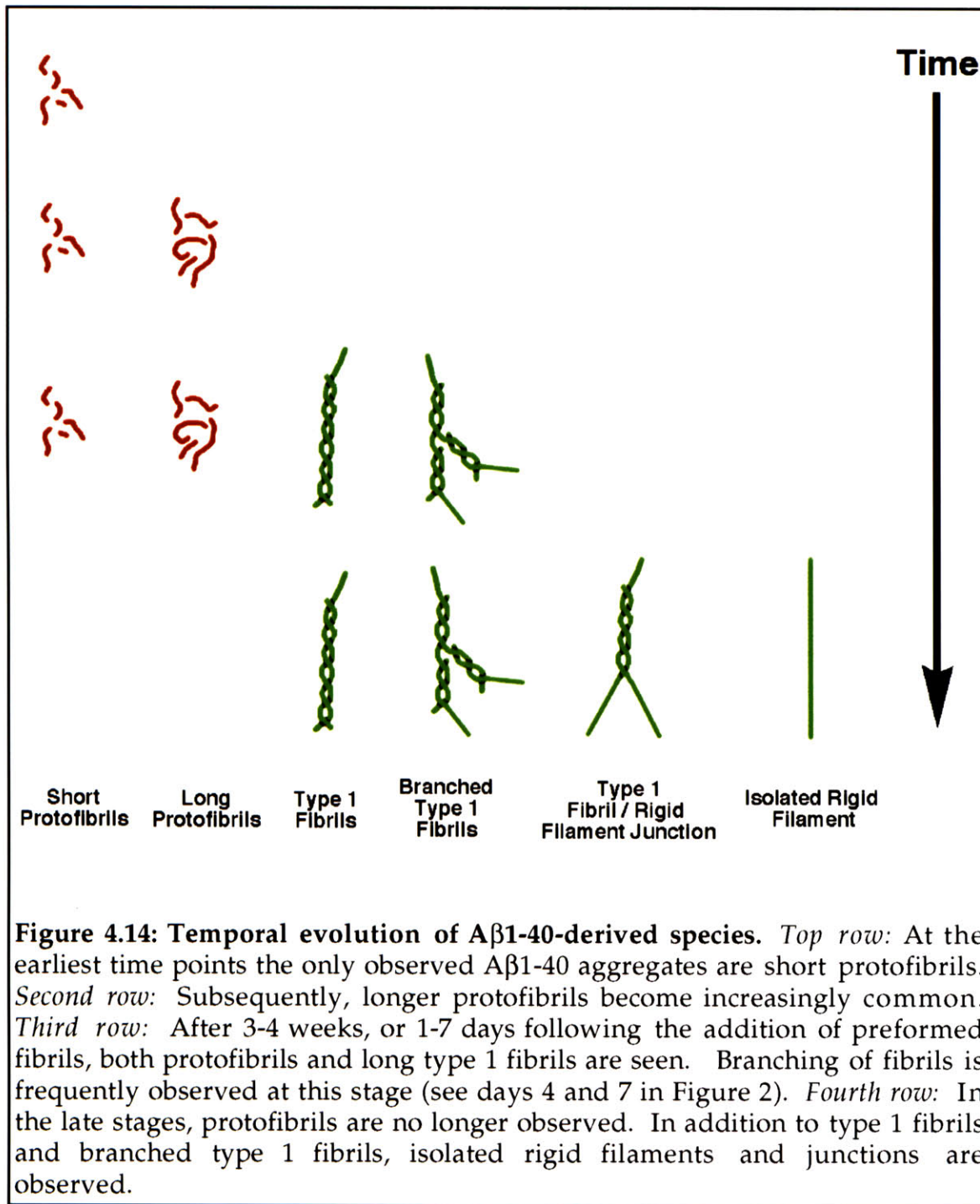
compared to fibrils and filaments. If filaments are the product of protofibril ligation in the context of type 1 fibrils, the increased resistance of filaments to denaturation compared to protofibrils could be explained if a stabilizing conformational change occurs during fibril assembly.

*Indications from differences between protofibrils and filaments.*

Simple end-to-end ligation of winding protofibrils should produce filaments with morphological features like protofibrils that differ only by increases in length. However the filament clearly differs from the protofibril in several ways. The small height increases along the length of the filaments shown in Figure 4.11 have a periodicity of ~40 nm. This distance is approximately twice the distance observed for periodic height increases along the protofibril (which have a ~20 nm period). Furthermore, when filaments are compared to fibrils they appear to be more rigid (they show much less curvature when adsorbed to the surface than protofibrils do). Finally, although the average diameter of filaments is similar to the protofibril (as discussed above), comparison with type 1 fibrils in the same image shows that filament diameters are about 40% of type 1 fibril diameters. This is less than the height of protofibrils relative to type 1 fibrils which is usually ~48% (Chapter 2). Each of these changes could be an indication that a conformational change occurs as protofibrils are incorporated into protofibrils.

## A Model For A $\beta$ Fibril Formation

A schematic summary of the temporal evolution of the A $\beta$ 1-40-derived species imaged herein is shown in Figure 4.14. The observed species fall into three classes, based on their dimensions and surface topography as determined by AFM. First to appear are the flexible protofibrils, which have an axial periodicity of *ca.* 20 nm, and are 3-4 nm in height. Protofibrils grow slowly (to *ca.* 200 nm) until type 1 fibrils are observed, then are rapidly consumed. The protofibrils are in equilibrium with monomeric A $\beta$ ; slow dissolution of protofibrils occurs at high dilution (data not shown). The next species to appear are type 1 fibrils; usually well over 1  $\mu$ m long, with a helical structure (axial periodicity of *ca.* 40 nm), and a height that is approximately 2.5-fold that of the protofibril. After the protofibrillar population has been consumed, filaments appear that are rigid and long like type 1 fibrils, have axial periodicity resembling the type 1 fibril, but have a height that is similar to that of the protofibril. The dimensions of these classes are consistent with a two-filament wound morphology for the type 1 fibril; this morphology is well-precedented (discussed in Chapter 2). The morphological differences between the rigid filaments and the flexible protofibrils may reflect a critical conformational change (red to green in Figure 4.13). A conformational change is also supported by the increased resistance of filaments and fibrils to denaturation by guanidine compared to protofibrils.



The intermediacy of the Aβ protofibril necessitates a modification of the nucleation-dependent polymerization model for amyloid formation. Our current hypothesis is based on four observations reported herein, the

transient population of the protofibril, the promoting effect of preincubation on the seeded transition to fibrils, the wound morphology of the fibril, and the fact that the filament morphology differs from protofibrils suggesting that a conformational change is coupled to protofibril incorporation into fibrils. A schematic version of this model is shown in Figure 4.15 and discussed below.

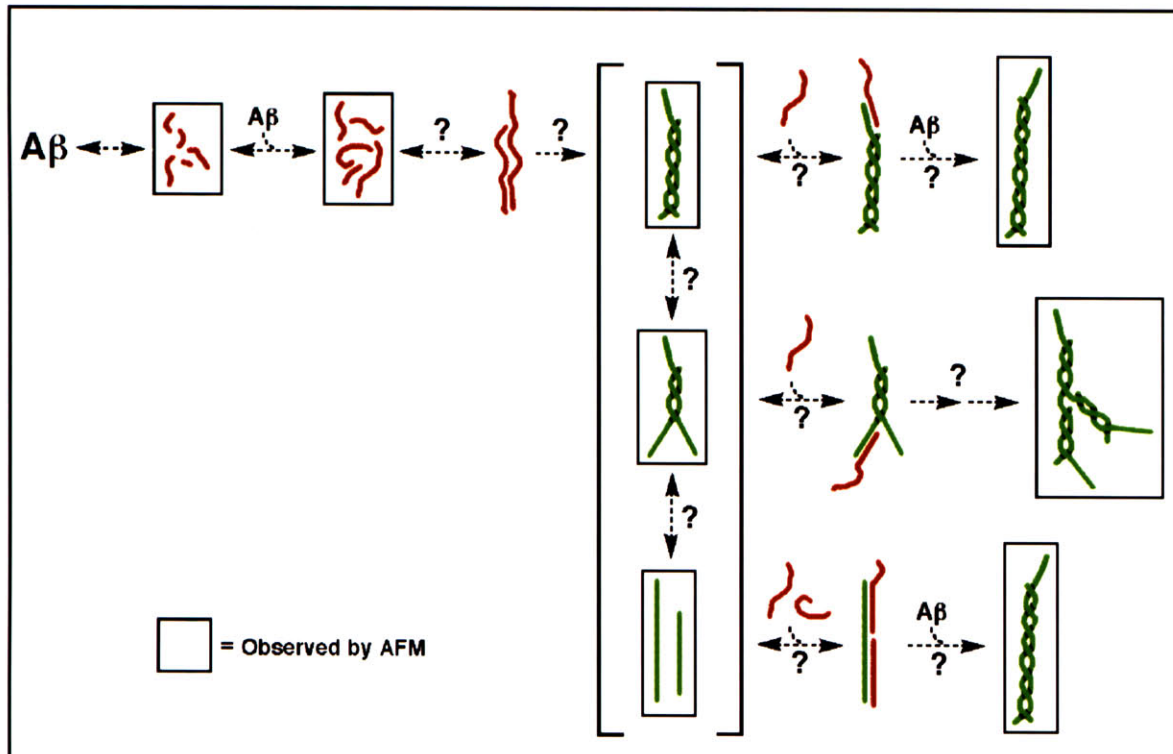


**Figure 4.15** A working hypothesis to explain seeded amyloid fibril growth. Oligomeric A $\beta$  species that have been directly observed by AFM are shown in boxes. Inferred species (not boxed) and hypothetical pathways to explain their interconversion (dashed arrows with question marks) are included.

In the earliest stages of fibril formation, monomeric (or dimeric)<sup>2</sup> A $\beta$  rapidly oligomerizes to form short protofibrils. The average length of the observed protofibrils (and the total amount)<sup>2</sup> increases with time. Nucleus

formation may involve annealing, winding, and an irreversible conformational change (red to green) to produce a type 1 fibril. The conformational change provides an explanation for the apparent cooperativity of fibril formation and could lead to a preorganized single-filament seed template that is an optimal binding site for addition of a subsequent protofibril. Addition of seed containing a mixture of fibrillar species (Figure 4.15, shown in brackets) bypasses nucleation. An exposed rigid filament could seed growth by catalyzing a conformational change in an added protofibril, analogous to the case in flagellar assembly.<sup>17</sup> Addition of a protofibril to an exposed filament could lead to unbranched elongation of a type 1 fibril (top, bottom), or to branched morphology (middle). Fibril elongation may also occur by addition of A $\beta$  monomer/small A $\beta$  oligomer onto filament ends.<sup>2,18,19</sup> Detailed kinetic studies, utilizing multiple methods to characterize and quantify all intermediates,<sup>2,9,20</sup> are required to test this model.

Information about unseeded A $\beta$  fibril growth can also be inferred from observations of seeded fibril formation. Since fibrils, but not protofibrils, are competent seeds, the nucleation-dependent step may be the protofibril-to-type 1 fibril transition, consistent with the sudden appearance of long type 1 fibrils as the earliest fibril morphology in both seeded and unseeded A $\beta$  solutions. The formation of the fibril nucleus could result from association and winding of two flexible protofibrils (unboxed aligned protofibrils in Figure 4.15) in

combination with a conformational change (red-to-green in Figure 4.15). Protofibril association to form a nucleus should depend on the area of the interacting surface and the frequency of collisions, and therefore, on the length and amount of protofibrils. Alternatively annealing and winding could be intramolecular; for example, *via* looping and supercoiling of a long protofibril.

The *in vitro* intermediacy of protofibrils suggests that they also exist *in vivo*. To demonstrate unequivocally the importance of the protofibrils in the *in vivo* pathogenic process, protofibrils must be identified in, or extracted from, AD brain tissue. Protofibrils have not been observed so far in AD brain tissue sections nor have they been purified from AD brain. This is not surprising since AD brain tissue is likely to represent the end-stage in the *in vivo* amyloid formation process when intermediates would be least likely to be found. Furthermore, even if protofibrils are present detection would be hampered by the problems associated observing such small, flexible structures in thin tissue sections, and by their potential instability to amyloid extraction procedures. Protofibrils are most likely to be found in the brains of individuals predisposed to develop AD such as young Down syndrome<sup>6</sup> and head trauma patients.<sup>21</sup> In both of these groups, significant deposition of A $\beta$ , in a non-fibrillar form called diffuse amyloid, precedes symptoms.<sup>6,21</sup> These diffuse amyloid deposits are the logical place to begin to search for protofibrils *in vivo*.

## Experimental Section

*Protein substrate.* Synthetic A $\beta$ 1-40 was purchased from Quality Controlled Biochemicals Inc. (Hopkinton, MA). All-D A $\beta$ 1-40 was kindly provided by Mike Vitek (Duke University)

*Preparation of seed-free A $\beta$ 1-40 stock solutions.* Stock solutions of A $\beta$ 1-40 in DMSO were prepared at a concentration of approximately 12 mg/ml. The peptide solution was then sonicated for 5 - 10 min and filtered through a 0.2  $\mu$ m nylon micro-spin filter (Whatman Inc., Clifton, NJ) to remove any undissolved seed. Final peptide concentrations of the DMSO stock solutions, as determined by quantitative amino analysis, were typically 2-2.5 mM.

*In vitro aggregation of A $\beta$ 1-40.* A $\beta$  aggregation was initiated by adding an aliquot of a concentrated DMSO stock of A $\beta$ 1-40 to aqueous buffer (10 mM phosphate, 137 mM NaCl, 27 mM KCl, pH 7.4) followed by immediate vortexing to mix thoroughly. After initial mixing the solutions were incubated at room temperature without further agitation except for gentle tapping to ensure homogeneous aliquots for AFM.

*Seeding experiments.* 100  $\mu$ M solutions of A $\beta$ 1-40, containing long protofibrils ( after > 1 week preincubation) were divided. One portion was left

unaltered and the other portion was seeded by adding pre-formed seed fibrils and filaments (approximately 1% of a molar equivalent based on initial total A $\beta$ 1-40 concentration), but no protofibrils (morphology confirmed by AFM just prior use). At the same time, a 100  $\mu$ M A $\beta$ 1-40 solution that was not preincubated was also seeded with the same amount of the identical seed stock. The seed stock was diluted into buffer containing no A $\beta$ 1-40 at the same ratio present in seeded samples and imaged to determine the contribution of seed fibrils to the observed images; no fibrils were detected, indicating that the observed fibrils in the seeded growth incubations are attributable to new growth, rather than the seed aliquot.

*GuHCl denaturation experiments.* Aliquots (3  $\mu$ L) of A $\beta$ 1-40 (50  $\mu$ M) either containing protofibrils and other small oligomers present prior to fibril formation, or containing fibril and filament morphologies but no protofibrils were diluted to a final A $\beta$ 1-40 concentration of 25  $\mu$ M in buffer containing no GuHCl, 1 M GuHCl, or 3 M GuHCl. Following incubation for 24 hours at room temperature, specimens were prepared on mica and analyzed by AFM.

*Atomic force microscopy.* Samples were mixed by gentle tapping to evenly suspend any aggregates, and 3-5  $\mu$ l aliquots were placed on freshly cleaved mica (Ted Pella, Redding, CA). After 30 sec, the mica was gently rinsed twice with 50  $\mu$ l of 0.2  $\mu$ m-filtered water to remove salt and loosely bound peptide.



Excess water was removed with a gentle stream of filtered compressed tetrafluoroethane, and the samples were imaged immediately. All images were obtained under ambient conditions with a Nanoscope IIIa Multimode scanning probe workstation (Digital Instruments, Santa Barbara, CA) operating in TappingMode™ using etched silicon NanoProbes™ (Probe Model TESP, Digital Instruments). Scanning parameters varied with individual tips and samples, but typical ranges were as follows: initial RMS amplitude, 1.2 V; setpoint, 0.9-1.1V; tapping frequency, 250-350 kHz; scan rate, 0.8-1.75 Hz. Carbon nanotube probes were made by Stanislaus Wong in Charles Lieber's lab (Harvard University) using published procedures.<sup>12</sup> Analysis of morphology dimensions was performed as described previously in Chapter 2.

## References for Chapter 4

1. Harper, J.D., Wong, S.S., Lieber, C.M., and Lansbury, P.T. Jr. Observation of metastable Abeta amyloid protofibrils by atomic force microscopy. *Chem. Biol.* **1997**, *4*, 119-125.
2. Walsh, D.M., Lomakin, A., Benedek, G.B., Condron, M.M., and Teplow, D.B. Amyloid beta-protein fibrillogenesis. Detection of a protofibrillar intermediate. *J. Biol. Chem.* **1997**, *272*, 22364-22372.
3. Selkoe, D.J. Alzheimer's disease: genotypes, phenotypes, and treatments. *Science* **1997**, *275*, 630-631.
4. Selkoe, D.J. Amyloid beta-protein and the genetics of Alzheimer's disease. *J. Biol. Chem.* **1996**, *271*, 18295-18298.
5. Gearing, M., Mori, H., and Mirra, S.S. Abeta-peptide length and apolipoprotein E genotype in Alzheimer's disease. *Ann. Neurol.* **1996**, *39*, 395-399.
6. Lemere, C.A., Blusztajn, J.K., Yamaguchi, H., Wisniewski, T., Saido, T.C., and Selkoe, D.J. Sequence of deposition of heterogeneous amyloid beta-peptides and APO E in Down syndrome: implications for initial events in amyloid plaque formation. *Neurobiol. Dis.* **1996**, *3*, 16-32.
7. Jarrett, J.T., Berger, E.P., and Lansbury, P.T., Jr. The carboxy terminus of the beta amyloid protein is critical for the seeding of amyloid formation: implications for the pathogenesis of Alzheimer's disease. *Biochemistry* **1993**, *32*, 4693-4697.
8. Evans, K.C., Berger, E.P., Cho, C.G., Weisgraber, K.H., and Lansbury, P.T., Jr. Apolipoprotein E is a kinetic but not a thermodynamic inhibitor of amyloid formation: implications for the pathogenesis and treatment of Alzheimer disease. *Proc. Natl. Acad. Sci. USA* **1995**, *92*, 763-767.
9. Wood, S.J., Chan, W., and Wetzel, R. An ApoE-Abeta inhibition complex in Abeta fibril extension. *Chem Biol* **1996**, *3*, 949-56.
10. Lansbury, P.T., Jr. A Reductionist view of Alzheimer's disease. *Acc. Chem. Res.* **1996**, *29*, 317-321.
11. Dai, H., Hafner, J.H., Rinzler, A.G., Colbert, D.T., and Smalley, R.E. Nanotubes as nanoprobe in scanning probe microscopy. *Nature* **1996**, *384*, 147-150.
12. Wong, S.S., Harper, J.D., Lansbury, P.T.J., and Lieber, C.M. Carbon nanotubes tips: High resolution probes for imaging biological systems. *J. Am. Chem. Soc.* **1998**, *120*, 603-604.
13. Ferrone, F.A., Hofrichter, J., and Eaton, W.A. Kinetics of sickle Hemoglobin polymerization. II. A double nucleation mechanism. *J. Mol. Biol.* **1985**, *183*, 611-631.
14. Shen, C.L. and Murphy, R.M. Solvent effects on self-assembly of beta-amyloid peptide. *Biophys. J.* **1995**, *69*, 640-651.
15. Howlett, D.R., Jennings, K.H., Lee, D.C., Clark, M.S., Brown, F., Wetzel, R., Wood, S.J., Camilleri, P., and Roberts, G.W. Aggregation state and

- neurotoxic properties of Alzheimer beta-amyloid peptide. *Neurodegeneration* **1995**, 4, 23-32.
16. Stine, W.B., Jr., Snyder, S.W., Lador, U.S., Wade, W.S., Miller, M.F., Perun, T.J., Holzman, T.F., and Krafft, G.A. The nanometer-scale structure of amyloid-beta visualized by atomic force microscopy. *J Protein. Chem.* **1996**, 15, 193-203.
  17. Asakura, L. Polymerization of flagellin and polymorphism of flagella. *Adv. Biophys.* **1970**, 1, 99-155.
  18. Esler, W.P., Stimson, E.R., Ghilardi, J.R., Vinters, H.V., Lee, J.P., Mantyh, P.W., and Maggio, J.E. In vitro growth of Alzheimer's disease beta-amyloid plaques displays first-order kinetics. *Biochemistry* **1996**, 35, 749-757.
  19. Naiki, H. and Nakakuki, K. First-order kinetic model of Alzheimer's beta-amyloid fibril extension in vitro. *Lab. Invest.* **1996**, 74, 374-383.
  20. Wood, S.J., Maleeff, B., Hart, T., and Wetzel, R. Physical, morphological and functional differences between pH 5.8 and 7.4 aggregates of the Alzheimer's amyloid peptide A $\beta$ . *J. Mol. Biol.* **1996**, 256, 870-7.
  21. Nicoll, J.A., Roberts, G.W., and Graham, D.I. Apolipoprotein E epsilon 4 allele is associated with deposition of amyloid beta-protein following head injury. *Nat. Med.* **1995**, 1, 135-7.